NASA CONTRACTOR REPORT

NASA CR-800

NASA CR-

v.1

c.1

TECH LIBRARY KAFB, NM

0060192

LOAN COPY: RETURN TO
AFWL (WLIL-2)
KIRTLAND AFB, N MEX

RESEARCH AND DEVELOPMENT OF HIGH-PERFORMANCE AXIAL-FLOW TURBOMACHINERY

Volume 1 - Design of Turbine-Compressor

by P. Bolan, R. Cohen, and W. K. Gilroy

Prepared by
PRATT & WHITNEY AIRCRAFT
East Hartford, Conn.
for Lewis Research Center

NATIONAL AERONAUTICS AND SPACE ADMINISTRATION • WASHINGTON, D. C. • MAY 1968

TECH LIBRARY KAFB, NM
0060192

NASA CR-800

RESEARCH AND DEVELOPMENT OF HIGH-PERFORMANCE AXIAL-FLOW TURBOMACHINERY

Volume 1 — Design of Turbine-Compressor

By P. Bolan, R. Cohen, and W. K. Gilroy

Distribution of this report is provided in the interest of information exchange. Responsibility for the contents resides in the author or organization that prepared it.

Prepared under Contract No. NAS 3-4179 by
PRATT & WHITNEY AIRCRAFT
East Hartford, Conn.

for Lewis Research Center

NATIONAL AERONAUTICS AND SPACE ADMINISTRATION

For sale by the Clearinghouse for Federal Scientific and Technical Information
Springfield, Virginia 22151 – CFSTI price $3.00

FOREWORD

This report was prepared in accordance with Contract NAS3-4179 under the technical management of Jack A. Heller of the Space Power System Division, and in consultation with Harold E. Rohlik, Calvin L. Ball, William J. Anderson, and George K. Fischer of the Fluid System Components Division, NASA Lewis Research Center, Cleveland, Ohio. It is published in three volumes, as follows:

Volume 1 CR-800 - - Design of Turbine-Compressor (Pratt & Whitney Aircraft)
Volume 2 CR-801 - - Design of Gas Bearings (Mechanical Technology Incorporated)
Volume 3 CR-802 - - Design of Backup Gas Bearings (The Franklin Institute Research Laboratories)

ABSTRACT

The National Aeronautics and Space Administration is conducting an evaluation of candidate Brayton-cycle turbomachinery configurations. As part of this program, Pratt & Whitney Aircraft has designed a turbine-compressor incorporating a single-stage axial-flow turbine driving a six-stage axial-flow compressor supported on gas bearings. The gas bearing rotor support system was successfully tested in a gas bearing dynamic simulator. A backup gas bearing system was designed and various experimental investigations were conducted to verify certain areas of the turbine-compressor design in addition to the gas bearing testing.

TABLE OF CONTENTS

VOLUME 1

Page

Foreword iii
Abstract v
Table of Contents vii
List of Figures viii
List of Tables x

I. Summary 1
II. Introduction 2
III. Description of Turbine-Compressor Design 5

- A. Aerodynamic Design 7
- B. Stress and Deflection Analyses 9
- C. Rotor Dynamics and Gas Bearing Designs 18
- D. Thermal Analysis 23
- E. Material Selection 29
- F. Recommendations on provisions to Install Instrumentation 32

IV. Summary of Gas Bearing Dynamic Simulator Testing 36

References 40

Appendix 1 - Backup Gas Bearing Design 41
Appendix 2 - Compressor Blade Retention Investigation 50
Appendix 3 - Gas Bearing Materials Investigation 53
Appendix 4 - Journal Bearing Heat Exchanger Investigation 55
Appendix 5 - Figures 57

LIST OF FIGURES

Number	Title	Page
1	Brayton-Cycle Turbomachinery	4
2	Brayton-Cycle Turbine-Compressor	62
3	Turbine-Compressor Rotor Assembly	63
4	Turbine Blades	64
5	Compressor Blades	65
6	Compressor Blade Retention	66
7	Number 2 Bearing Heat Exchanger	67
8	Thrust Runner	68
9	Turbine-Compressor Gas Bearing Design. Thrust Bearing and No. 1 Journal Bearing	69
10	Main (Forward) Thrust Stator and Support	70
11	Compressor Research Package Vane and Shroud Assembly	71
12	Gas Cooling Flow Path	72
13	Turbine-Compressor Gas Bearing Design. No. 2 Journal Bearing	73
14	Trailing Edge View of Turbine Nozzle Assembly	74
15	Turbine Nozzle Vane Casting	75
16	Estimated Compressor Efficiency from Inlet Flange to Scroll Exit Flange	76
17	Predicted Turbine Weight Flow Parameter	77
18	Estimated Turbine Off-Design Parameter	78
19	Rotor Runaway Condition	79
20	Turbine Blade Stress	80
21	Temperature Map of Scroll Area	81
22	Mass Distribution of Rotor Assembly	82
23	Distribution of Polar Moment of Inertia of Rotor Assembly	83
24	Turbine-Compressor Rotor Response at 50,000 rpm with 0.002 Ounce-Inch of Turbine Unbalance	84
25	Front Journal Bearing Pads	85
26	High Spring Rate Flexures	86
27	Low Spring Rate Flexures	87
28	Turbine End of Number 2 Bearing	88
29	Number 1 Bearing Support and Rear Thrust Stator	89
30	Temperature Map of Number 2 Bearing (Initial Design)	90
31	Temperature Map of Number 2 Bearing (Final Design)	91
32	Temperature Map of Number 1 Bearing (Initial Design)	92
33	Temperature Map of Number 1 Bearing (Final Design)	93
34	Temperature Map of Turbine-Compressor Inlet Duct	94
35	Thrust Bearing Coolant Performance	95
36	Turbine-Compressor Temperature Map	96
37	Temperature Transient in Number 2 Bearing (Initial Design)	97
38	Temperature Transient in Number 1 Bearing (Initial Design)	98
39	Transient Temperature Response of Thrust Bearing. No Stator Cooling. No Mount Ring Heat	99
40	Transient Temperature Response of Thrust Bearing. Stator Cooling at T_O = 150°F. Mount Ring Heated	100
41	Transient Temperature Response of Thrust Bearing. No Stator Cooling. Mount Ring Heated	101
42	Turbine Thermal Transient	102
43	Inter-Scroll Structure Thermal Transient	103
44	Dynamic Simulator of Turbine-Compressor Gas Bearing System	104
45	Cross-Section of Dynamic Simulator	105
46	Shaft of Dynamic Simulator and Turbine-End View Showing Heat Exchanger Brazed Inside Bearing Journal	106
47	Dynamic Simulator Installed in Vertical Position with Compressor Inlet Up	107
48	Control Panel and Instrumentation Readout Equipment for Dynamic Simulator	108
49	Dynamic Simulator Test Results. Traces of Number 2 Journal Bearing (Initial Design)	109

LIST OF FIGURES (Cont'd)

Number | Title | Page

50 Dynamic Simulator Test Results. Pad-to-Shaft Film Thickness of Number 1 Journal Bearing (Initial Design) 110

51 Modified Configuration of Number 2 Journal Bearing Pads 111

APPENDIX 1

52 Number 1 Bearing Area with Sleeve Concept 112

53 Temperature Map of Number 1 Bearing with Sleeve Concept 113

54 Shaft Temperature vs Length of Number 1 Bearing with Sleeve Concept 114

55 Temperature Map of Number 1 Bearing with Cooling Jacket Concept 115

56 Shaft Temperature vs Length at Number 1 Bearing with Cooling Jacket Concept 116

57 Number 1 Bearing Area with Gas Cooling 117

58 Temperature Map of Number 1 Bearing with Gas Cooling Concept No. 1 118

59 Shaft Temperature vs Length at Number 1 Bearing with Gas Cooling Concept No. 1 119

60 Temperature Map of Number 1 Bearing with Gas Cooling Concept No. 2 120

61 Shaft Temperature vs Length at Number 1 Bearing with Gas Cooling Concept No. 2 121

62 Temperature Map of Number 2 Bearing with Gas Cooling Concept No. 1 (0.5% Gas Flow) 122

63 Temperature Map of Number 2 Bearing with Gas Cooling Concept No. 1 (1.0% Gas Flow) 123

64 Temperature Map of Number 2 Bearing with Gas Cooling Concept No. 1 (1.5% Gas Flow) 124

65 Temperature vs Axial Distance at Number 2 Bearing with Gas Cooling Concept No. 1 125

66 Temperature Map of Number 2 Bearing 126

67 Temperature vs Axial Distance at Number 2 Bearing 127

68 Temperature Map of Number 1 Bearing and Thrust Bearing 128

69 Turbine-Compressor Backup Gas Bearing Design. Thrust Bearing and No. 1 Journal Bearing 129

Number | Title | Page

70 Turbine-Compressor Backup Gas Bearing Design. No. 2 Journal Bearing 130

71 Turbine-Compressor with Backup Gas Bearings 131

APPENDIX 2

72 Compressor Blade-Locking Pin Installed 132

73 Compressor Research Package Disc, Blades, and Lock Pins 133

74 Aluminum Blade Locking Pin Test Results 134

75 Aluminum Blade Locking Pins 135

76 Silver-Plated Copper Blade Locking Pins 136

77 Solid Copper Pin Deformation Test Results 137

78 Relieved Copper Pin Deformation Test Results 138

79 Drilled Copper Blade Locking Pin Showing Deformed Head Sheared Off after Blade Removal 139

80 Drilled Copper Blade Locking Pins 140

81 Relieved Copper Pin Deformation Test Results 141

82 Drilled Copper Blade Locking Pin Showing Upset Deformation after 125-Pound Load 142

83 Deformed Rivet Head of Drilled Copper Blade Locking Pin after 125-Pound Load 143

84 Simulated Compressor Blade Root Test Parts 144

85 Test Setup for Applying Simulated Centrifugal Load to Compressor Blade Root Test Pieces 145

APPENDIX 3

86 Linde LC-4 Process Bond Strength Specimens before and after Test 146

87 Waspaloy and Aluminum with Chrome Oxide Coating Applied by Linde LC-4 Process 147

88 M-1 Tool Steel and Titanium with Chrome Oxide Coating Applied by Linde LC-4 Process 148

89 Cup/Bend Specimens Coated by Linde LC-4 Process and Plasma-Spray Process after Test 149

90 Thermally-Cycled Specimens of Linde LC-4 Coating and Plasma-Spray Coating on Waspaloy 150

APPENDIX 4

91 Two Views of Finned Element of Heat Exchanger for Number 2 Bearing 151

92 Simulated Shaft Assembly Mounted in Braze Retort 152

LIST OF TABLES

Number	Title	Page
1	Estimated Compressor Performance at Design Operating Conditions	7
2	Estimated Turbine Performance at Design Operating Conditions	8
3	Compressor Blade Stress Summary	9
4	Dovetail Stresses in Fifth Stage of Compressor	10
5	Compressor Blade Natural Frequencies at 50, 000 rpm	10
6	Turbine Blade Natural Frequencies	11
7	Turbine Gooseneck Stresses	12
8	Number 2 Bearing Journal Growth	12
9	Number 1 Bearing Journal Growth	12
10	Number 2 Bearing Heat Exchanger Stresses	13
11	Thrust Bearing Distortion at Assembly	14
12	Thrust Bearing Distortion at Operating Conditions	14
13	Significant Stresses in Number 1 Journal and Thrust Bearings	15
14	Significant Stresses in the Compressor and Turbine Scroll Area	16
15	Significant Transient Stresses in the Turbine Casing	17
16	Vibrational Characteristics of Static Structure	17
17	Turbine-Compressor Gas Bearing Design Parameters and Calculated Performance Characteristics	20
18	Summary of Tests Conducted on Turbine-Compressor Gas Bearing Dynamic Simulator	38
19	Summary of Test Conditions to Establish Whirl Threshold of Rear Journal Bearing	39

I. SUMMARY

Pratt & Whitney Aircraft has conducted the design of an axial-flow turbine-compressor as candidate turbomachinery for a Brayton-cycle space powerplant. The overall design of the turbine-compressor is discussed and the results of gas bearing test programs are presented. Tests of the rotor support system using a rotor dynamics simulator have demonstrated satisfactory gas bearing operation at the design speed of 50, 000 rpm and at 120 per cent of design speed. During this testing the gas bearing cooling provisions also demonstrated satisfactory performance. Tests were conducted on air and argon at ambient pressure levels of 14.7 and 7 psia, in both horizontal and vertical orientations with mass unbalance introduced in the rotor to simulate end-of-life conditions. Thrust loads above expected levels were tested on the hydrodynamic thrust bearing and loads up to 100 pounds were tested on the hydrostatic thrust bearing to simulate maximum anticipated startup conditions. Bearing temperatures up to 310°F were demonstrated as well as hydrodynamic startup on the journal bearings.

II. INTRODUCTION

The National Aeronautics and Space Administration has embarked on the Apollo program to put man on the moon. This trip is planned to take a few days and the spacecraft is equipped with three 2-kilowatt fuel cells for onboard electrical power requirements. Future space missions now being planned are for extended periods lasting about one year and requiring power in the tens of kilowatts. For these future missions, nuclear and solar heat sources are being considered with a variety of power-conversion systems. These include static and dynamic systems. One of the dynamic power-conversion systems being considered is the Brayton cycle. This system offers the potential of high efficiency and a well-developed technology based upon that of aircraft gas turbines. As part of the continuing research activity being conducted by the National Aeronautics & Space Administration, Pratt & Whitney Aircraft designed an axial-flow turbine-compressor as a candidate for the Brayton-cycle powerplant.

The objective of the turbine-compressor research package was to evaluate two basic areas of technical uncertainty. First, efficiency of the turbomachinery in a Brayton-cycle powerplant affects the overall system characteristics to a high degree. Therefore, high aerodynamic efficiency and low parasitic power loss must be achieved. The aerodynamic efficiency of small-size low-flow turbomachinery is inadequately documented and the turbine-compressor and associated aerodynamic rigs were intended to be used to acquire this needed data. Secondly, the use of gas bearings for this application appeared to be desirable because of the elimination of possible contamination of the cycle gas with oil in a closed-loop powerplant for the lifetimes considered. However, the technology of gas bearings in this type of environment was limited. Therefore, it was decided to use as much well-documented technology as possible in all areas of the turbine-compressor design, and concentrate on conservative engineering practice in extrapolating known technology in the two least documented areas. The aerodynamic rigs discussed in References 1 and 2 were delivered to the NASA for the aerodynamic test evaluation. The initial gas bearings designed for the turbine-compressor and tested in a rotor dynamic simulator demonstrated successful operation early in the test program, but with higher than desired power loss. The initial gas bearing design was modified and at significantly reduced power loss demonstrated early successful operation at the design speed of 50,000 rpm and at 120 per cent of design speed.

The turbine-compressor research package was designed to provide a high-performance unit using axial-flow aerodynamic components. The design of this unit is discussed in this report as well as the test activities conducted in an effort to verify the design. The rotating system is supported on gas bearings designed by Mechanical Technology Incorporated and described in Volume 2 (report CR-801). A backup gas bearing rotor support system designed by The

Franklin Institute Research Laboratories is described in Volume 3 (report CR-802), and the integration of these bearings in the turbine-compressor is described in Appendix 1 of Volume 1. The compressor, turbine, and bearings are intended to be operated in argon. The mechanical design of the turbine-compressor, shown in Figure 1 with the turboalternator designed under Contract NAS3-6013, is intended to provide a unit that will meet the environmental conditions specified in Contract NAS3-4179, will be capable of 10,000 hours operating life, and will provide a versatile arrangement with ease of assembly and disassembly. The following conditions were specified in the design of the turbine-compressor research package:

working fluid, including bearings	argon
weight flow	0.611 lb/sec
inlet total temperature - compressor	536°R
inlet total temperature - turbine	1950°R
inlet total pressure - compressor	6.0 psia
inlet total pressure - turbine	13.2 psia
pressure ratio, total-to-total - compressor	2.30
pressure ratio, total-to-total - turbine	1.56
speed capability, per cent of design speed	120

The turboalternator shown with the turbine-compressor on Figure 1 produces 12 KW at 400 cps and 0.8 power factor and operates at 12,000 rpm.

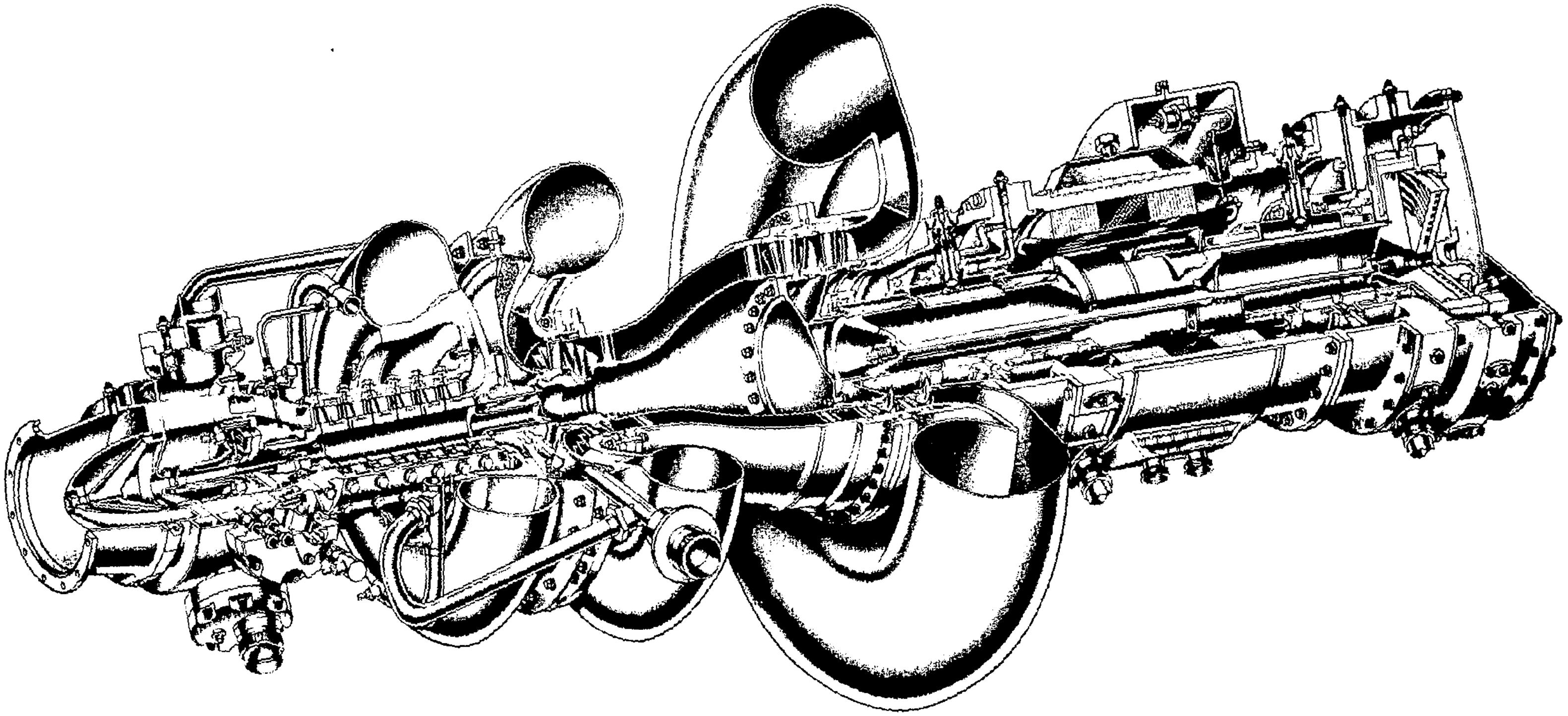

Figure 1 **BRAYTON CYCLE TURBOMACHINERY**

III. DESCRIPTION OF TURBINE-COMPRESSOR DESIGN

The turbine-compressor research package design is shown in Figure 2. The basic cycle flow enters the compressor through the inlet duct and around the housing which contains the thrust bearing and Number 1 radial bearing. The argon flows through the six-stage axial-flow compressor, the radial diffuser, and then the exit scroll and ducting. It is heated to 1950°R external to the unit and the argon is returned to the turbine inlet ducting and scroll. The Number 2 radial bearing is located between the compressor exit and turbine inlet. The argon flows through the single-stage axial-flow turbine which drives the compressor directly. It then exhausts through the exit ducting which is designed to match the turboalternator turbine.

The rotor of the turbine-compressor shown in Figure 3 consists of a single Waspaloy shaft with an integral turbine rotor, brazed heat exchangers and mechanically-attached compressor blades and thrust bearing runner. The single shaft was selected to provide a rigid rotor, good configuration for balancing, and space to incorporate bearing cooling heat exchangers. The turbine blades defined in Reference 1 and shown in the turbine rig in Figure 4 are machined integrally with the disk which connects with the shaft through a gooseneck. The compressor blades defined in Reference 2 and shown in the compressor rig in Figure 5 are made of titanium alloy and are attached to the rotor by dovetails. The blades are located axially by radial copper pins which are upset into a slot in the bottom of the blade to ensure retention as shown in Figure 6 and discussed in Appendix 2. Cylindrical surfaces, which are coated with chrome oxide based on Appendix 3 and Volume 2 (report CR-801), on each end of the compressor, serve as bearing journals. A nickel heat exchanger shown in Figure 7 is brazed under each journal to provide for gas cooling of the bearings. Investigation of heat exchanger fabrication is discussed in Appendix 4. The titanium alloy thrust runner shown in Figure 8 is bolted to the end of the shaft by a method that provides minimum distortion of the thrust face.

The compressor inlet section shown in Figure 9 contains the inlet gas passage and guide vanes as well as the Number 1 radial bearings and the thrust bearing. The journal bearing is located in the plane of the guide vanes and holes are provided in the guide vanes for bearing pivot adjustment. An aluminum thrust plate shown in Figure 10 forms the main (forward) stationary part of the thrust bearing. It is mounted on a tubular support which provides flexibility. The plate is cooled by liquid to minimize thermal distortion. Gas lines are included to provide high pressure gas for external pressurization during starting.

The compressor stator vanes are airfoils defined in Reference 2 and brazed in shrouds as shown in Figure 11. The brazed stator assemblies are split to permit assembly and they are located by pins and secured by bolts in the outer casing of the compressor to assure proper location. The outer shrouds constitute the outer wall of the gas passage in the compressor. To provide the close clearances required in this type of machine, the stators are assembled in the outer casing and final-machined.

Compressor exit gas is bled from the compressor discharge, cooled, fed through the leading edge of the inlet struts and flows down the center of the shaft as shown in Figure 12. About 3.8 per cent of the cycle flow, cooled to 100°F, is required at the compressor inlet strut at a pressure of 12.8 psia. This gas flows through heat exchangers in the journal of each bearing to cool the radial bearings and is discharged into the Number 2 bearing compartment as shown in Figure 13. Some of this gas flows through a metering hole in the rotor into the compartment behind the turbine disk and prevents circulation of hot turbine discharge gas in this area. Part of the gas flows through the labyrinth seal and up the front face of the turbine disk. Approximately 0.9 per cent of the cycle flow is bled from the Number 2 bearing compartment and is returned uncooled to the Number 1 bearing area to heat the radial bearing support as shown in Figure 9. This gas leaks through the labyrinth seal upstream of the compressor first stage.

The turbine gas flow enters the turbine scroll through an inlet port and is evenly distributed circumferentially in the scroll. The inlet gas then flows radially in the inlet duct struts and is turned to flow axially through the turbine nozzles shown in the turbine rig on Figure 14. The nozzle vanes, shown on Figure 15, are located axially by an intermediate ring in the duct flange and are restrained circumferentially by slots and pins. The turbine inlet duct and scroll is connected to the compressor exit duct by a flange and conical section. Since the turbine inlet temperature is 1950°R and the compressor exit temperature is approximately 800°R, the interconnecting structure has been designed to minimize the thermal loss consistent with the integrity of the parts. The Number 2 journal bearing pivots are straddle-mounted from the bearing support ring on the back surface of the compressor exit diffuser. The turbine inlet is insulated to reduce heat transfer from the turbine inlet gas to the bearing compartment.

The turbine exit duct is bolted to a flange which also contains the turbine nozzle vanes. The exit duct is a welded structure made of AMS 5754 with the critical dimensions machined after welding. The exit ducting is located by a bolted flange which incorporates a composite metal seal to prevent gas leakage. The bolts are plated to assure satisfactory disassembly. The mount system supports the unit at the flange between the compressor and turbine scrolls and at the flange on the compressor inlet.

A. Aerodynamic Design

The basic objective in the aerodynamic design of the Brayton-cycle axial-flow compressor was to provide a machine of high efficiency at the design operation conditions. Of particular importance, in an axial compressor of the small size and type required, is attention to Reynolds number losses, clearance losses and exit ducting losses. To minimize the Reynolds number effects, conservatively loaded airfoils of reasonable size are required. Clearance losses are reduced by providing the minimum clearances consistent with mechanical integrity. Low velocities and reasonable diffusion rates are necessary to minimize exit duct losses.

A six-stage compressor with constant inner diameter utilizing NACA 4-digit airfoils was selected. Axial gas velocities at the inlet and exit are 404 and 300 feet per second respectively. Estimated performance at the design operating conditions is listed in Table 1. The complete estimated performance map from inlet flange to exit flange is shown on Figure 16.

TABLE 1

Estimated Compressor Performance at
Design Operating Conditions

inlet flange total pressure	6.0 psia
inlet flange total temperature	536°R
scroll exit flange total pressure	13.8 psia
scroll exit flange total temperature	793°R
flow	0.611 lb/sec
speed	50,000 rpm
pressure ratio, total-to-total, inlet flange to scroll exit flange	2.3
efficiency, total-to-total, inlet flange to scroll exit flange	82.5 per cent
pressure ratio, total-to-total, inlet flange to compressor exit	2.365
efficiency, total-to-total, inlet flange to compressor exit	85.8 per cent
pressure ratio, total-to-static, inlet flange to compressor exit	2.28
efficiency, total-to-static, inlet flange to compressor exit	84.4 per cent

The turbine blading for the axial-flow Brayton-cycle turbine-compressor was selected with the objective of producing high efficiency and high reliability potential. Preliminary studies indicated that an efficient turbine could be designed for this application over a moderate range of speeds. Therefore, a rotational speed of 50,000 rpm was selected based on compressor design requirements. With the compressor work, speed, and flow defined, the first major turbine design selections were the size or diameter of the turbine wheel and the number of stages. This choice was governed by the most significant turbine design variable, the isentropic velocity ratio. A high mean velocity ratio of 0.697 was selected to provide high efficiency potential. This resulted in a mean blade diameter of 4.1 inches for a single-stage turbine. Coupled with the high velocity ratio, high reaction was selected in the interest of high efficiency.

Estimated turbine performance at the design operating conditions is listed in Table 2. The overall performance of the turbine is given on Figures 17 and 18.

TABLE 2

Estimated Turbine Performance at
Design Operating Conditions

stage work	32.82 Btu/lb
rotational speed	50,000 rpm
pressure ratio across turbine	
total to total	1.531
total to static	1.577
pressure ratio, flange to flange	
total to total	1.545
total to static	1.556
velocity ratio (actual)	0.697
axial gas velocity to mean blade velocity ratio	0.387
exit axial Mach number	0.187
total-to-total efficiency	86.7 per cent
total-to-static efficiency	81.2 per cent
exit gas angle (mean)	80.0 degrees
hub-tip diameter ratio	0.596
blade root static pressure ratio	1.11
flange-to-flange total-to-total efficiency	84.2 per cent
flange-to-flange total-to-static efficiency	83.3 per cent

B. Stress and Deflection Analyses

The design of the turbine-compressor is based on conservative stresses and deflections in both the rotating and stationary parts to provide a machine with long life potential and with the ability to operate at the small clearances necessary for high aerodynamic efficiency and proper bearing performance. The turbine-compressor is designed to withstand the environments defined by NASA Specification P0055-1 dated July 15, 1963 with ample margin.

The compressor blades are designed with margin. The blades are made of AMS 4928 which is a high strength titanium alloy containing aluminum and vanadium. The centrifugal stresses and unrestrained bending stresses at the design speed of 50,000 rpm are low in respect to the allowable stress of approximately 50,000 psi. The blade stresses are summarized in the following table:

TABLE 3

Compressor Blade Stress Summary

Stage	Unrestored Gas Bending Stress, psi	Centrifugal Stress at 50,000 rpm, psi
1	700	10,000
2	800	10,000
3	600	9,000
4	600	9,000
5	700	9,000
6	700	9,000

The compressor blades are twisted and a centrifugal untwist moment is applied at design conditions. The stresses associated with the untwist are about 5000 psi. The combined blade stresses including the untwisting moment at the design conditions and the 20 per cent overspeed conditions are well below the allowable stress for the titanium alloy.

The blades are retained in the shaft by dovetails as shown in Figure 6. The fifth-stage compressor dovetail is the most critical and the dovetail attachment stresses in this stage are summarized in the following table:

TABLE 4

Dovetail Stresses in Fifth Stage of Compressor

Stress, psi	Allowable Stress, psi	Type
13,000	47,000	combined bending and tensile (blade)
19,000	69,000	max. bearing stress on dovetail shoulder (blade)
4,000	42,000	shearing stress in dovetail (blade)
6,000	58,000	tensile stress in dovetail neck (blade)
6,000	76,000	bending stress in disk lug (shaft)

The compressor blades have a flutter margin in torsion of approximately 2 1/2 and they have about twice this margin in bending. The first, second, and third natural frequencies in bending and the first and second in torsion are summarized in the following table at design speed for the stage indicated. Since Stages 4 and 5 are practically the same as Stages 3 and 6, the natural frequencies of Stages 4 and 5 are not computed. The centrifugal stiffening effects on the natural frequencies of the blades are small.

TABLE 5

Compressor Blade Natural Frequencies at 50,000 rpm

Stage	First Bending, cps	Second Bending, cps	Third Bending, cps	First Torsion, cps	Second Torsion, cps
1	5070	21,900	46,400	12,400	34,900
2	4330	19,600	46,000	14,300	39,500
3	5370	25,500	51,200	15,900	45,000
6	5770	27,700	52,900	15,300	53,500

The blades have natural frequencies removed from major sources of excitation. The major sources of excitation are the four inlet struts and the twelve inlet guide vanes. At design speed the wakes from these members produce some excitation at 3333 cps and 10,000 cps, frequencies well removed from the natural frequency of any of the blades. The stator vanes also produce some excitation. The wakes of the first-stage stators excite the second-stage blades at 16,667 cps and the other blades at this same frequency to a lesser extent. The 24 vanes in the following stages produce wake excitation at 20,000 cps, primarily affecting the third through sixth-stage blades. The airfoils were designed to avoid natural frequencies which correspond to the sources of excitation.

The natural frequencies of the turbine blades are summarized in the following table, and they exhibit very little centrifugal stiffening effect.

TABLE 6

Turbine Blade Natural Frequencies

First Bending, cps	Second Bending, cps	Third Bending, cps	First Torsion, cps	Second Torsion, cps
7250	17,300	29,200	13,200	26,200

The turbine blade natural frequencies are removed from the probable sources of excitation which are associated with the inlet ducting, 833 and 1667 cps, and the nozzle wakes, 25,000 cps.

The turbine disk has been designed to provide low creep in 10,000 hours of operation and to provide ample failure margin. The turbine disk is predicted to yield at a rotational speed above 75,000 rpm and to burst at a speed above 86,000 rpm. An operational condition which might lead to overspeeding the turbine has been examined to determine the possibility of a disk failure. If the compressor became completely unloaded the turbine would probably accelerate the rotor in approximately 1.5 seconds to failure as indicated in Figure 19. The possibility of such a failure is very remote.

The turbine blades and disk are designed to provide low creep rates. In 10,000 hours less than 2 per cent creep is predicted as shown in Figure 20. The possibility of unsymmetric creep exists and a pessimistic estimate of the resulting unbalance indicates that it should be less than 0.002 ounce-inch at the completion of 10,000 hours of operation. The design of the rotor forging requires radial grain orientation in the turbine which should minimize unsymmetric creep, and provide significantly less turbine unbalance at the end of 10,000 hours.

The gooseneck between the Number 2 bearing journal and the turbine disk is designed to limit turbine heat flow into the bearing area and to cause as little centrifugal growth in the journal as possible. Distortion at the bearing end of the gooseneck is 0.00073 inch. However, there is sufficient shaft length between this point and the journal so that distortion becomes negligible in the journal area. Gooseneck stresses are moderate and are listed in the following table:

TABLE 7

Turbine Gooseneck Stresses

Location	Temperature, °F	Bending Stresses at 60, 000 rpm, psi	0.2% Yield Strength, psi
bearing end of gooseneck	320	28, 000	117, 000
turbine end of gooseneck	1030	38, 300	110, 000

Shaft journal growth for the Number 2 radial bearing is given in Table 8.

TABLE 8

Number 2 Bearing Journal Growth

	50, 000 rpm	60, 000 rpm
centrifugal	0. 00059 in.	0. 00085 in.
thermal (70-330°F)	0. 00198 in.	0. 00198 in.
total growth	0. 00257 in.	0. 00283 in.

The journal growth for the Number 1 bearing is given in Table 9.

TABLE 9

Number 1 Bearing Journal Growth

	50, 000 rpm	60, 000 rpm
centrifugal	0. 00019 in.	0. 00028 in.
thermal (70-200°F)	0. 00050 in.	0. 00050 in.
total growth	0. 00069 in.	0. 00078 in.

The heat exchanger under the Number 2 bearing is designed to introduce no journal distortions and to introduce no direct tensile stresses in the braze between the fins and the journal, to assure proper bearing clearance and structural integrity of the heat exchanger-journal bond. The possibility of direct tensile stress in the braze is eliminated by canting the heat exchanger fins as shown in Figure 7. The heat exchanger is made of TD nickel and, at 300°F, has a 0.2 per cent yield strength of 40, 000 psi and an ultimate strength of 50, 000 psi. The silver braze has an ultimate strength of 61, 000 psi at 350°F. The stresses in the Number 2 bearing heat exchanger are summarized in the following table.

TABLE 10

Number 2 Bearing Heat Exchanger Stresses

Speed	50,000 rpm		60,000 rpm	
Location	Fin Root	Braze (Fin Tip)	Fin Root	Braze (Fin Tip)
Nominal Dimensions				
centrifugal stress - psi	15,700	5,960	22,600	8,190
thermal stress - psi	5,900	-2,150	5,900	-2,150
total stress - psi	21,600	3,810*	28,500	6,040*
Minimum Tolerances				
centrifugal stress - psi	25,200	7,400	36,200	10,600
thermal stress - psi	3,700	-1,820	3,700	-1,820
total stress -psi	28,900	5,580*	39,900	8,780*

* Bending stress, no direct tension

The brazing procedure was investigated to determine the correct preparation and temperatures to be used. This investigation showed satisfactory results on laboratory test specimens. A further discussion of this investigation is presented in Appendix 4.

The thrust bearing runner located at the front end of the turbine-compressor rotor is subjected to assembly and operating applied loads which can introduce distortion. The assembly loads are due to the radial snap fit between the runner and shaft and the axial bolt-up load as the runner is secured into the shaft. Operating loads are due to the centrifugal force on the thrust runner, the difference in thermal expansion between the thrust runner and shaft materials (titanium vs Waspaloy) and the axial load on the face of the thrust runner due to the operating thrust load. Dead material is provided and various stiffnesses are designed in the thrust runner to limit distortions. Distortions due to assembly loads (radial snap fit and axial bolt preload) are shown in Table 11. Positive deflection is an axial movement of the tip of the runner rearward (towards the turbine).

TABLE 11

Thrust Bearing Distortion at Assembly

	Assembly Deflections	
	Minimum	Maximum
0.0004 - 0.0006 inch radial snap tightness	0.329 mil	0.493 mil
0.004 - 0.005 inch axial preload (200 - 280 lb preload)	-0.082	-0.115
total assembly deflection	0.214 mil	0.411 mil

Assembly deflections can be inspected with an optical flat.

The distortions during operation are shown in Table 12 and are additive to the total assembly deflection.

TABLE 12

Thrust Bearing Distortion at Operating Conditions

	Operating Deflections	
	50,000 rpm	60,000 rpm
centrifugal	0.064 mil	0.092 mil
radial temperature change (70 to 200°F)	-0.156	-0.156*
axial temperature change (70 to 200°F)	-0.025	-0.025*
15 lb forward rotor thrust	0.020	0.020
total operating deflection	-0.097 mil	-0.069 mil

* Temperatures at overspeed conditions (60,000 rpm) are assumed to be the same as at 50,000 rpm.

The total deflection obtained by adding both assembly and operating deflections falls between 0.117 and 0.314 mils in the rearward direction (toward the turbine). However, an examination of the details of this deflection in the thrust runner shows the largest amount of curvature between the inside radius of the runner and the inside radius of the hydrodynamic bearing. Therefore, less than half of the above distortion is present across the face of the hydrodynamic thrust bearing. This is an acceptable situation for operation of the thrust bearing.

The thrust runner coupling was designed to provide sufficient flexibility in order to minimize distortion due to thermal expansion. A maraging steel was selected for the bolt material to provide a high strength to modulus ratio. Significant stresses in the Number 1 bearing journal and rotating portions of the thrust bearing are summarized in Table 13.

TABLE 13

Significant Stresses in Number 1 Journal and Thrust Bearings

Location	Operating Condition	Stress, psi	Material	0.2 Per Cent Yield Stress psi
heat exchanger fin root	60000 rpm 180°F	49,000 [1]	TD nickel	43,000
heat exchanger braze	60000 rpm 180°F	6,400 [2]	silver braze	64,000
heat exchanger inner ring	60000 rpm 180°F	15,000	TD nickel	43,000
journal	60000 rpm 200°F	15,000	Waspaloy	119,000
thrust runner cylinder	60000 rpm 200°F	65,000	titanium alloy	89,000
coupling bolt read	assembly preload 150°F	191,000	18% Ni maraging steel	244,000

[1] Minimum tolerance, maximum speed condition, 24 per cent ductility available

[2] Bending stress, no direct tension

Stresses throughout the static structure induced by temperature, pressure and assembly loads, are designed at an acceptable level in order to assure the integrity of the turbine-compressor and provide sufficient rigidity to the bearing supports and seals. The highest stresses are located in the flange between the compressor exit scroll and the turbine inlet scroll and are primarily caused by the seal compression requirements. Actually the flange stresses are well below the 0.2 per cent yield strength of the materials and flange loads significantly above the yield strength are permissible. Therefore, there is a significant margin in the flange design. Figure 21 indicates the normal operating temperatures in this area. The circled numbers in this figure indicate the locations of the stresses in Table 14.

TABLE 14

Significant Stresses in the Compressor and Turbine Scroll Area

	Location	Operating Condition	Stress, psi	Material	0.2 Per Cent Yield Strength, psi
1.	compressor scroll vanes	22 psi 340°F	5,700	Inconel 718	143,000
2.	turbine scroll vanes	22 psi 1490°F	6,300	Hastelloy X	25,000
3.	compressor scroll cone	design thermal stress	35,000	Inconel 718	140,000
4.	turbine scroll cone	design thermal stress	39,000	Waspaloy	84,000
5.	compressor scroll flange	seal load	70,000	Inconel 718	128,000
6.	turbine scroll flange	seal load	54,000	Waspaloy	96,000

The compressor exit diffuser wall is designed to introduce a minimum distortion at the bearing supports. Also, the bearing pad support material is selected to match thermal expansion in the bearings. The effects of centrifugal growth on bearing clearance were indicated previously. The bearing clearance changes due to gas pressure are in the order of 0.00003 inch and can be neglected.

The thermal transient conditions in the turbine area have been examined and found to introduce some stresses beyond the yield point of the materials employed. However, there is sufficient ductility to avoid failure. The stresses in the turbine casing during the most severe thermal transient are summarized in the following table. These stresses only occur during rapid startup and shutdown but low cycle fatigue should not be a factor in the anticipated use of this equipment (less than 100 starts).

TABLE 15

Significant Transient Stresses in the Turbine Casing

	Location	Stress, psi	Material	0.2 Per Cent Yield Stress, psi
1.	turbine case	65, 000	Hastelloy X	42, 000
2.	turbine flange	135, 000	Waspaloy	102, 000

The vibrational characteristics of the static structure result in small amplitudes of motion. At the design condition, the deflection at the front and rear bearing supports is about 0. 000001 inch. The resonant frequency, mode shape, and amplitudes of motion of the static structure are presented in Table 16. The

TABLE 16

Vibrational Characteristics of Static Structure

Mode No.	Resonant Frequency, rpm	Mode Shape	Deflection at Resonance for amplification of 20	Location of Deflection
1	3, 000	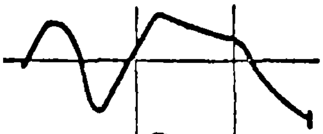	0.22×10^{-4} in	No. 2 Bearing
2	13, 000	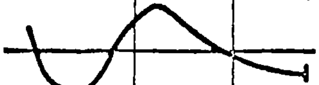	3.0×10^{-4} in	No. 2 Bearing
3	25, 000	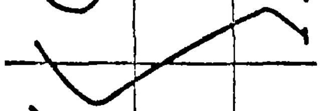	1.04×10^{-4} in	No. 1 Bearing
4	41, 000	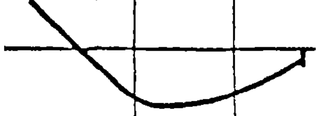	1.06×10^{-5} in	*Turbine Rear Seal
5	63, 000	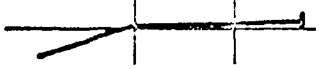	0.58×10^{-5} in	*Turbine Rear Seal

* Deflection at bearings is negligible

resonance with the largest amplitude occurs at 13, 000 rpm and the predicted deflection at this condition is only 0. 0003 inch.

The turbine-compressor is designed to withstand the required launch environmental conditions. However, practically no data is available on the ability of the gas bearings to survive the shock and vibration environments. The launch, lift-off and boost condition represent the most severe shock and vibration conditions. A test program is recommended to determine the capability of the gas bearings under the anticipated environments. If the bearings prove to be unsatisfactory when subjected to these conditions, one of two approaches can be taken: (1) shock mount the machinery, or (2) restrain the rotor in the inoperative condition. The rest of the static and rotating structure is designed to be capable of meeting the requirements. Therefore, shock mounts do not appear necessary.

C. Rotor Dynamics and Gas Bearing Designs

The rotor of the turbine-compressor weights 10. 64 pounds and its center of gravity is located 6. 82 inches from the centerline of the front radial bearing. The rotor mass distribution is shown in Figure 22. The total polar moment of inertia is 0. 308 in-lb-sec^2 with the distribution shown in Figure 23. The transverse moment of inertia about the center of gravity is 0. 605 in-lb-sec^2.

The free-shaft critical speed of the rotor is 88, 000 rpm, a value which provides ample margin over the design speed of 50, 000 rpm and the operating overspeed of 60, 000 rpm to limit the shaft distortion due to dynamic forces. The rotor response at 50, 000 rpm for 0. 002 ounce-inch of unbalance in the turbine wheel is predicted in Figure 24. The rotor must pass through rigid-body critical speeds at about 11, 000 and 12, 000 rpm when accelerating to design conditions. Since these two critical speeds are primarily dependent on the gas bearing characteristics, they are discussed further in Volume 2 (report CR-801).

The detailed gas bearing designs and test program are presented in Volume 2 of this report. That volume also includes the determination of the radial bearing loads experienced in supporting the rotor weight of 10. 64 pounds, both in the rotor vertical position (zero g condition for the journal bearings) and in one horizontal attitude.

The aerodynamic thrust load when the unit is operating at the design point in the horizontal attitude (zero g condition for the thrust bearing) is 15 pounds towards the compressor inlet. The unit is also required to operate vertically with the compressor inlet up, in which case the net rotor thrust at the design point is approximately 4 pounds towards the compressor inlet.

The aerodynamic thrust during startup and shutdown is difficult to predict, in fact the thrust direction may be reversed during part of the acceleration, depending on the method of starting. Transient thrust loads of 100 pounds in the forward direction and 50 pounds in the reverse direction were selected as design requirements. Additional design requirements for the bearings were:

1) Stable operation at any ambient pressure above 12 psia,
2) Stable operation with an unbalance of 0.002 ounce-inch in the plane of the turbine wheel, and
3) Ability to withstand vibrational and thermal transients during startup and shutdown.

Only limited technology was available for the design of gas bearings to operate satisfactorily under these conditions for the 10,000-hour planned mission. Pivoted-pad flexure-mounted journal bearings were selected with hydrodynamic lift-off, and a hydrodynamic spiral-groove main or forward thrust bearing with hydrostatic lift-off. The hydrostatic reverse thrust bearing is needed only during startup or shutdown and has no hydrodynamic capability. The bearing designs, the data for which is listed in Table 17, include the following features:

1) Four 80 degree arc pads with provision to adjust pivot radial position
2) chrome oxide as the surfacing material
3) hydrodynamic lift-off of journal bearings
4) startup thrust loads supported by a hydrostatic bearing built into a spiral-groove self-acting thrust bearing
5) internally-brazed axial-finned nickel heat exchangers to remove journal bearing friction heat
6) liquid-cooled aluminum thrust stator
7) titanium thrust runner
8) miniaturized capacitance probes embedded near the pivot to measure journal pad-to-shaft film thickness and
9) capacitive probes to measure pad and shaft dynamic behavior.

The initial design, whose parameters are listed in Table 17, was based on conservative design practice to assure that the bearing system would operate adequately. After early successful operation was demonstrated, the initial design was modified to reduce friction power loss and increase bearing tolerance for transient thermal differentials. The result was the final design whose parameters are also listed in Table 17.

A set of pivoted pads for the front journal bearing is shown in Figure 25. Figure 26 shows the flexures with high spring rate used in each journal bearing of the initial design. Figure 27 shows the flexures with low spring rate used at the two upper pad locations at each journal bearing in the final design. Figure 28 shows the rear journal bearing with the journal removed as it was installed in the dynamic simulator. The front journal bearing support and reverse thrust stator is shown in Figure 29.

TABLE 17

Turbine-Compressor Gas Bearing Design Parameters and Calculated Performance Characteristics

All data given below is based on the following gas-bearing operating conditions

rotor speed	50,000 rpm
lubricant gas	argon
bearing-cavity ambient pressure	12.0 psi

Journal Bearing

	Initial Design	Final Design
configuration	pivoted-pad (with hydrodynamic lift-off)	pivoted-pad (with hydrodynamic lift-off)
journal diameter, inches		
No. 1 (forward) bearing	1.500	1.500
No. 2 (turbine end) bearing	2.125	2.125
bearing length-to-diameter ratio (L/D)		
No. 1 bearing	1.0	1.0
No. 2 bearing	1.0	1.0
number of pads per bearing	4	4
pad orientation (with reference to horizontal orientation of the rotor)	rotor weight between pivots	rotor weight between pivots
arc length (θ) of pad, degrees	80.0	80.0
pivot location (β / θ) from leading edge	0.65	0.65
pad clearance ratio (C_p/R)		
No. 1 bearing	0.0010	0.0018
No. 2 bearing	0.0010	0.0030
pivot ball diameter, inches		
No. 1 bearing	0.2500	0.2500
No. 2 bearing	0.3750	0.3750
pivot socket diameter, inches		
No. 1 bearing	0.2550	0.2550
No. 2 bearing	0.3824	0.3824
bearing number (Λ)		
No. 1 bearing	10.7	2.98
No. 2 bearing	11.5	1.23

TABLE 17 (Cont'd)

Journal Bearing

	Initial Design	Final Design
measured pivot support radial stiffness, lb/in		
No. 1 bearing	50,000 (all pads)	9,800 (upper pads) 50,000 (lower pads)
No. 2 bearing	70,000 (all pads)	8,400 (upper pads) 70,000 (lower pads)
bearing load, pounds		
horizontal orientation (rotor weight)		
No. 1 bearing	3.63	3.63
No. 2 bearing	7.72	7.72
space operation (due to 0.002 ounce-inch of mass unbalance in turbine plane)		
No. 1 bearing	1.01	0.38
No. 2 bearing	1.67	1.23
operating clearance at pivot, inches		
horizontal orientation (loaded pads)		
No. 1 bearing	0.00033	0.00057
No. 2 bearing	0.00046	0.00058
space operation (all pads)		
No. 1 bearing	0.00037	0.00067
No. 2 bearing	0.00053	0.00067
friction loss per journal, watts		
horizontal orientation		
No. 1 bearing	110.5	57.4
No. 2 bearing	336.0	235.8
space operation		
No. 1 bearing	109.0	56.5
No. 2 bearing	331.0	232.5
radial gas-film stiffness, lb/in		
horizontal orientation		
No. 1 bearing	73,000	34,400
No. 2 bearing	104,100	75,000
space operation		
No. 1 bearing	70,940	33,100
No. 2 bearing	100,900	72,200
gas film temperature, °F		
No. 1 bearing	213	175*
No. 2 bearing	376	310*

TABLE 17 (Cont'd)

Journal Bearing

	Initial Design	Final Design
shaft temperature, °F		
No. 1 bearing	192	165*
No. 2 bearing	342	285*
pad temperature, °F		
No. 1 bearing	213	175*
No. 2 bearing	377	310*
shaft material	Waspaloy	Waspaloy
pad material	M-1 tool steel	M-1 tool steel
pivot material	M-1 tool steel	M-1 tool steel
journal and pad surfacing material	chrome oxide	chrome oxide

Forward Thrust Bearing

	Initial Design	Final Design
configuration	spiral groove with hydrostatic lift-off	spiral groove with hydrostatic lift-off
thrust plate diameter, inches	3.25	3.25
spiral-groove bearing O.D., inches	3.25	3.25
spiral-groove bearing I.D., inches	1.38	1.38
groove depth, inches	0.002	0.002
number of grooves	20	20
design load (aerodynamic) for spiral-groove bearing, pounds**	15	15
operating clearance of spiral-groove bearing, inches	0.00095	0.00095
friction loss at design load, watts	108.0	108.0
orifice diameter, inches	0.040	0.040
number of orifices	20	5
hydrostatic gas supply pressure at start up, psia	100.0	100.0
hydrostatic bearing load at startup, pounds	100.0	100.0
hydrostatic film clearance at startup, inches	0.0015	0.0008
stator support stiffness in axial direction, lb/in	670,000	670,000

TABLE 17 (Cont'd)

Forward Thrust Bearing

	Initial Design	Final Design
stator support stiffness in tilt direction, in-lb/rad	34,200	34,200
stator temperature, °F	175.0	175.0
runner temperature, °F	216.0	216.0
runner material	titanium	titanium
stator material	AMS-4027 (aluminum)	AMS-4027 (aluminum)
stator and runner surfacing material	chrome oxide	chrome oxide

Reverse Thrust Bearing

	Initial Design	Final Design
configuration	hydrostatic	hydrostatic
orifice diameter, inches	0.040	0.040
number of orifices	15	15
supply gas pressure, psia	100.0	100.0
design load, pounds	50.0	50.0
hydrostatic clearance at startup, inches	0.0013	0.0013
stator material	AMS-6415 (steel)	AMS-6415 (steel)
stator surfacing material	chrome oxide	chrome oxide

* Final journal bearing temperatures are based on same cooling gas-flow as the initial design. However, further thermal investigations are required as discussed in the next section of the report.

** The hydrodynamic thrust bearing was designed to support a design thrust load of about 25 pounds which corresponds to the unit operating vertically with the compressor inlet down. However, this requirement was later cancelled but the thrust bearing design was not changed.

D. Thermal Analysis

The turbine-compressor design is based on steady-state and transient thermal analyses of critical areas. The thermal conditions within the unit determine the basic clearances of blade tips, seals, and bearings as well as providing a basis for material selection. The heat generated in the bearings must be removed to limit the bearing operating temperatures and to control the bearing clearances. Of course, this requirement is common to practically all bearing systems. There are three methods of removing heat which are usually considered:

1) conduction to an environmental heat sink
2) forced convection by a circulating lubricant
3) forced convection by another cooling fluid

All of these techniques were examined for the turbine-compressor application. Since the journal bearing between the compressor and the turbine is in the most severe thermal environment and since this bearing has the highest predicted heat generation, the heat removal from this bearing will be discussed here.

The bearing cooling requirements are determined by the selection of the bearing design and the design of the bearing environment. The bearing mount is located on the compressor discharge duct and the compressor discharge gas temperature is about 350°F. The shaft between the bearing and the turbine is reduced in cross-section to limit the heat conducted from the turbine to the bearing area. Since the gas pressure at the exit of the turbine nozzle is lower than the compressor exit pressure, some argon flows through the bearing compartment from the compressor to the turbine, but this flow is limited by labyrinth seals. This leakage gas cools the shaft between the bearing and the turbine to aid in the thermal isolation of the turbine. In addition to the requirements imposed by the design, bearing thermal design objectives were also chosen including a maximum bearing operating temperature of 400°F.

In an effort to find a simple low-loss heat-rejection system, the possibility of removing the heat generated in the bearing by the gas leaking from the compressor to the turbine, coupled with heat conduction from the bearing along the shaft into the argon in the compressor, was examined. The resulting maximum bearing temperature was between 800 and 900°F and obviously unsatisfactory. In order to improve the shaft conduction, silver was added to the bore of the shaft. In an effort to improve the gas cooling, the labyrinth seal clearances were enlarged to permit a larger leakage flow. This configuration had a reasonably uniform temperature distribution but the maximum temperature of the bearing was 670°F and the design was considered unsatisfactory.

Evidently, additional cooling is required and since liquid cooling is used elsewhere in the powerplant, it was considered for this application. A stationary cooling jacket was designed to encase the bearing and the shaft in the immediate area of the bearing. Since the bearing shoes and the shaft must be free to move, a clearance of 0.010 inch was provided between the jacket and the bearings. The clearance space was filled with argon at compressor discharge pressure, which provided the bearing lubricant. The gas clearance space also represented a thermal barrier and the resulting temperature of 615°F did not meet the design criteria. Adding silver to the bore of the shaft to improve the conduction improved the bearing temperature to 470°F but the liquid jacket and silver in the bore were not sufficient to meet the objectives. Instead of adding silver in the shaft, a stationary cooling plug was added in the shaft inside the bearing. Because of the tolerances and the thermal expansions during transient operation, a gap of 0.025 inch was used between the plug and shaft. The liquid-cooled jacket on the outside of the bearing and liquid-cooled plug on the inside of the shaft did not provide a satisfactory bearing temperature.

In order to use liquid cooling effectively, it should be introduced as close to the source of heat generation as possible. Therefore, liquid cooling directly in the pads was examined. The net result was excellent. With liquid flowing through the pads at about 310°F, the bearing operated at 350°F. This approach is very satisfactory except for one factor. In a tilting-pad bearing the pads must be free to move. Restraint of the pads can lead to unstable operation of the rotor system. The basic bearing system design philosophy for this unit was to employ established practice as much as possible. Since liquid-cooled pads had not been demonstrated experimentally and since the liquid lines would introduce pad restraints, the liquid-cooled pad concept was rejected for the radial bearings.

As the liquid cooling results demonstrated, the coolant should be introduced as close to the heat source as possible. A gas-cooling system was examined in which the gas was introduced in heat exchangers in the shaft to effectively remove the bearing heat generation in the journals. The cooling flow path is shown in Figure 12.

About 3.8 per cent of the cycle flow is bled from the compressor discharge and cooled in an external heat exchanger to 100°F. This bleed flow is introduced to the center of the shaft through struts in the inlet section. The cooling gas passes through a finned heat exchanger under the Number 1 bearing journal, down the shaft and back through a finned heat exchanger in the shaft under the Number 2 journal. The cooling gas passes out through radial holes in the shaft forward of the Number 2 bearing, passes over the Number 2 bearing pads, and then splits in three directions. Approximately 1.32 per cent of the cycle flow passes through a seal and up the front face of the turbine and 1.54 per cent is returned through metering holes in the shaft to the cavity behind the turbine and enters the main stream through the rear turbine seal. The remaining 0.92 per cent is piped from the area between the scrolls to the Number 1 bearing area where it pressurizes the bearing and controls the temperature of the bearing support. This portion of the cooling gas leaks through the labyrinth seal at the front of the compressor. Therefore cooling gas is used for three purposes in this design: 1) to cool the journal areas, 2) to provide the seal leakage flow, and 3) to provide the gas for the bearings at proper pressure. The system provides a fairly uniform temperature distribution in the bearing and provides bearing operating temperatures within the design objectives. This type of bearing cooling has been successfully applied to other gas bearing applications and has been selected as the basis for this design.

A detailed thermal map of the Number 2 bearing area at design operating conditions is presented in Figure 30. The bearing design operating temperature is about 350°F. In the selection of the design configuration various methods of reducing heat generation were considered, including a larger bearing clearance and a smaller diameter. The smaller diameter adversely affects shaft stiffness and the bent-shaft critical speed. A larger bearing clearance was analyzed and tested which resulted in a reduction in power loss in the Number 2 bearing from 340 to 240 watts. Further reduction of the power loss by increasing the operating clearance caused rotor whirl, as discussed in Volume 2 (report CR-801). The predicted thermal map at the reduced power loss for this bearing is shown in Figure 31. This bearing operates at about 300°F if the initial design coolant system and cooling gas flow rates are retained.

The detailed thermal map of the Number 1 bearing (initial design) and thrust bearing is presented in Figure 32 at design operating conditions. Figure 33 shows the thermal conditions in the Number 1 bearing with the larger clearance if the initial design coolant system and cooling gas flow rates are retained. Heat is generated in the journal bearing and on both sides of the thrust bearing. The radial bearing is cooled by the argon which flows through a heat exchanger in the journal before it flows to the Number 2 bearing area. The Number 1 bearing support ring is located by three pilots on the compressor inlet case under the guide vanes. In order to produce the desired thermal conditions in the Number 1 bearing area, warm gas is ducted through the guide vanes to the bearing support ring and then it leaks through the labyrinth seal. This small bleed flow is taken from the Number 2 bearing compartment after it has cooled the Number 1 and Number 2 bearings and provides the labyrinth leakage at the inlet of the compressor rotor. Therefore, this arrangement does not require any additional bleed flow from the system. The Number 1 bearing support system does not impose a severe thermal gradient on the wall of the compressor duct. Figure 34 presents a thermal map of the compressor inlet inner wall which includes one of the three Number 1 bearing support ring pilots.

While the final-design journal bearings will operate satisfactorily at the design operating point with thermal conditions as shown on Figures 31 and 33, the rear journal would require negative zero-speed room temperature setup clearance. To permit practical setup clearance, it has been determined that the steady-state design-point rear journal and pad temperatures will have to be increased to 400°F and 425°F respectively. The design has not been revised to accomplish these temperatures; however the probable solution is to reduce the cooling gas flow through the rear journal heat exchanger by adding metering holes in the rear shaft plug. The turbine disc rear labyrinth seal flow shown on Figure 12 can then partially or totally bypass the heat exchanger.

Gas cooling of the thrust bearing was examined and found to be inadequate to minimize thermal distortions. A number of thrust bearings have demonstrated satisfactory performance with restraint of the stationary member introduced by the support system. Since the liquid lines would not appreciably increase this restraint, liquid cooling has been selected for the thrust bearing. Versilube F-50 was assumed to be the heat transfer medium as requested by NASA although the liquid coolant system can accommodate glycol. Thrust bearing liquid coolant performance data is shown in Figure 35. With the unit running at design conditions and with a coolant flow of 200 lb/hr of Versilube F-50, the pressure drop through the thrust stator is 8 psi, the coolant temperature rise is 9°F and the mean coolant-to-metal temperature difference is 28°F. As shown in Figure 35 the liquid coolant enters the aluminum thrust bearing stator through one inlet and flows in two streams circumferentially 180 degrees where the two streams combine. The flow travels again in circumferential grooves 360 degrees and exits from the stator at an outlet located diametrically opposite to the inlet. The inlet and outlet coolant fittings are located opposite to each other, to prevent unsymmetrical restraint of the thrust stator by the coolant tubes.

The overall temperature map of the turbine-compressor is shown in Figure 36.

Journal bearing clearances depend on maintaining nearly isothermal conditions in the shaft, pads and support for the initial bearing design because of the relatively small flexibility of the bearing support. Transient thermal analysis of the Number 2 bearing shown in Figure 37 indicates that these components are not completely isothermal during a rapid startup. However, the journal bearing spring mounts will partially compensate for the more rapid thermal growth of the shaft. Electric heaters are provided on the forward and rear diffuser walls of the compressor to permit adjustment of the bearing clearance during transients for various startup rates and to correct anomalies not predicted because of the complex nature of the transient. The heater capacities are sufficient to control the rate of change of the bearing clearance for a step change in rotor speed from zero to 50,000 rpm. The proper amount of heater operation is dependent on the startup process used, and is established during the test program. The temperature band shown in Figure 37 is the required diffuser temperature for bearing clearance control with the forward and rear diffuser walls at the same temperature. The allowable clearance variation represented by the limits of the temperature range is ±0.00015 inch. No deflection of the bearing flexure is assumed for conservative limits. The flexure would permit double the temperature range shown. The Number 1 bearing support is also provided with an electric heater to adjust the bearing clearance during the startup transient. The heater capacity is sufficient to control the bearing clearance for an extreme startup rate and the proper heat rate is dictated by the startup rate desired during the test program. Figure 38 shows the thermal response of the components of the Number 1 bearing during a rapid startup process. The temperature range shown in Figure 38 is the required support ring temperature for a bearing clearance control of ±0.00011 inch. Because flexure operation was neglected in setting the temperature range, the temperature band width shown is about half the allowable range for the initial design.

The thermal transient response of the journal bearing systems has been significantly changed by the larger bearing clearances and the lower springrate flexures. The lower power loss associated with the increased radial clearance decreases the rate of temperature rise of the journals. The larger radial clearance and the reduction of stiffness of the upper flexures permit larger mismatches of journal and bearing support temperatures, while maintaining reasonable bearing clearances. Shaft-to-housing mismatches of plus* 94°F to minus 105°F for the front bearing and plus 46°F to plus 226°F for the rear bearing can be accommodated. The system flexibility should control the various temperatures within the acceptable variations during startup and shutdown.

A detailed analysis of the distortion of the turbine-compressor thrust runner during a rapid startup was conducted and the distortion was found to be acceptable. For this analysis, a step increase in speed from zero to 50, 000 rpm was assumed, and the operating thrust used is that produced during vertical operation with the thrust bearing on the bottom so that the results would be conservative. The effects of introducing liquid coolant into the thrust stator during starting and the influence of electrical heat input in the Number 1 journal bearing mount ring were evaluated. The distortion of the thrust runner is an axial motion of the outer portion in the downstream direction. A deflection of 0. 00032 inch occurs with the use of liquid coolant in the thrust stator and heat input to the Number 1 journal bearing support ring. A deflection of 0. 00034 inch occurs without coolant flow and without heat input to the Number 1 journal support ring. However, the deflection is reduced 33 per cent by supplying cooling a short period after starting has been initiated. The transient temperatures produced with no coolant flow and with no electrical heat input to the Number 1 journal bearing support ring are shown in Figure 39. The corresponding temperatures produced with coolant flow and with electrical heat input are shown in Figure 40. Figure 41 shows the transient bearing temperatures produced by delaying the coolant flow until after the initial period of startup. As a result of these studies, the maximum deflections predicted for the thrust runner during a rapid start with the system oriented horizontally is between 0. 00023 and 0. 0001 inch, depending on the use of electrical heat input to the Number 1 journal bearing mount ring. These deflections are produced by initiating the liquid coolant flow about one minute after a rapid startup. These deflections are acceptable since the thrust bearing operating clearance is 0. 001 inch with the unit operating in the horizontal position.

---

* A plus temperature difference means a shaft temperature higher than the bearing mount temperature

The thermal transient behavior of the turbine and the support between the turbine and compressor scrolls is shown, respectively, in Figures 42 and 43 for a rapid start with full design turbine inlet temperature and pressure. The most highly stressed area is the diaphragm between the mount ring (point 3) and the turbine scroll (point 1) in Figure 43. This thermal gradient will cause about 1 per cent yield in the diaphragm during a rapid start. However, the diaphragm is fabricated of Waspaloy which has sufficient ductility and low cycle fatigue should not be a problem for at least 300 start cycles. The turbine blade tip cold clearance (0.020 inch) and seal clearance (0.010 inch) are selected to permit rapid starting based on these transient results.

Compressor blade tip cold clearance (0.007 inch) and seal clearance (0.006 inch) include provision for full temperature in the rotor and ambient temperature in the compressor case. Axial growth of the rotor and static structure is provided for in the axial clearance (0.055 inch) between blades and vanes.

E. Material Selection

The turbine-compressor materials were selected to provide high integrity for a 10,000-hour mission and to withstand the handling and storage environments. Materials were employed which have long and successful records in aircraft gas turbine service. Also, stainless materials were included where possible, to prevent corrosion in storage and handling.

The most complex single part in the turbine-compressor is the shaft with integrally-machined turbine blades. Since the turbine blades are stressed and in a high temperature environment PWA-1007 Waspaloy was selected for this part.

Laboratory stress rupture and creep strength data are generally limited to 1,000 hours or less and standard procedures for extrapolating this data to longer times, such as 10,000 hours, are to use the Larson-Miller extrapolation method. Field experience on jet engine blades of Waspaloy, however, indicates that this method of extrapolation is optimistic. Examination of long-time blades used in jet engines indicates that lower stress rupture and creep strengths are obtained than would be expected by use of the Larson-Miller method. When exposed to high temperatures for long times, Waspaloy, like any high temperature precipitation hardening alloy, will overage which is not in itself necessarily harmful but does result in a reduction of strength. In setting allowable stresses for the Brayton-cycle turbine this reduction in strength due to overaging has been taken into account. As can be seen in Figure 20, the resulting allowable stresses are still appreciably above calculated centrifugal P/A stresses, indicating that the Brayton-cycle turbine should have a high degree of reliability for 10,000 hours of life. In predicting blade life and safety margins, only the centrifugal P/A stress was considered, because gas and centrifugal bending stresses are small and with time would be reduced further by local creep.

Of course, there are several major differences between the environmental conditions for the Brayton-cycle turbine blading and jet engine blading which indicate that the design approach for the turbine-compressor is conservative. The Brayton-cycle turbine operates in an inert atmosphere, at constant temperature, with a uniform inlet temperature distribution spanwise.

AMS 5382 (X-40) cobalt-base alloy was chosen as the turbine vane material. In addition to its corrosion resistance, the alloy was chosen for its extremely good castability which permits better control of trailing edge thicknesses. Pratt & Whitney Aircraft has used this alloy successfully as a turbine blade and vane material for over 14 years.

The compressor blades are of AMS 4928 titanium to reduce the rotating mass and to reduce unbalance due to difference in blade weight. This is an alpha-beta (Ti-6Al-4V) alloy used in the annealed condition by Pratt & Whitney Aircraft. Its general corrosion and oxidation resistance are excellent to 900°F. This material as JT4(J75) compressor blading has accumulated more than 6 million hours of military and commercial flight time.

The compressor blades are retained by pinning with AMS 4500 or AMS 4701 commercially pure copper pins. An alternate material, soft aluminum, presents a possible galvanic corrosion problem in an air environment with an electrical potential difference between it and titanium.

The compressor diffuser is fabricated of PWA 1009 (Inconel 718) to match the thermal expansion coefficient of the shaft. Although Inconel and Hastelloy X would have been adequate from the standpoint of corrosion resistance and general strength, the necessity for high strength in the threaded areas precluded their use. Strength comparison of these alloys is shown below:

	UTS	0.2% YS	ELONG. (%)
Inconel	70, 000 min.	30, 000 min.	10 min. (spec.)
Hastelloy X	65, 000	45, 000	15 (typical)
Inconel 718	125, 000 min.	110, 000 min.	5 min. (spec.)

Inconel 718 is a precipitation-hardenable nickel-base alloy with a composition which imparts sluggishness in the hardening reaction, allowing traversing of the hardening temperature range without sudden local changes in structure that could cause cracking. Extensive testing and experimental use has shown the alloy to be stable to about 1200°F and well suited for use in low and intermediate temperature assemblies. A major virtue of Inconel 718 is its excellent weldability by virtue of its low susceptibility to cracking. In addition, it is brazeable.

The compressor inlet case is fabricated of AMS 5665 Inconel with AMS 5646 (AISI 347) stainless steel vanes. Inconel is a nickel-base alloy, richly alloyed primarily with chromium. It is nonhardenable by heat treatment and is used in the solution heat-treated (annealed) condition. Yield strength of the alloy (30, 000 psi minimum at 70°F) is retained at temperatures up to about 1100°F. Fabricability is similar to that of the austenitic stainless steels. Oxidation resistance is superior to that of the austenitic stainless steels but slightly inferior to that of Hastelloy X. AMS 5645 (AISI 321) and AMS 5646 (AISI 347) stainless steels were chosen for the inlet case vanes, nosecone and various bosses, rings and fittings. These are highly corrosion resistant, austenitic type stainless steels which can be used advantageously where high expansion and low strength (approximately 30, 000 psi min. 0. 2 per cent yield strength at 70°F) are not deterrents. They are easily welded and brazed and require at most only a simple stress relief after welding.

The compressor stators are brazed assemblies consisting of Inconel (AMS 5665) vanes and inner shrouds and Hastelloy X (AMS 5754) outer shrouds. The assemblies are low temperature silver (AMS 4773) furnace-brazed. Inconel was originally chosen for the outer shroud but higher strength requirements in the threaded areas necessitated use of a stronger alloy. Since Hastelloy X was considered an adequate improvement over Inconel for this application, it was chosen over Inconel 718, due to greater ease of fabrication.

The turbine inlet duct, scroll and exit diffuser are Hastelloy X. Hastelloy X is a nickel-base alloy, richly alloyed primarily with chromium. It is essentially nonhardenable by heat treatment and is normally used in the solution heat-treated condition. Yield and rupture strengths are superior to those of Inconel. Oxidation resistance is outstanding at temperatures up to 2200°F and is superior to that of Inconel.

The turbine shroud flange is machined from PWA-1010 (Inconel 718) because of the high-temperature high-strength requirement for rapid startup and shutdown.

F. Recommendations on Provisions to Install Instrumentation

The aerodynamic instrumentation for the turbine-compressor research package is to be essentially the same as that suggested for the inlet and exit of the turbine research package and the compressor research package, so that performance figures are as nearly comparable as possible. Interstage instrumentation, scroll static pressure taps, traverse bosses, and other internal aerodynamic instrumentation are not suggested for the turbine-compressor combined unit.

Compressor

Inlet (plane located upstream of four front struts) - Three total pressure probes and three half-shielded thermocouple probes installed in the gas stream midway between the walls.

Scroll Exit - (upstream of flange)

1) Two total pressure rakes with three taps per rake,
2) Two total temperature rakes with three taps per rake, and
3) Four static pressure taps.

Turbine

Scroll Inlet - (downstream of flange)

1) Two total pressure rakes with three taps per rake,
2) One total temperature rake with three thermocouples per rake, and
3) Four static pressure taps.

Exit - (plane of three rear struts)

1) Three total pressure rakes with three taps per rake,
2) Three total temperature rakes with three thermocouples per rake, and
3) Three static pressure taps.

It is recommended that thermocouples be located at various points of the static structure where variation from the calculated thermal map could affect bearing operation, running clearances, or internal stresses. At the front bearing location, two 36-pin connectors (18 thermocouples each) can be included, as shown on Figure 2, to measure temperatures in the front journal and thrust bearing area, as follows:

Quantity	Location
4	radial gradient around forward thrust stator support
4	radial gradient around rear face of reverse thrust bearing stator
2	on No. 1 journal bearing support
8	on No. 1 journal bearing pads
6	radial gradient around inner surface of inlet case inner wall
12	spare

At the rear bearing location, two 36-pin connectors can be incorporated to connect the following internal thermocouples:

Quantity	Location
8	on No. 2 journal bearing pads
2	inside mount ring between the two scrolls
8	radial and circumferential gradient on rear wall of compressor diffuser
6	radial and circumferential gradient on turbine inlet heat shield
5	radial and circumferential gradient on front wall of turbine inlet
7	spare

Separately connected external thermocouples are recommended as follows:

Quantity	Location
8	radial and circumferential gradient around front wall of compressor diffuser
4	circumferential gradient around rear wall of turbine inlet

Quantity	Location
2	turbine casing in plane of rotor
8	circumferential and axial gradients of turbine exhaust case

The recommended rotor dynamic behavior instrumentation and speed instrumentation is as follows:

Thrust Bearing and Journal Bearing No. 1

Position	Purpose	Number of Sensors
thrust bearing ground to thrust stator	dynamic movement of stator	1
thrust bearing bearing to runner	thrust bearing film thickness (Figure 10)	3
reverse thrust bearing ground to runner	reverse thrust bearing film thickness (Figure 29)	3
shaft ground to shaft	dynamic movement of shaft	2 at 90 deg.
pad pad to shaft	film thickness between each pad and shaft (Figure 25)	4 at 90 deg.
pad flutter ground to back of pad	pad flutter in pitch direction (unloaded pad)	1
pad flutter ground to back of pad	pad flutter in roll direction (unloaded pad)	1

These probes are also used as speed pickups. This can be achieved by a small interruption on the surface of the thrust runner and proper treatment of the resulting signals.

Journal Bearing No. 2

Position	Purpose	Number of Sensors
pad pad to shaft	film thickness between each pad and shaft	4 at 90 deg.
pad flutter pad to shaft	dynamic movement between pad and shaft in roll direction (unloaded pad)	1
shaft ground to shaft	dynamic movement of shaft (Figure 28)	2 at 90 deg.
pad flutter ground to back of pad	pad flutter in the pitch direction (unloaded pad) (Figure 28)	1

It is recommended that various pressures and temperatures of coolant flows, bearing compartments, and areas critical to the thrust balance be measured. One thermocouple or pressure tap at each of the following locations is recommended. Unless otherwise specified the instrumentation is located in plumbing external to the turbine-compressor research package.

1) Temperature of liquid coolant to thrust stator
2) Pressure of liquid coolant to thrust stator
3) Temperature of liquid coolant from thrust stator
4) Pressure of liquid coolant from thrust stator
5) Pressure of jacking gas to hydrostatic thrust bearing
6) Temperature of gas coolant bled from compressor discharge
7) Pressure of gas coolant bled from compressor discharge
8) Temperature of gas coolant fed to front struts
9) Pressure of gas coolant fed to front struts
10) Pressure at front compartment pressure regulating bleed
11) Temperature of gas used to heat front bearing support ring
12) Pressure of gas used to heat front bearing support ring
13) Pressure in rear journal bearing compartment-install fitting in one bearing adjustment access plug
14) Pressure in compartment behind turbine disc-redesign struts in turbine exit plane to thicken airfoil and drill hole radially through vane

IV. SUMMARY OF GAS BEARING DYNAMIC SIMULATOR TESTING

A test program was set up with the following objectives:

1) to evaluate the rotor-bearing and coolant systems under the predicted turbine-compressor operating conditions,
2) to identify and correct any problems,
3) to reduce bearing power loss, and
4) to decrease flexure spring rate and provide greater transient thermal tolerance.

A rotor system dynamic simulator was built to duplicate the turbine-compressor rotor mass, distribution of mass and stiffness, and the transverse and polar moments of inertia of the rotor. The bearings and method of support were substantially the same as those designed for the turbine-compressor research package. Figure 44 shows the simulator mounted in the two attitudes to be tested. Figure 45 shows the internal configuration of the simulator. The shaft included an integral impulse drive turbine, journal bearing heat exchangers, and balance provisions as shown in Figure 46.

Figure 47 shows the simulator mounted for test behind the control panel and instrumentation readout equipment is shown on Figure 48. Shop air or bottled nitrogen were used to drive the turbine. A vacuum pump was used to reduce bearing ambient pressures to the test levels. Filtered shop air or argon were used to supply the bearings. Filtered shop air was used in the thrust loading chambers. Speed was controlled by turbine inlet pressure and measured by magnetic speed pickup which received its input from six slots machined in the shaft, where the second-stage compressor blades would be located in the turbine-compressor research package.

Thermocouples on the bearings and bearing mounts were recorded sequentially on a strip chart potentiometer. Signals from the capacitance proximity probe were displayed on oscilloscopes after being conditioned in Wayne Kerr or Microdyne distant-measuring equipment. The Microdyne console, three of which can be seen in Figure 48, is an integrated system including improved stability, switching, and readout equipment to facilitate data presentation in various forms. The ground-to-shaft probes, spaced 90 degrees apart at each journal, are displayed on the X and Y axes of a dual-beam oscilloscope, as shown in Figure 49. The large squares in the four views represent the maximum displacement of the journal when rotated against the pads manually. The corners of the square are located midway between adjacent pivots. Probes other than the ground-to-shaft type are displayed versus a time scale as shown on Figure 50.

The initial bearing design was tested in the simulator as outlined in Table 18. The bearing and cooling systems operated satisfactorily with one exception. Pneumatic hammer occurred in the forward hydrostatic thrust bearing and was quickly eliminated by reducing the number of jacking gas supply orifices.

To reduce the bearing friction power loss and to decrease the journal bearing radial stiffness, the bearings in the simulator were revised by:

1) Increasing the machined clearance ratio of the front and rear journal bearings from 0.001 to 0.0018 and 0.003 inch respectively. This permitted use of an increased running clearance, upon which power loss is strongly dependent.
2) Decreasing the springrate of the upper flexures of the front and rear journal bearings from 50,000 and 70,000 pounds per inch to 9,800 and 8,400 pounds per inch respectively.
3) Adding weights to the rear bearing pads, as shown on Figure 51, to lower the pad natural roll frequency.

The test program as outlined above the dashed line in Table 18, plus a thermal test using argon with one cooling gas flow rate was completed. However, rotor instability at the rear journal bearing prevented operation at full desired diametral clearance, which was 0.00317 inch as compared to 0.00088 inch for the initial design. The maximum diametral clearance attained was 0.0021 inch when operating at 50,000 rpm in air at a bearing ambient pressure of 14.7 psia. At these conditions the rotor developed a whirl motion with a frequency of approximately 125 cps. The whirl amplitude increased with bearing clearance. The tests were completed at a diametral clearance of 0.0017 inch using argon at 12 psia in the bearing compartments, without encountering whirl.

A third series of tests was run to establish the design clearance for the rear journal bearing that would minimize the friction power loss and, at the same time, assure whirl-free operation over the entire spectrum of anticipated operating conditions. The only change made to the bearing parts was the removal of the weights from the rear journal bearing pads. Since the bearing would be operating at reduced clearance and thus at greater film stiffness, the roll natural frequency of the light pad was predicted to be above the design speed as in the initial design.

The simulator was run with a balanced rotor at 20,000, 30,000, 40,000, 50,000 and 60,000 rpm at each of the test conditions listed in Table 19. During each run the diametral clearance of the rear journal bearings was slowly increased by thermally expanding the flexure mount ring. A check point with the rotor unbalanced by 0.0034 ounce-inch in the turbine plane was made with the shaft vertical in air at an ambient pressure of 14.7 psia. As a result of these tests, the final design diametral clearance of 0.00135 inch was established.

TABLE 18

Summary of Tests Conducted on Turbine-Compressor Gas Bearing Dynamic Simulator

Speed, rpm	Ambient Air Pressure, psia	Thrust Bearing Load, Pounds			Journal Bearings			
		Hydrostatic		Hydrodynamic	Residual Unbalance		0.0024 oz-in Unbalance in Turbine Plane	
		Forward	Reverse	Forward	Hor.	Vert.	Hor.	Vert.
50,000	14.7	100	50	25, 3	X	X	X	
	12.0	100, 0	50	40, 15, 3	X	X	X	X
	7.5			30, 15, 3			X	X
60,000	14.7	100		15	X			
	12.0	100	50	20, 15, 7	X	X	X	X
	7.5	0						
thermal tests	14.7							
50,000	air	five different cooling air flow rates						
40,000	14.7			25	X			
	air	five different cooling air flow rates						
50,000	12.0			15			X	
	argon	two different cooling gas flow rates						

To verify the final design, the simulator was tested as outlined above the dashed line in Table 18 plus a thermal test using argon with one cooling gas flow rate. The thrust bearings were run hydrostatically at low speeds and hydrodynamically at high speeds.

TABLE 19

Summary of Test Conditions to Establish Whirl Threshold of Rear Journal Bearing

Rotor Orientation	Lubricant Gas	Ambient Pressure, psia
horizontal	air	14.7
horizontal	air	10.0
vertical	air	14.7
vertical	air	10.0
vertical	argon	10.0

Test Results

The journal bearings and hydrodynamic thrust bearing as initially designed performed satisfactorily. Pneumatic hammer was encountered in the forward hydrostatic thrust bearing, but was eliminated by reducing the number of jacking gas supply orifices from 20 to 5, as indicated in Table 17.

The roll natural frequency of the initial design of the rear journal bearing was significantly above design speed. The larger clearance investigated resulted in lower gas film stiffness, and the roll natural frequency of the pads was predicted to be near design speed. The addition of the weights shown on Figure 51 lowered the roll natural frequency below design speed. The pads displayed acceptable stability when passing through their natural frequency.

The bearings of the final design performed satisfactorily over the anticipated operating spectrum of the turbine-compressor research package. The final design represents a reduction in the front and rear journal bearing power losses of 50 and 34 per cent respectively. The low springrate upper flexures permitted operation with satisfactory pad film thickness over wide variations in temperature differential between the bearing parts.

See Volume 2 (report CR-801) for a more complete discussion of the gas-bearing test program.

REFERENCES

1. Turbine Research Package for Research and Development of High-Performance Axial-Flow Turbine-Compressor, Report PWA-2822, NASA CR-54883, Contract NAS3-4179, December 1966

2. Compressor Research Package for Research and Development of High-Performance Axial-Flow Turbine-Compressor, Report PWA-2933, NASA CR-54884, Contract NAS3-4179, March 1967

APPENDIX 1

Backup Gas Bearing Design

The purpose of the backup gas-bearing effort was to design a rotor support system that could be incorporated into the turbine-compressor if the initial gas bearing system proved unsatisfactory upon testing. Therefore, as much as possible of the turbine-compressor design was maintained to provide an economical substitution of bearing systems. The Franklin Institute Research Laboratories provided the gas bearing performance and dynamic analyses and furnished design requirements for the backup bearings during the design investigation. The gas bearing design and analysis is presented as Volume 3 (report CR-802) which was prepared by The Franklin Institute Research Laboratories. The major areas of design integration included bearing performance, thermal control, and bearing mechanical support design. The thermal and mechanical design of the backup bearing system is presented in this appendix.

The design of the backup gas bearings initially consisted of a 2-inch diameter deadended thrust bearing, a 2-inch diameter Number 1 journal bearing and a 2-1/8-inch diameter Number 2 journal bearing. The corresponding friction losses were 20, 89, and 117 watts at minimum film clearances of 0.0007, 0.0012, and 0.0014 inch, respectively.

The Number 1 journal bearing was investigated first because this area presented the opportunity for a variety of approaches to the cooling scheme, and because the design of this radial bearing could affect the design of the thrust bearing. Three methods of cooling the Number 1 journal bearing were investigated, including axial conduction to the liquid-cooled forward thrust stator, radial conduction through a 0.010-inch argon gap to a cooled jacket surrounding the pads, and gas cooling through heat exchangers in the shaft.

Initially, cooling the Number 1 journal bearing by axial conduction was considered. This configuration would employ a thrust runner and Number 1 journal which would be an integral part of the shaft. The heat would be conducted from the Number 1 journal bearing through the shaft and across the 0.0007-inch thrust bearing gap. Thermal analysis of this configuration indicated an axial temperature gradient in the journal of about 125°F, which would result in unacceptable distortion. To reduce the axial temperature gradient, copper was added inside the shaft underneath the journal. A configuration shown in Figure 52 was considered to permit fabrication while maintaining one-piece construction for heat conduction. The resulting axial temperature map in the Number 1 journal bearing with a copper thickness of 0.125 inch is shown in Figure 53 and the temperature gradient shown on Figure 54 is acceptable. However, the radial growth of the journal due to thermal expansion and the centrifugal load of the copper is 0.005 inch, which is excessive. Because of mechanical considerations, the axial conduction method of cooling the Number 1 journal bearing was rejected. In order to reduce friction losses, the journal diameter was reduced to 1.5 inches.

Cooling the Number 1 journal bearing by radial conduction to a liquid-cooled jacket surrounding the pads and separated from the back of the pads by an argon gap 0.010 inch thick was investigated. The resulting thermal map for a 1.5-inch diameter bearing is shown in Figure 55. The bearing temperature level of 333°F is within acceptable limits and the resulting temperature gradient of 24°F shown in Figure 56 is satisfactory. However, this cooling scheme produces distortion of the film clearance in the thrust bearing. The 333°F Number 1 journal temperature causes the journal to grow radially by 0.0015 inch. The two bottom journal bearing pads are supported on the compressor inlet case and operate at an essentially constant temperature of 76°F. Since the upper shoe is spring-mounted, the shaft centerline will experience a radial motion of 0.0015 inch. The Number 2 journal bearing pads are mounted to the compressor exit scroll at 350°F and the two bottom pads will expand radially outward, tending to compensate for the growth of the Number 2 journal. Therefore, the 0.0015-inch radial motion of the front end of the shaft tilts the face of the thrust bearing. A total axial runout of 0.0003 inch in the thrust runner will result. Since the thrust bearing is designed to operate at clearances down to 0.0007 inch, this distortion is not acceptable.

Two methods of gas-cooling the radial bearings were investigated. First a system that would require a minimum cooling flow was studied. In this scheme, the cooling gas was introduced in the Number 2 bearing compartment at 100°F. The cooling gas would flow radially into the Number 2 journal heat exchanger and then through the Number 1 journal heat exchanger. It would exit from the front end of the shaft through holes just behind the thrust runner. The gas would then flow into the Number 1 journal bearing and thrust bearing areas and enter the compressor upstream of the first stage rotor. This configuration is shown in Figure 57. The ambient pressure in the Number 1 bearing compartment would be 5.2 psia and the cooling gas flow would be 1.0 per cent of the cycle flow through the shaft heat exchangers with an additional 1.8 per cent gas flow through the turbine labyrinth seals. The resulting temperature map and temperature gradient are presented in Figures 58 and 59. The 325°F bearing temperature produces a tilt in the thrust runner as in the previous case. Therefore, this system of gas cooling was rejected.

The second gas-cooling system is substantially the same as the system employed in the turbine-compressor design incorporating the Mechanical Technology Incorporated bearings. The cooling gas is introduced in the Number 1 bearing compartment at 12.8 psia and 100°F. It flows into the shaft behind the thrust runner, through the Number 1 journal heat exchanger and Number 2 journal heat exchanger, into the Number 2 bearing compartment. About 3.8 per cent of the cycle flow is employed. About 2.8 per cent of the cycle flow passes into the shaft and the remaining 1.0 per cent passes through the labyrinth seal and rejoins the main cycle at the leading edge of the first compressor blade row. This gas-cooling scheme maintains low Number 1 journal temperatures and low temperature gradients, as indicated in Figures 60 and 61. The resulting thrust bearing axial runout for this cooling system with a journal temperature of 160°F is 0.0001 inch which is satisfactory. Although this cooling system requires 1 per cent more bleed flow than the first gas-cooling scheme, it was selected for cooling the journal bearings because it should provide better thrust bearing performance.

Gas cooling of the Number 2 journal bearing was investigated over a range of gas flow rates from 0.5 to 1.5 per cent of system flow with the cooling gas introduced at 100°F in the Number 2 bearing compartment, consistent with the first gas-cooling scheme for the Number 1 bearing. Figures 62, 63, and 64 show the temperature maps in the Number 2 bearing for various gas flow rates in the heat exchanger. The resulting bearing temperature gradients for these cases are shown in Figure 65. A minimum flow of 0.5 per cent is required inside of the turbine rotor for cooling the gooseneck and preventing back flow of hot turbine gas through the rear labyrinth seal of the turbine. A flow rate of 1.0 per cent through the heat exchanger results in an acceptable temperature gradient of 43°F. This cooling scheme for the Number 2 journal bearing was not considered further because it is not compatible with the selected cooling scheme for the Number 1 journal bearing.

The Number 2 bearing temperature map consistent with the related cooling scheme for the Number 1 bearing is shown in Figure 66 and the corresponding temperature gradients are shown on Figure 67. The journal temperature of 260°F with a gradient of 21°F is satisfactory.

The thrust bearing diameter was increased from 2 to 2.80 inches to provide adequate clearance during startup due to a maximum forward thrust of 100 pounds and a maximum rearward thrust of 50 pounds. These startup loads are supported by the hydrostatic portions of the forward and reverse thrust bearings. At the 100-pound forward thrust load the clearance is 0.93 mils on the forward thrust bearing, and at 50 pounds rearward thrust the clearance is 2 mils on the reverse thrust bearing. The power loss at the design speed of 50,000 rpm increased from 20 to 41 watts due to the larger thrust bearing. Figure 68 is the map for this configuration of the Number 1 journal bearing-thrust bearing area. Because of the possibility of an accidental thrust reversal at design speed, the reverse hydrostatic thrust bearing design was revised to incorporate a step bearing with the hydrostatic ports located in the lands.

Further analysis of the distortion in the thrust bearing clearance due to radial motion of the journal bearings indicated an increase of distortion from 0.0001 to 0.0002 inch for the larger thrust bearing diameter. This amount is acceptable because of the increase in the thrust bearing clearance at design conditions due to the increased diameter of the thrust bearing. The thrust bearing clearance at design conditions is 0.0011 inch.

The thrust bearing runner located at the front of the turbine-compressor rotor is subjected to assembly and operating applied loads that can introduce sufficient distortion to warrant a structural study. The assembly loads are due to the radial snap fit between the runner and shaft and the axial boltup load as the runner is secured into the shaft. Operating loads are due to the centrifugal force on the thrust runner, the difference in thermal expansion between the thrust runner and shaft materials (titanium versus Waspaloy) and the axial load on the face of the thrust runner due to the operating thrust load. Material has been added and various stiffnesses have been adjusted in the thrust runner to limit distortions. Distortions due to assembly loads (radial snap fit and axial bolt preload) are shown in Table 1-1. Positive deflection is an axial movement of the tip of the runner rearward (towards the turbine).

TABLE 1-1

Thrust Bearing Distortion at Assembly

	Assembly Deflections, Mils	
	Minimum	Maximum
0.004 to 0.006-inch radial snap tightness	0.224	0.336
0.005 to 0.004-inch axial preload (280 to 200 lb preload)	-0.092	-0.066
total assembly deflection	0.132	0.270

The distortions during operation are shown in Table 1-2 and are additive to the total assembly deflection.

TABLE 1-2

Thrust Bearing Distortion at Operating Conditions

	Operating Deflections, Mils	
	50,000 rpm	60,000 rpm
centrifugal	0.030	0.043
steady-state radial thermal change (70 to 145°F)	-0.005	-0.005*
steady-state axial thermal change (70 to 145°F)	-0.014	-0.014*
15 lb forward rotor thrust	0.009	0.009
total operating deflection	0.020	0.033

*Temperatures at overspeed condition (60,000 rpm) are assumed to be the same as at 50,000 rpm

The resultant distortions should permit satisfactory bearing operation.

The final mechanical design of the backup gas bearing system incorporates a 2.80-inch diameter deadended thrust bearing, a 1-1/2 inch diameter by 1-1/2 inch long Number 1 journal bearing and a 2-1/8 inch diameter by 2-1/8 inch long Number 2 journal bearing. The thrust bearing as shown in Figure 69 includes a liquid-cooled aluminum forward thrust stator, a titanium thrust runner and a steel reverse thrust stator. The thrust stators incorporate hydrostatic jacking provisions in addition to the hydrodynamic provisions. The forward stator only is supported by a diaphragm. This diaphragm can be machined if more flexibility is required. The journal bearings incorporate three 100-degree tilting pads with the two bottom pad supports rigidly mounted, and the top pad preloaded about 8 to 9 pounds by a spring with a spring rate of 91 pounds / inch. Hydrostatic jacking provisions are incorporated in all of the pads. The Number 2 journal bearing area is shown on Figure 70. Table 1-3 is a summary of gas bearing design parameters for the turbine-compressor backup bearings.

An overall view of the turbine-compressor incorporating the backup gas bearings is shown in Figure 71.

TABLE 1-3

Turbine-Compressor
Backup Gas Bearing Design Parameters

Journal Bearings

configuration	tilting pad, hydrostatic lift-off
journal radius, inches	
Number 1 (forward) bearing	0.750
Number 2 (turbine end) bearing	1.062
axial length, inches	
Number 1 bearing	1.500
Number 2 bearing	2.125
number of pads	3
pad orientation	2 loaded (hor. oper.)
orifice orientation	at pivot on all pads
pivot location from leading edge/ arc length	0.65
arc length of pad, degrees	100
ball radius, inches	
Number 1 bearing	0.6
Number 2 bearing	0.6

TABLE 1-3 (Cont'd)

Journal Bearings (Cont'd)

socket radius, inches	
Number 1 bearing	∞
Number 2 bearing	∞
clearance ratio	
Number 1 bearing	0.00267
Number 2 bearing	0.00272
operating clearance at pivot, inches	
space operation	
Number 1 bearing	0.00063
Number 2 bearing	0.00120
Design Λ	1.5
friction loss per journal, watts	
space operation	
Number 1 bearing	48
Number 2 bearing	102
radial gas film stiffness, lbs/inch	
space operation	
Number 1 bearing	9.15×10^3
Number 2 bearing	5.0×10^3
radial support stiffness, lbs/inch	
Number 1 bearing	91
Number 2 bearing	91
load, pounds	
space operation	
Number 1 bearing	8.0
Number 2 bearing	9.0
rotor speed, rpm	50,000
gas	argon
ambient pressure, psia	12.0
gas film temperature °F	
Number 1 bearing	159
Number 2 bearing	267
shaft temperature, °F	
Number 1 bearing	144
Number 2 bearing	256

TABLE 1-3 (Cont'd)

Journal Bearings (Cont'd)

pad temperature, °F	
Number 1 bearing	160
Number 2 bearing	269
shaft material	PWA 1007 (Waspaloy)
pad material	AMS 6440 steel
pivot material	AMS 5616 (Greek Ascoloy)
coating	chrome oxide

Thrust Bearing

configuration	spiral groove hydrostatic lift-off
diameter, inches	2.800
spiral groove outside diam., inches	2.667
spiral groove inside diam., inches	1.600
groove depth, inches	0.0037
number of grooves	15
load, pounds	15
clearance, inches	0.0011
friction loss, watts	41
orifice diameter, inches	0.032
number of orifices	20
hydrostatic gas supply pressure at startup, psia	100
hydrostatic bearing design load at startup, pounds	100
hydrostatic film clearance at startup, inches	0.00093
axial support stiffness, lbs/inch	1×10^5
torsional support stiffness, inch-lbs/rad	5×10^4
stator temperature, °F	115
runner temperature, °F	145
runner material	AMS 4928 titanium
stator material	AMS 4025 aluminum
coating	chrome oxide

TABLE 1-3 (Cont'd)

Reverse Bearing

configuration	step hydrodynamic, hydrostatic lift-off
orifice diameter, inches	0.032
number of orifices	28
supply gas pressure, psia	100
design load, pounds	50
hydrostatic clearance at startup, inches	0.0015
stator material	AMS-6415 steel
coating	chrome oxide

APPENDIX 2

Compressor Blade Retention Investigation

The two-fold purpose of the compressor blade retention investigation was to determine an adequate pin-locking method for attaching the compressor blades to the disk and to determine whether small dovetail blade attachments deform under the expected blade radial loads.

A. Compressor Blade Locking Method

The rivet pin method of blade locking was selected for the Brayton-cycle compressor due to lack of space in which to install more conventional blade locks. In this method, a pin is passed through a radial hole in the shaft under each blade. The pin engages a slot machined across the bottom of the blade platform. A special tool is used to apply force on the pin so that the pin is deformed in the slot to prevent the pin from falling out of the shaft hole, thus providing a positive mechanical lock. Figure 72 shows how the blade pin is installed. Figure 73 is a photograph of the corresponding parts.

Aluminum (AMS 4102) and copper (AMS 4701) were selected as the candidate pin materials. All of the pins used had a basic diameter of 0.062 inch with 0.0003 to 0.0006 inch of silver plating. A block with slots and sample blades was used for this testing and is described later in the Appendix. Force on the pin was applied with a hydraulic materials testing machine.

Test results for aluminum pins are shown in Figure 74. The amount of force used to reduce (upset) pin length is shown for three configurations in which the width of the slot in the blade was varied from 0.040 to 0.060 inch. After the pins were installed, the blade was forced to move in the dovetail to shear the pin. A force of about 70 pounds was needed to shear the aluminum pins. No damage to the titanium blades or block was evident. The load applied to the pins was increased to 300 pounds to get an improved rivet effect. A typical pin before and after use as a blade lock can be seen in Figure 75. The right-hand pin section shows shear marks which occurred at the point of pin separation during blade removal. The left-hand pin is unused. Aluminum pin testing was dropped after titanium was selected as the blade material, because of the potential electrolytic reaction in air between these pin and blade materials.

Solid copper pins were tested with upset loads up to 150 pounds. These pins did not deform adequately to provide a positive blade lock as shown on Figure 76. The left-hand sheared-off section shows the inadequate deformation. An unused solid pin is shown at the right for comparison. Figure 77 shows the solid pin deflection to be approximately 0.038 inch at 150 pounds load.

To give better pin deflection characteristics, holes were drilled 0.047 inch in diameter and to depths of 0.030 and 0.060 inch, respectively, in the end of the copper pin to be upset. Both relieved configurations of the silver-flashed copper pins provided consistent blade locks and met all design requirements. The test results for the two relieved configurations show that a deflection in excess of 0.059 inch is obtained at a 150-pound load (Figure 78.) Views of typical pins shown in Figures 79 and 80 indicate the deflection to be completely adequate at 150 pounds. The width of the deformed head is about 0.095 inch. The right-hand pin in Figure 80 is an unused one.

The force required to shear the locked blade from its simulated disk was approximately 105 pounds in all of the copper pin tests. Separate evaluations were conducted to determine the pure shear value of the pin in its solid area and in its hollow-relief area. These were found to be approximately 75 and 26 pounds, respectively. The difference between the shear force of 105 pounds for the locked blade and 75 pounds for the solid copper pin represents the friction force required to slide the blade from its slot. The high shear force also indicates that providing relief in the pin to give adequate upset deformation does not compromise the positive blade lock.

To obtain the optimum fit of the rivet pin in the disk hole, loose diametral fits of 0.0015, 0.0025, 0.0035, and 0.0055 inch were evaluated. The resultant curves shown in Figure 81 indicate the optimum fit to be 0.0025 inch loose. Insufficient data was available on the 0.0015-inch fit to be plotted in the curves, but data available was not as good at any point as that of the 0.0025-inch fit.

As a final evaluation of the rivet pin effect, several pins were upset in a revised block which simulated the blade root configuration but permitted studies of the pin upset without having to shear the pin. A typical pin (Figures 82 and 83) shows that the walls of the hollow pin hole have elongated and that opposing walls at one point have been pressed together.

Rivet type pins provide positive locking of the compressor blades to the disk. Silver-plated copper pins with a relief hole in the upset end provide consistent pin deformation characteristics which meet all design requirements.

The optimum blade locking fit of the pin to the disk hole is 0.0025 inch loose. The 105-pound force required to remove a locked blade exceeds the aerodynamic gas force of 0.5 pound. The selected blade lock pin is a silver-flashed copper pin with a relief hole 0.047 inch in diameter and 0.045 inch deep in the upset end.

B. Blade Radial Motion Tests

Brayton-cycle axial-flow compressor blades are expected to exert a radial pull of about 340 pounds per blade when operating at the maximum speed (60,000 rpm). Significant unsymmetric deformation of the blade root or disc slot under the radial load would cause unbalance of the rotor assembly. Blade samples consisting of titanium strips with machined dovetails were mounted in a block machined from Waspaloy and containing broached slots as shown in Figure 84. Five blade samples were mounted in the block and tensile load was applied to simulate centrifugal blade loads as shown in Figure 85. Tensile loads of 300, 600, and 1000 pounds per blade were applied and the distances between a gage point on the broached block and on each blade sample were measured.

No measurable (< 0.0001 inch) relative motion between the blade samples and the broached block existed under the loads applied indicating that the dovetail blade attachment is satisfactory for the Brayton-cycle axial-flow compressor.

APPENDIX 3

Gas Bearing Materials Investigation

Pratt & Whitney Aircraft conducted an evaluation test program of two methods of applying a chrome oxide coating to the turbine-compressor bearing materials. Mechanical Technology Incorporated had previously performed a materials test program of candidate coatings as discussed in Volume 2 (report CR-801), with the result that chrome oxide was selected as the coating for all bearing surfaces. The Pratt & Whitney Aircraft tests were conducted to evaluate the bond strength of the selected coating. The substrate specimens were 1-inch diameter bars, finished on the end to be coated to an 8-microinch AA surface. Coating tests included an evaluation of mechanical bond strength, cup/bend tests, and thermal cycle tests.

The results of bond strength tests on chrome oxide coatings applied to four substrate materials by two methods of application are shown in the following table:

Substrate	Coating Thickness, mils	Mechanical Bond Strength, psi Linde LC-4 Process	Plasma-Spray Process
Waspaloy, PWA-686	3	7,380*	12,050
aluminum, AMS-4117	2	8,050	9,200
tool steel, AISI M-1	2	9,500	8,780
titanium, AMS-4928	2	11,600	7,900**

* 10% coating bond failure
** 70% coating bond failure

Photographs of bond strength specimens coated by the Linde LC-4 process are shown before and after test in Figure 86. Figures 87 and 88 are micrographs of the LC-4 coating on the four substrates.

Figure 89 shows cup/bend specimens after test, coated by the Linde LC-4 process and the plasma-spray process, respectively. The cup/bend tests represented extreme off-design overstress conditions, but the Linde LC-4 coating indicated somewhat better adherence than the plasma-spray process.

Waspaloy cylinders simulating the Number 2 bearing journal were chrome-oxide coated by the two processes (coating surface unground) and the specimens were thermally cycled 500 times at rates simulating the turbine-compressor gas bearing environment, as shown in the following table.

Coating Method	Coating Thickness, mils	Temperature Range, °F	Rate of Temp. Change
Linde LC-4	2	80 - 380	1°F/sec
plasma-spray process	5	80 - 380	1°F/sec

Figure 90 shows micrographs of specimens coated by the Linde LC-4 process and the plasma-spray process, respectively, after thermal cycling tests. Although the plasma-spray coating appeared somewhat laminar and stratified, both methods of coating were judged to have similar bond strength characteristics.

APPENDIX 4

Journal Bearing Heat Exchanger Investigation

Pratt & Whitney Aircraft conducted an investigation of the techniques to fabricate the internal heat exhcnagers under the two journal bearings. The features to be evaluated were: machining with thin canted heat exchanger fins, uniformity of braze coverage and fillets, and distortion of the shaft assembly due to the braze cycle. The results of these evaluations indicate that a turbine-compressor shaft assembly can be successfully fabricated.

The requirements of high heat transfer coefficient and thermal growth characteristics comparable with the basic shaft material, Waspaloy, led to the selection of TD nickel for the heat exchangers. TD nickel is a dispersion containing 98 per cent nickel and 2 per cent thorium oxide. The machinability of this material into the desired configuration was investigated using two different methods of machining the canted fins.

The Number 2 bearing heat exchanger shown in Figure 91 was successfully fabricated by grinding. The other method of machining, electrical discharge (EDM), was extremely slow and resulted in excessive electrode wear. Fabrication of this heat exchanger was stopped upon the satisfactory completion of the first unit. The completed heat exchanger proved the feasibility of maintaining fin thickness tolerances within the range desired to assure uniform heat flow and minimum mechanical unbalance.

The design requirements of uniform shaft temperature distribution and close control of the circumferential mass distribution and shaft bowing to minimize unbalance necessitated investigation of the brazing technique. Several areas related to the braze technique were considered and the following evaluations were made:

1) braze coverage and filleting resulting with plated braze alloys,
2) effect of rotation of the part during braze, and
3) axial and circumferential distortions due to the braze thermal cycle.

A simulated shaft of Waspaloy was made and nickel plate 0.001 inch thick was applied to the inside. The various constituents of a braze material containing copper, silver, and tin were plated in separate layers on the heat exchanger fin tips. The shaft and heat exchanger were assembled with a very light interference fit due to the plating and mounted in a sealed retort as shown in Figure 92. The retort was rotated during the braze cycle and purged with a reducing atmosphere of hydrogen. The braze cycle of 1425°F for 10 minutes did not produce an acceptable bond. The resulting distortion of the shaft was less than 0.00015 inch both in roundness and bowing, and is significantly less than the design objective of less than 0.0005 inch to allow balance correction.

Standard T-shaped test specimens were prepared to further investigate the braze. Waspaloy plates were nickel-plated and TD nickel plates were plated on the edge with the various braze alloy constituents as described for the shaft and heat exchanger. Strength, coverage, and filleting of the braze were found to be excellent if the braze temperature of 1425°F was maintained for sufficient time to completely melt the braze constituents. The shaft distortion and T-specimen braze results obtained to date indicate that a satisfactory turbine-compressor shaft assembly can be fabricated. A second shaft assembly braze trial is recommended to verify the technique.

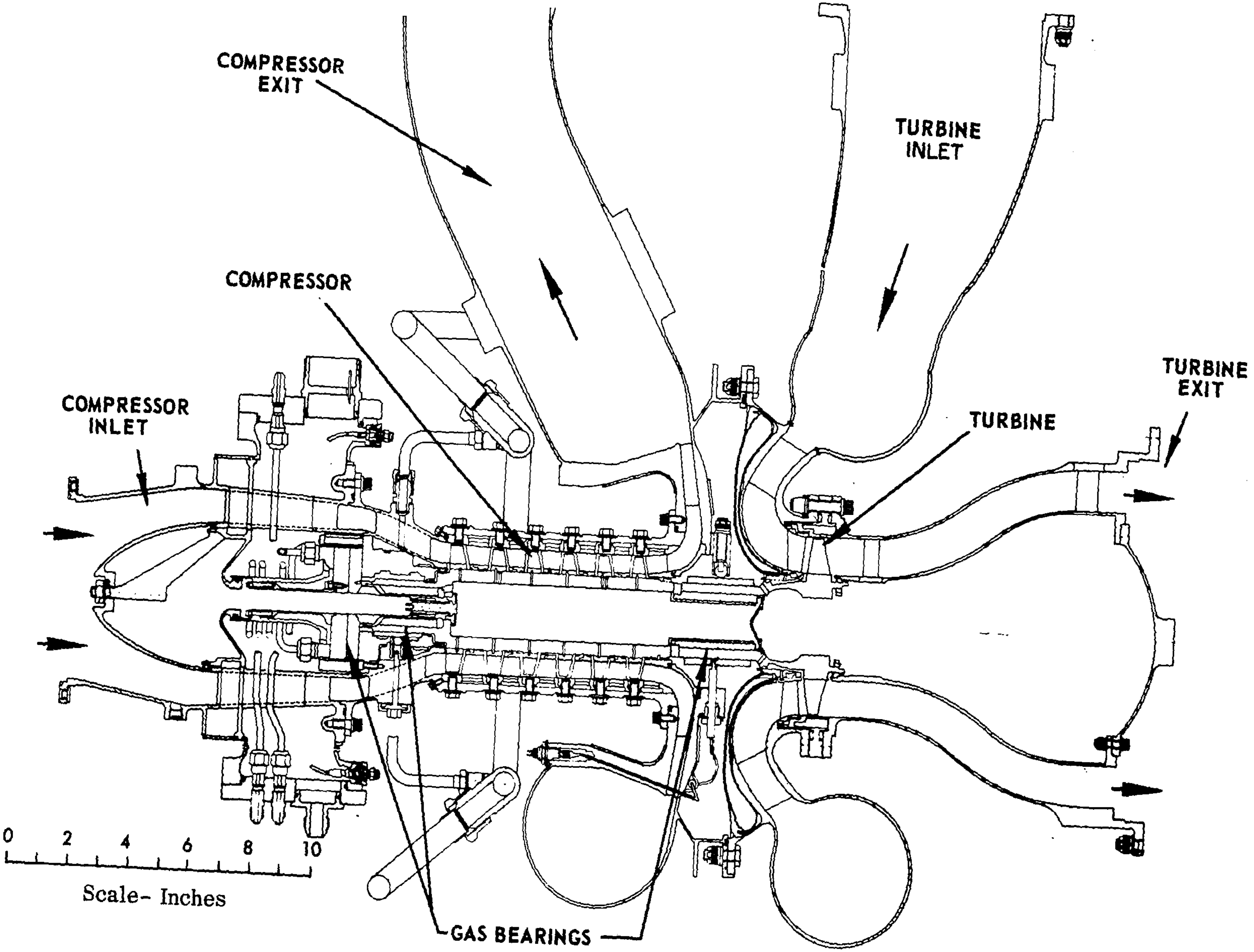
COMPRESSOR EXIT
TURBINE INLET
COMPRESSOR
TURBINE EXIT
COMPRESSOR INLET
TURBINE
0
2
4
6
8
10
Scale- Inches
GAS BEARINGS

Figure 2 Brayton-Cycle Turbine-Compressor

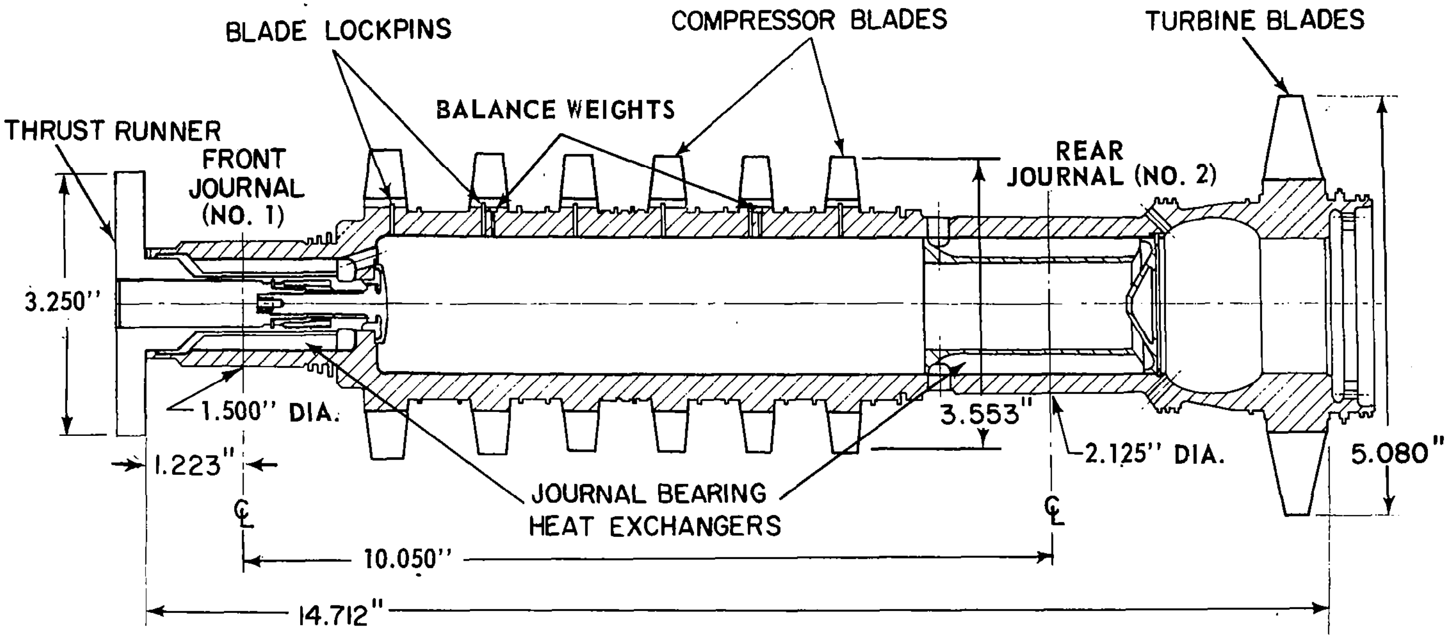
BLADE LOCKPINS
COMPRESSOR BLADES
TURBINE BLADES
BALANCE WEIGHTS
THRUST RUNNER
FRONT JOURNAL (NO. 1)
REAR JOURNAL (NO. 2)
3.250"
1.500" DIA.
1.223"
℄
JOURNAL BEARING HEAT EXCHANGERS
3.553"
2.125" DIA.
5.080"
℄
10.050"
14.712"

Figure 3 Turbine-Compressor Rotor Assembly

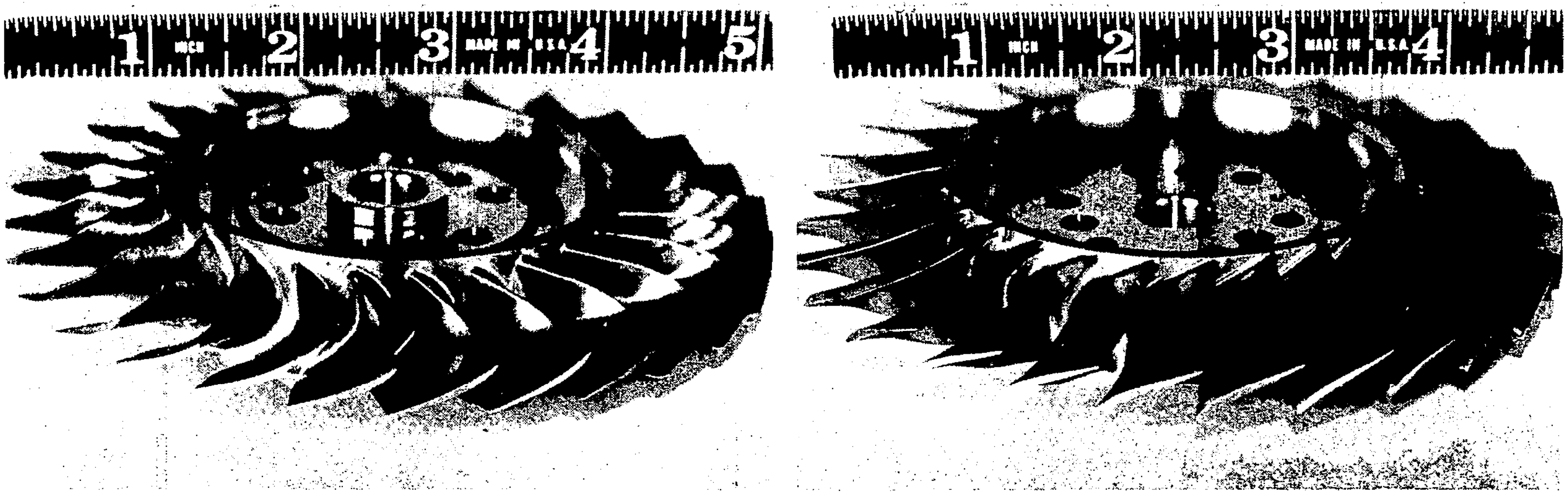
1
INCH
2
3
MADE IN U.S.A.
4
5
1
INCH
2
3
MADE IN U.S.A.
4

LEADING EDGE VIEW

TRAILING EDGE VIEW

Figure 4 Turbine Blades

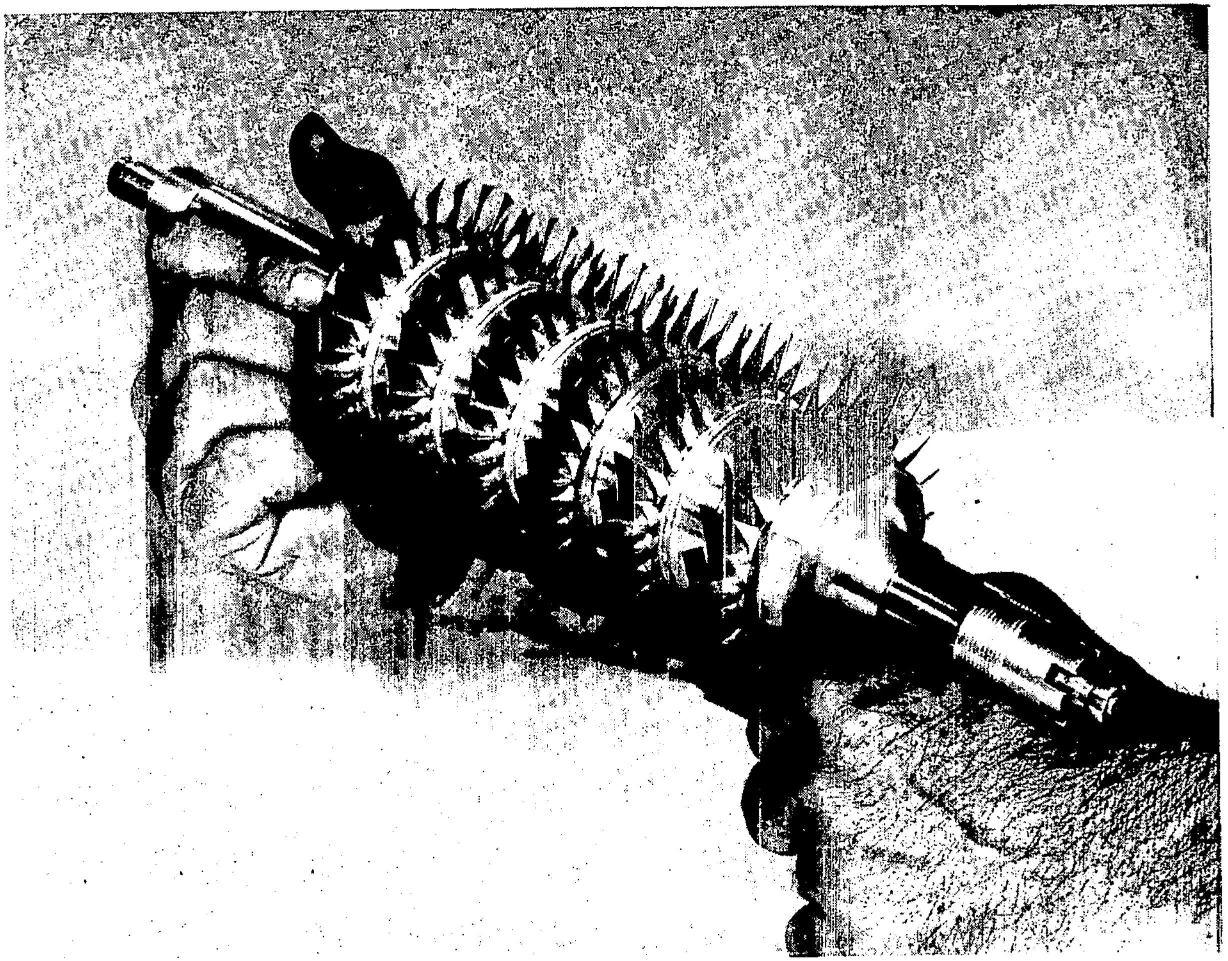

Figure 5 Compressor Blades

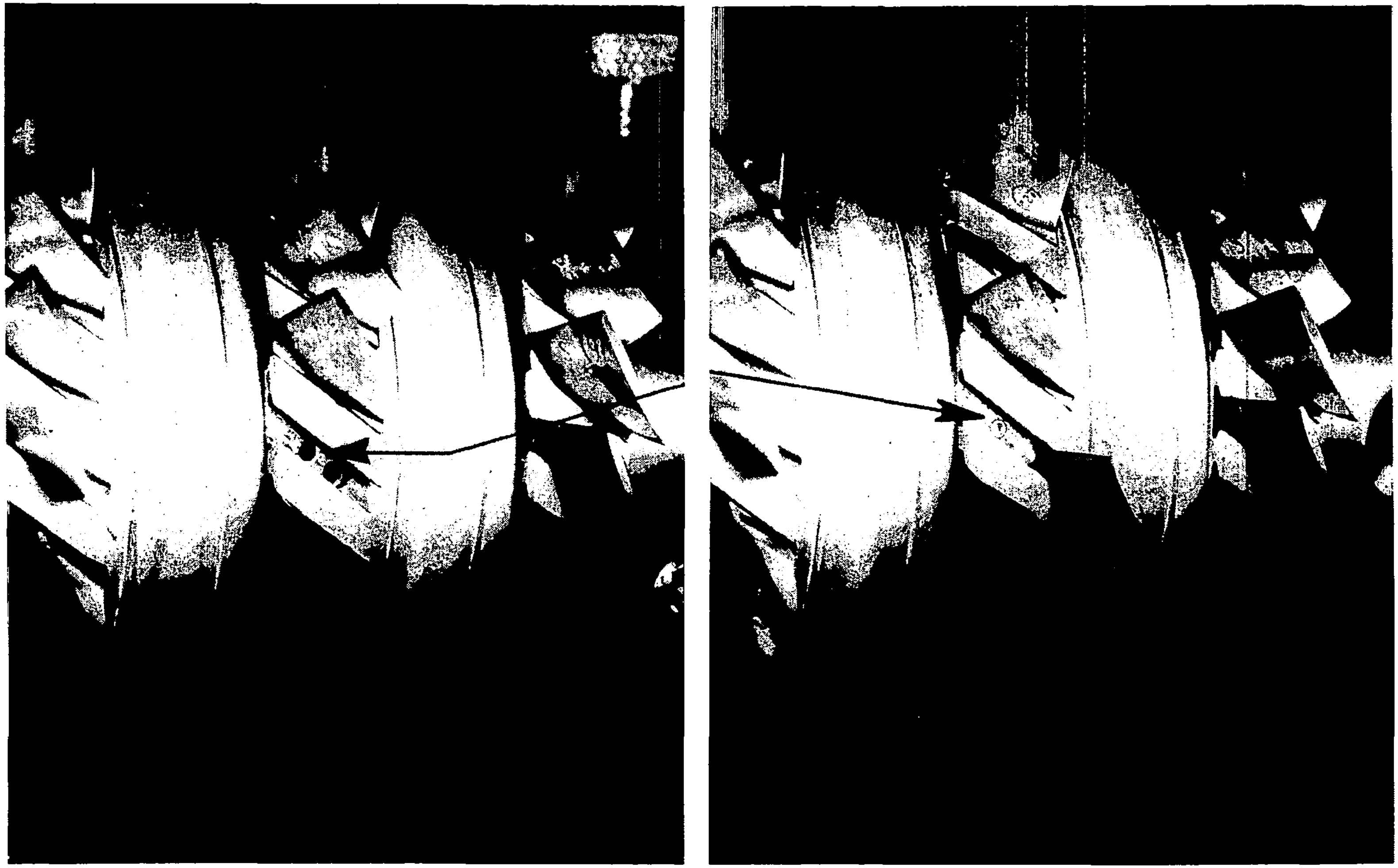

Figure 6 Compressor Blade Retention

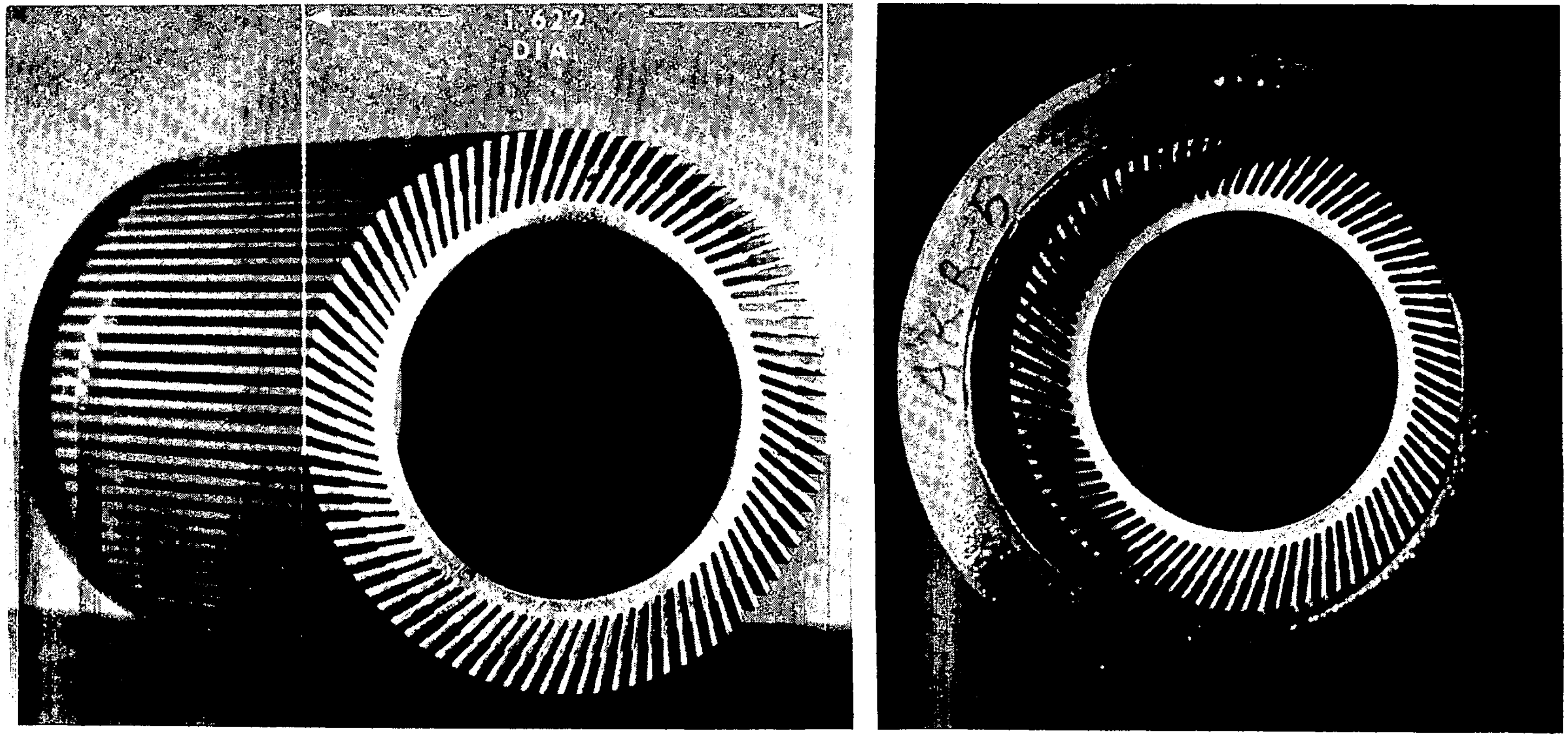

Figure 7 Number 2 Bearing Heat Exchanger

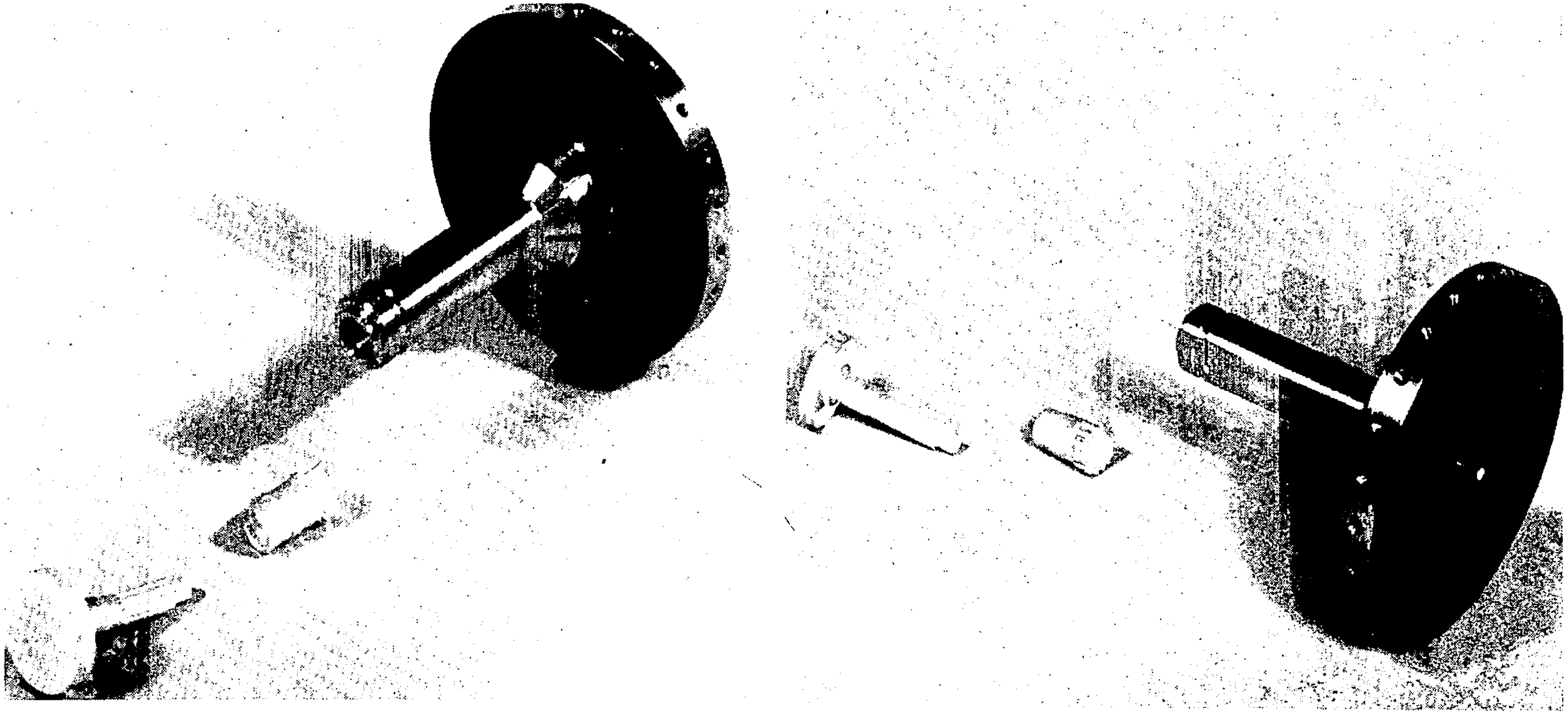

Figure 8 Thrust Runner

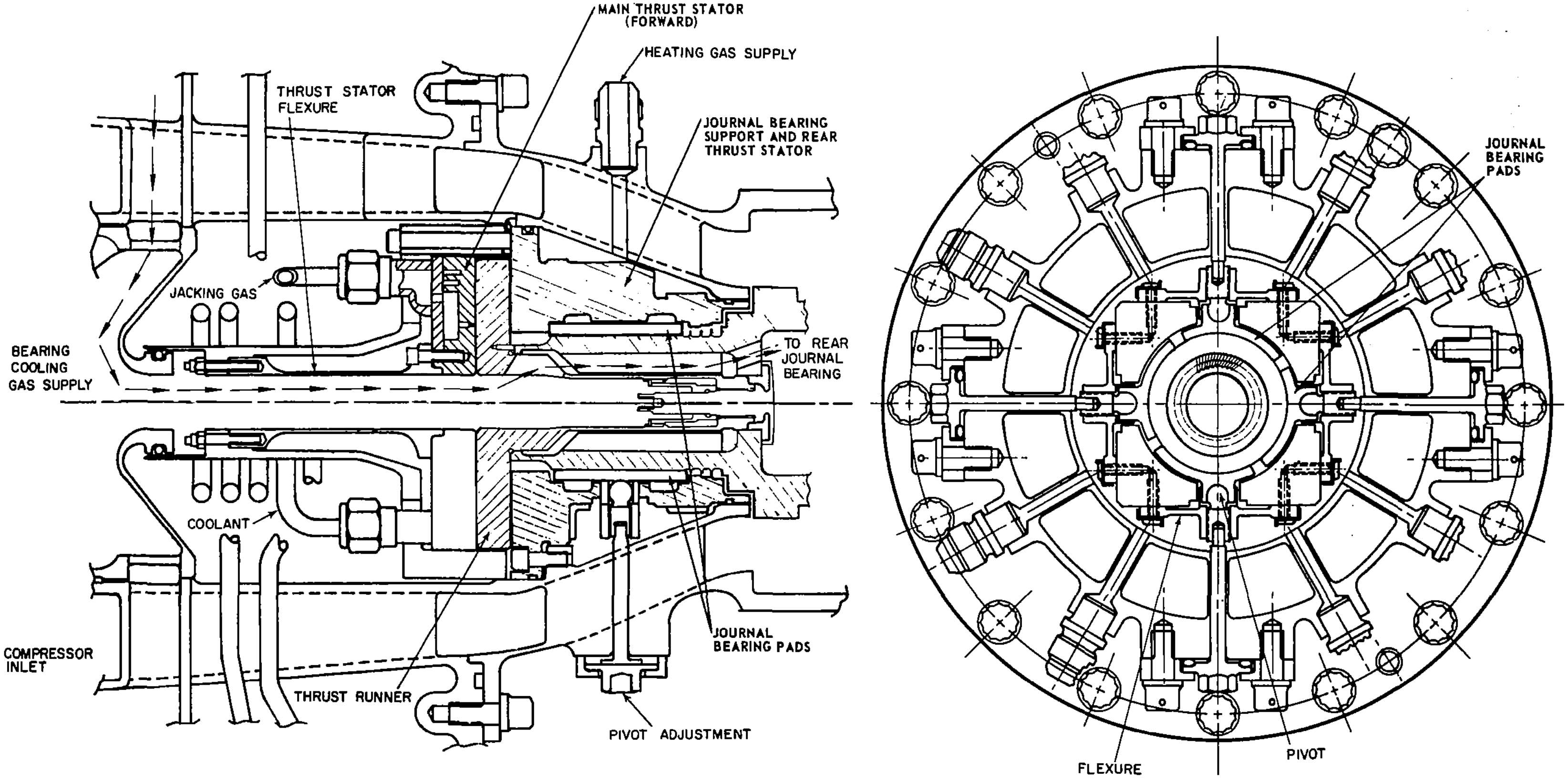
MAIN THRUST STATOR (FORWARD)
HEATING GAS SUPPLY
THRUST STATOR FLEXURE
JOURNAL BEARING SUPPORT AND REAR THRUST STATOR
JACKING GAS
BEARING COOLING GAS SUPPLY
TO REAR JOURNAL BEARING
COOLANT
COMPRESSOR INLET
THRUST RUNNER
JOURNAL BEARING PADS
PIVOT ADJUSTMENT
JOURNAL BEARING PADS
FLEXURE
PIVOT

Figure 9 Turbine-Compressor Gas Bearing Design. Thrust Bearing and No. 1 Journal Bearing

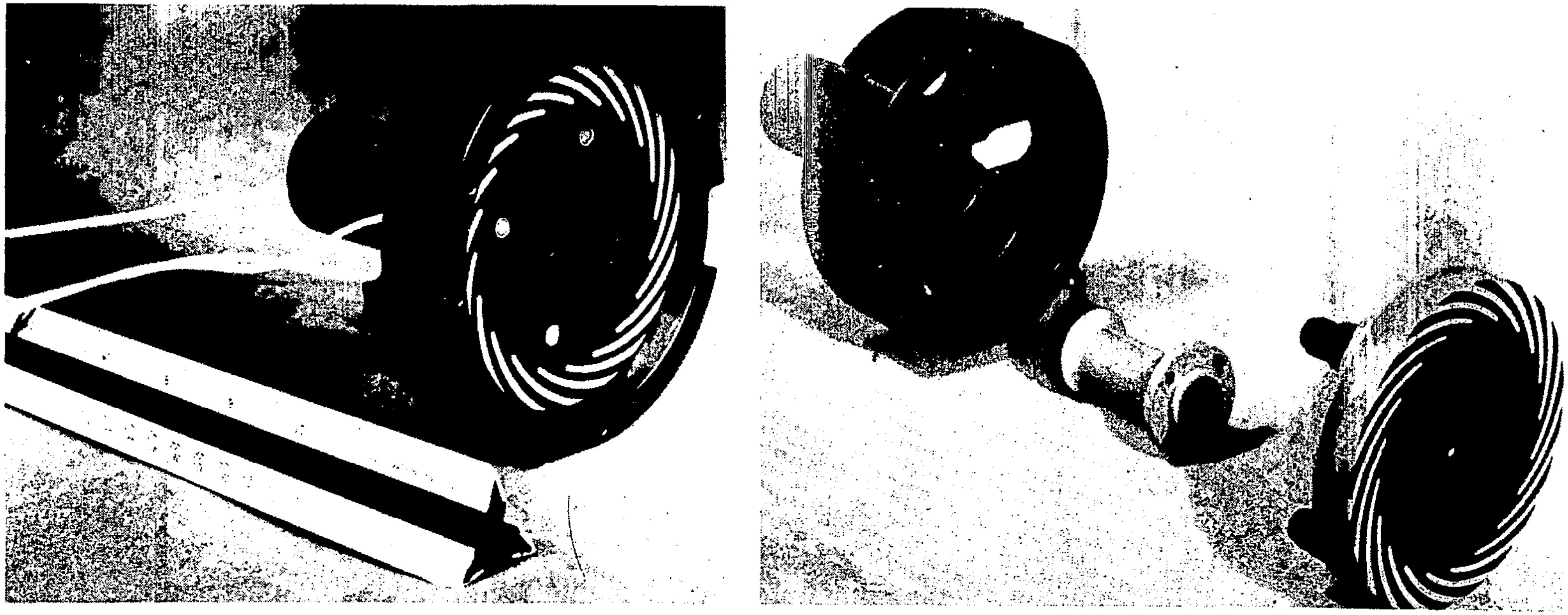

Figure 10 Main (Forward) Thrust Stator and Support

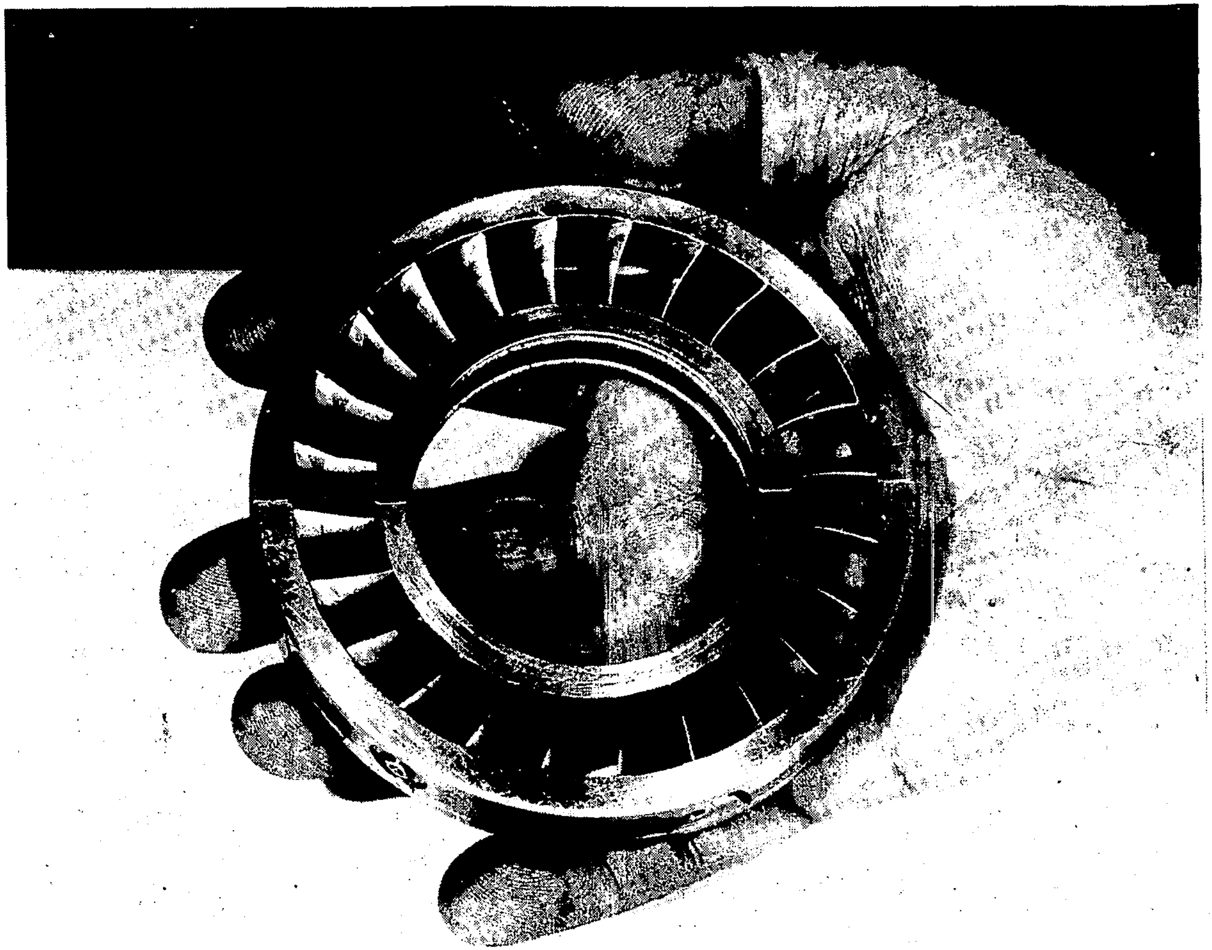

Figure 11 Compressor Research Package Vane and Shroud Assembly

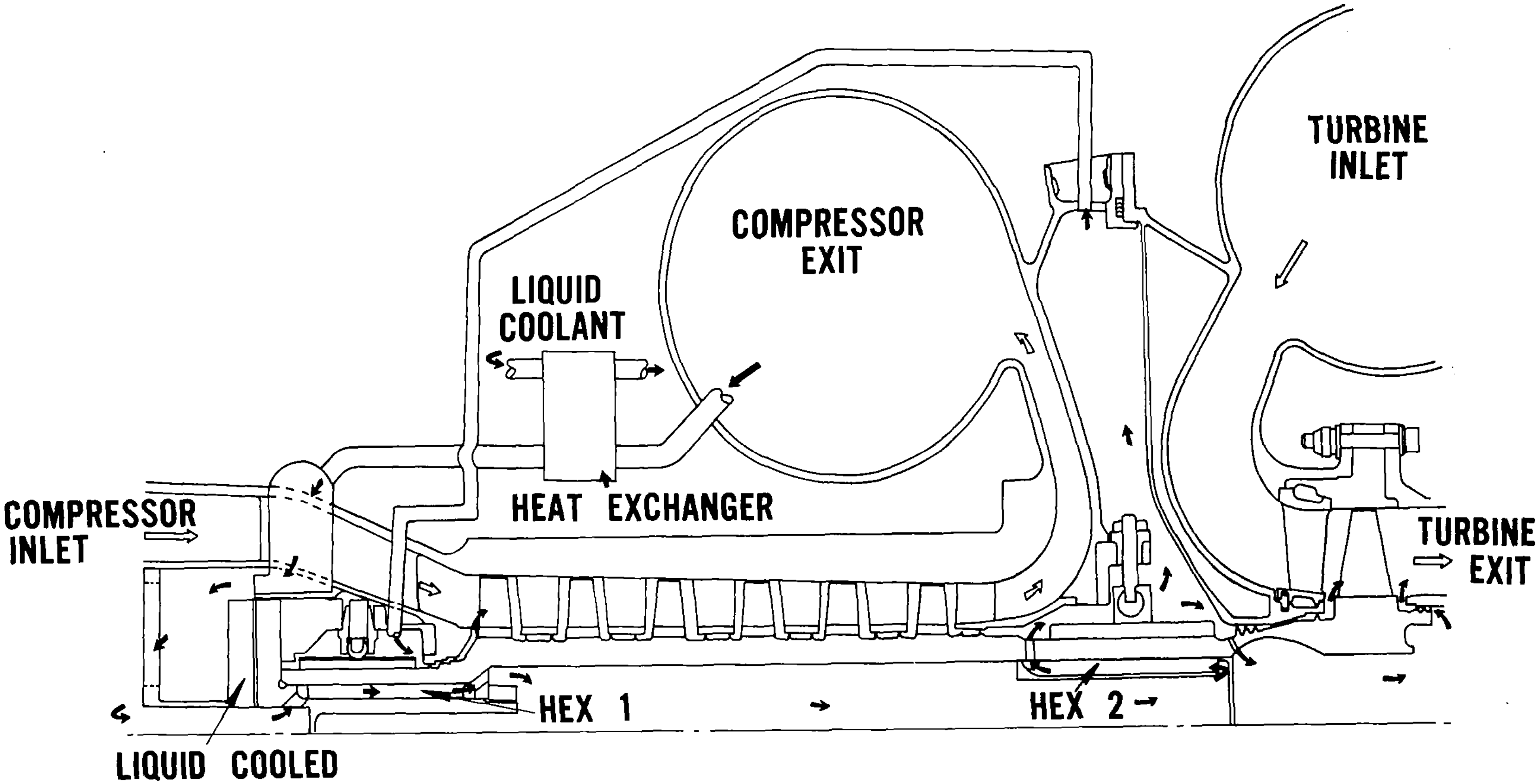
TURBINE INLET
COMPRESSOR EXIT
LIQUID COOLANT
HEAT EXCHANGER
COMPRESSOR INLET
TURBINE EXIT
HEX 1
HEX 2
LIQUID COOLED

Figure 12 Gas Cooling Flow Path

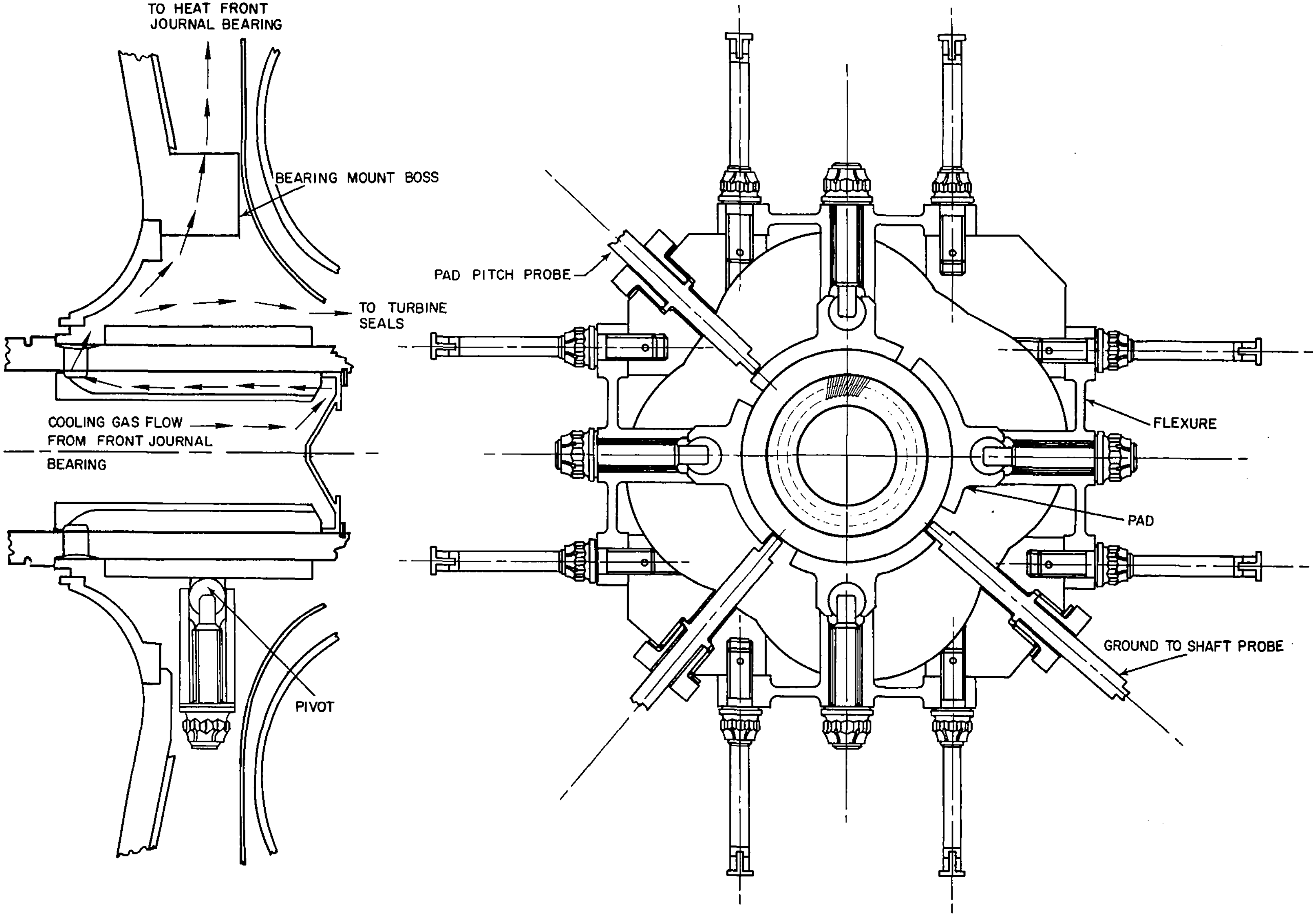
TO HEAT FRONT JOURNAL BEARING
BEARING MOUNT BOSS
TO TURBINE SEALS
COOLING GAS FLOW FROM FRONT JOURNAL BEARING
PIVOT
PAD PITCH PROBE
FLEXURE
PAD
GROUND TO SHAFT PROBE

Figure 13 Turbine-Compressor Gas Bearing Design. No. 2 Journal Bearing

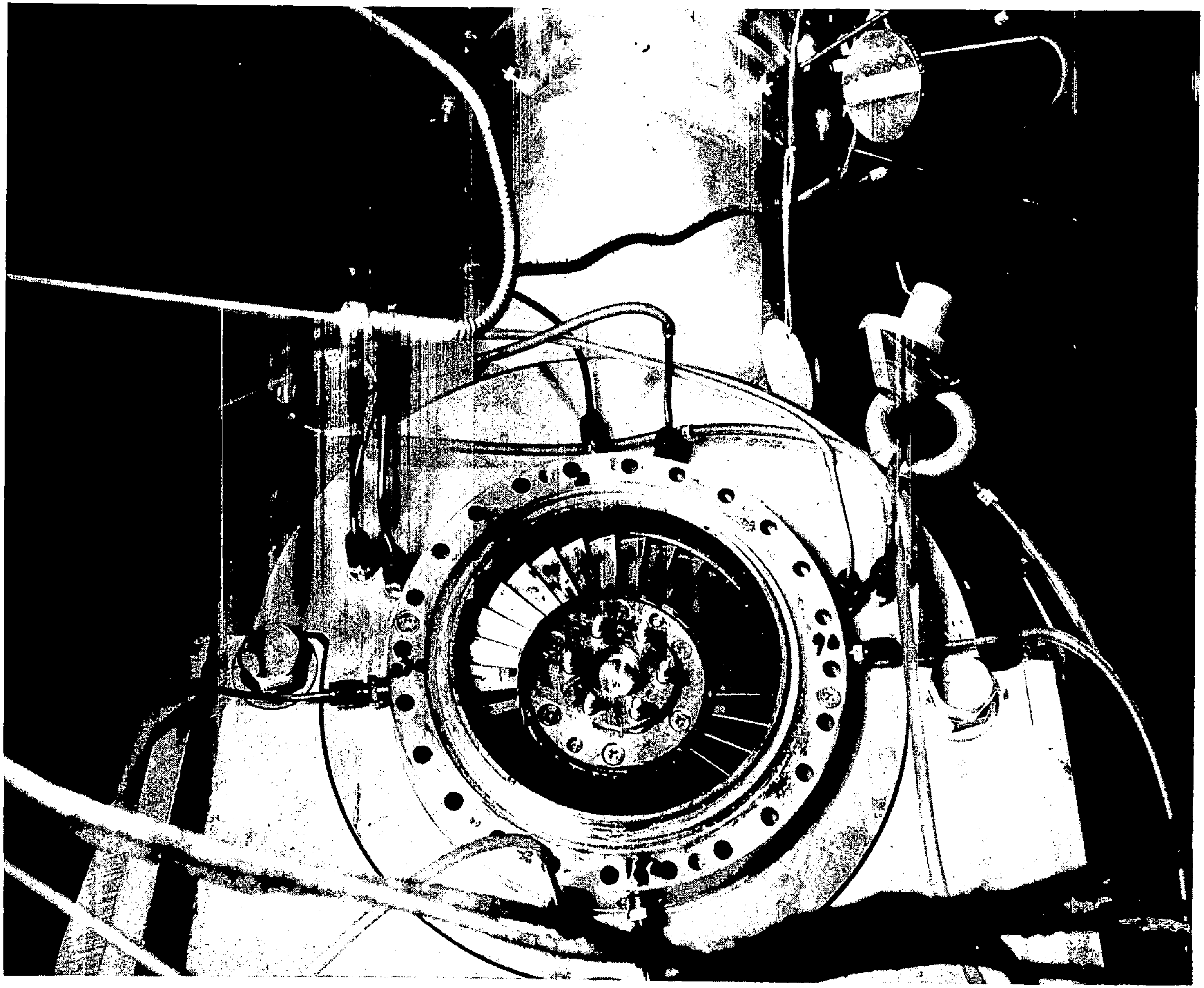

Figure 14 Trailing Edge View of Turbine Nozzle Assembly

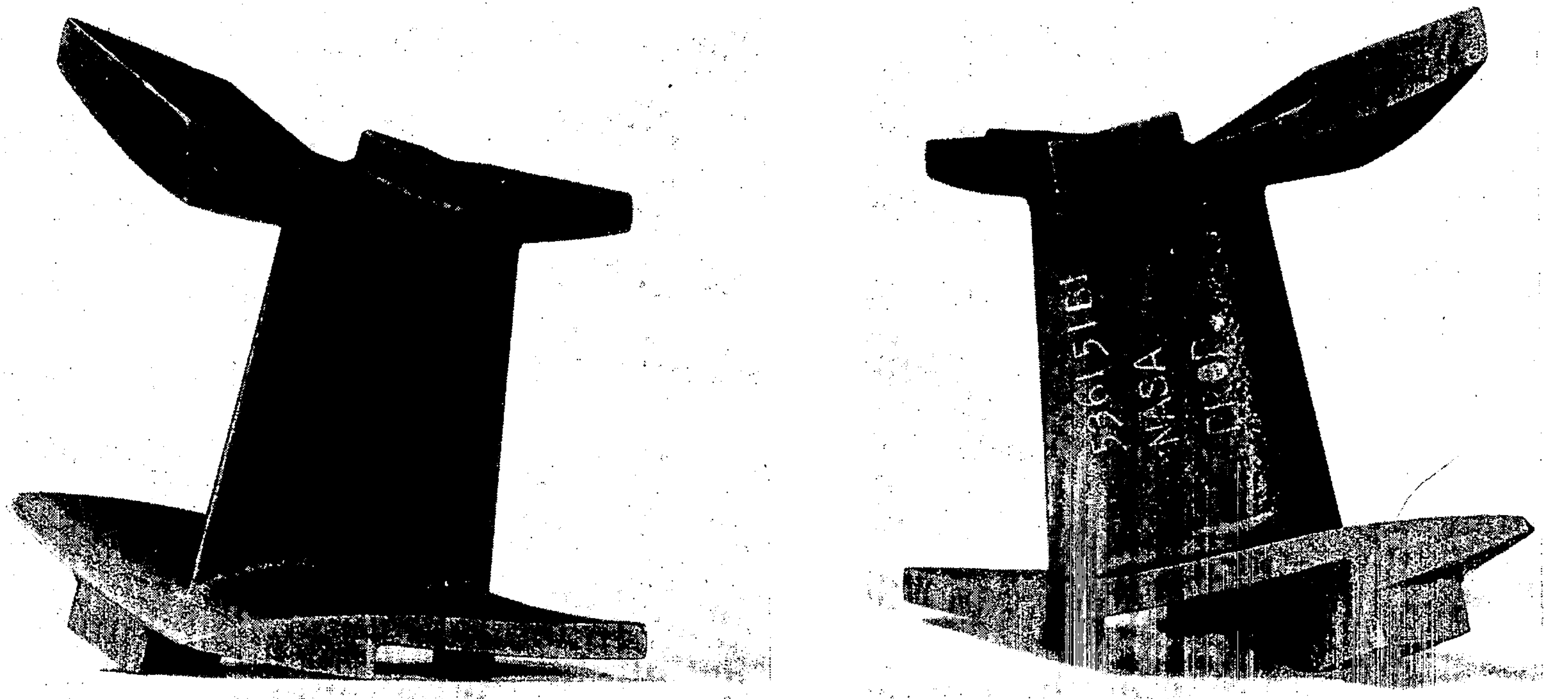

Figure 15 Turbine Nozzle Vane Casting

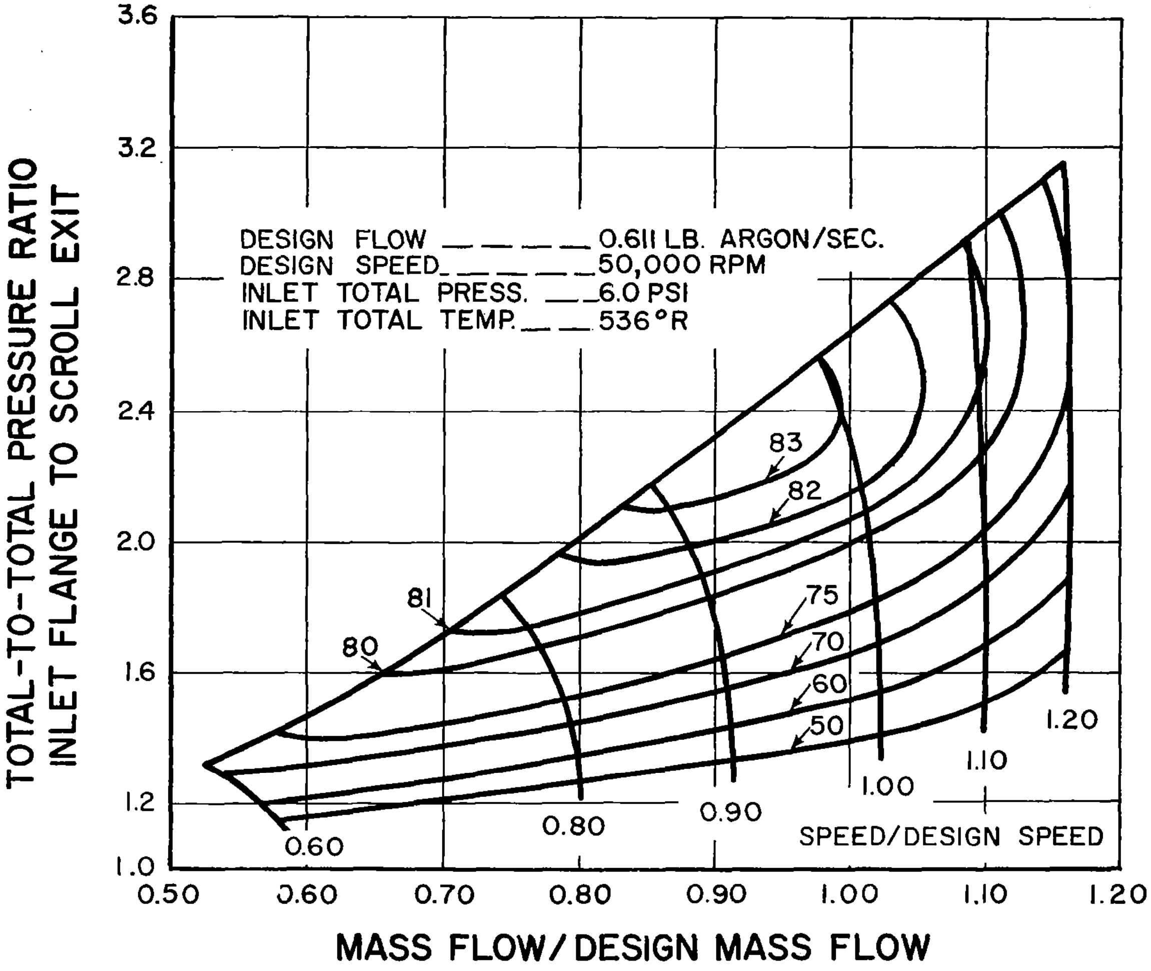

Figure 16 Estimated Compressor Efficiency from Inlet Flange to Scroll Exit Flange

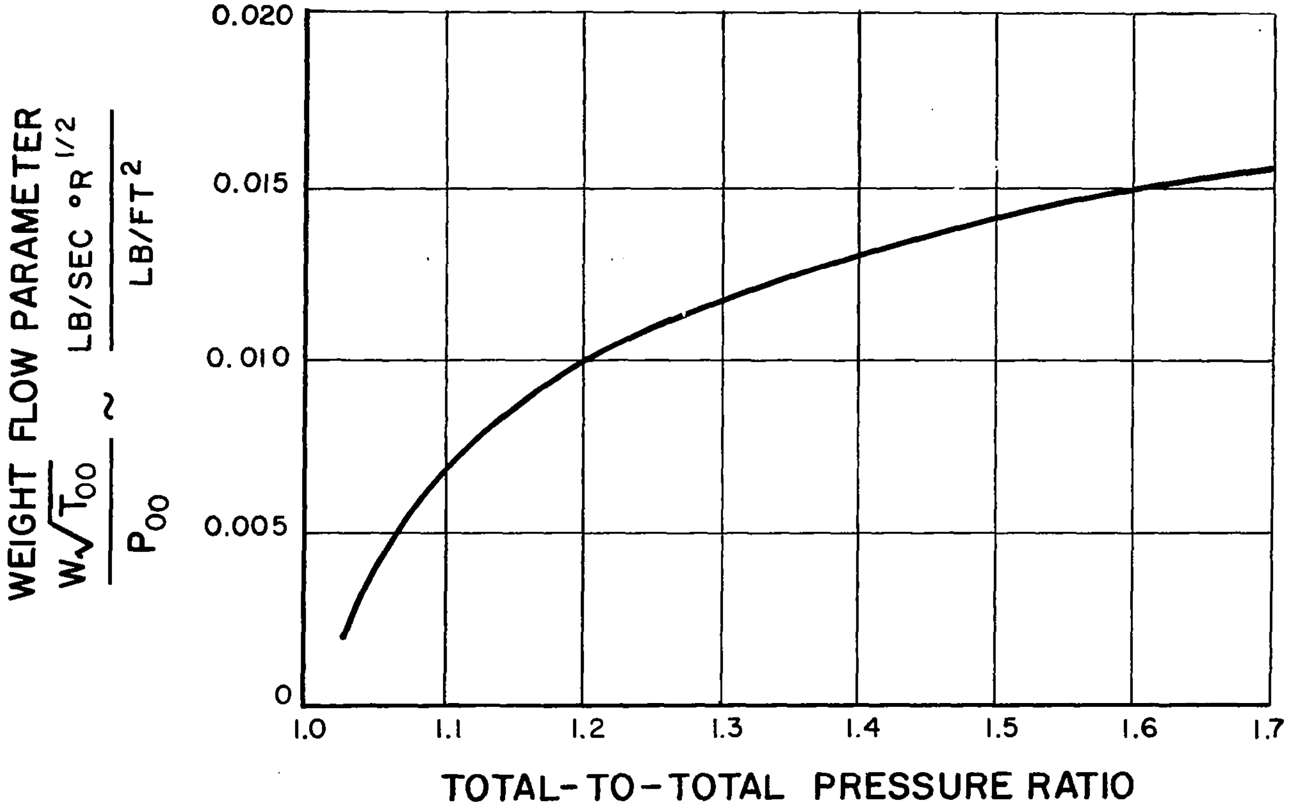

Figure 17 Predicted Turbine Weight Flow Parameter

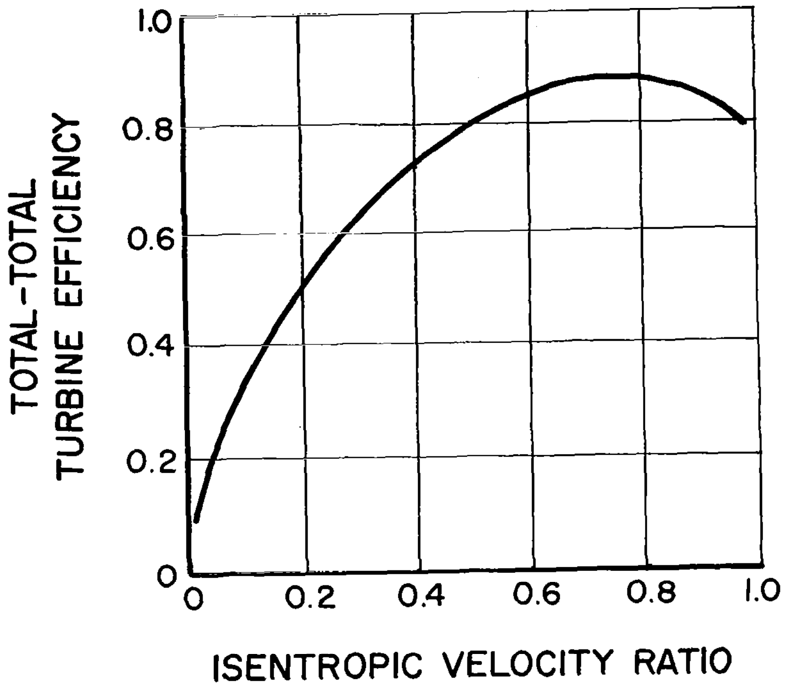

Figure 18 Estimated Turbine Off-Design Performance

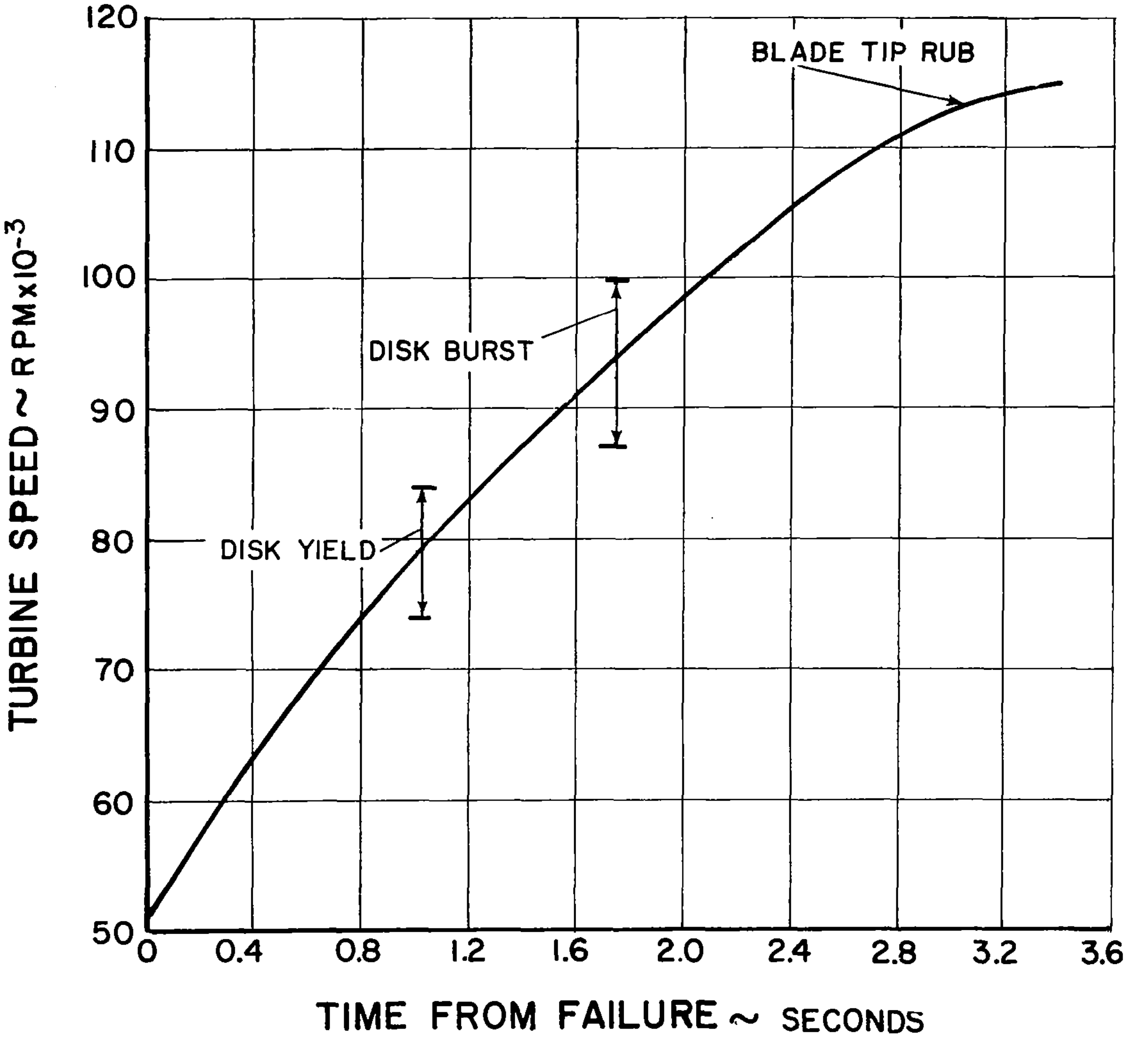

Figure 19 Rotor Runaway Condition

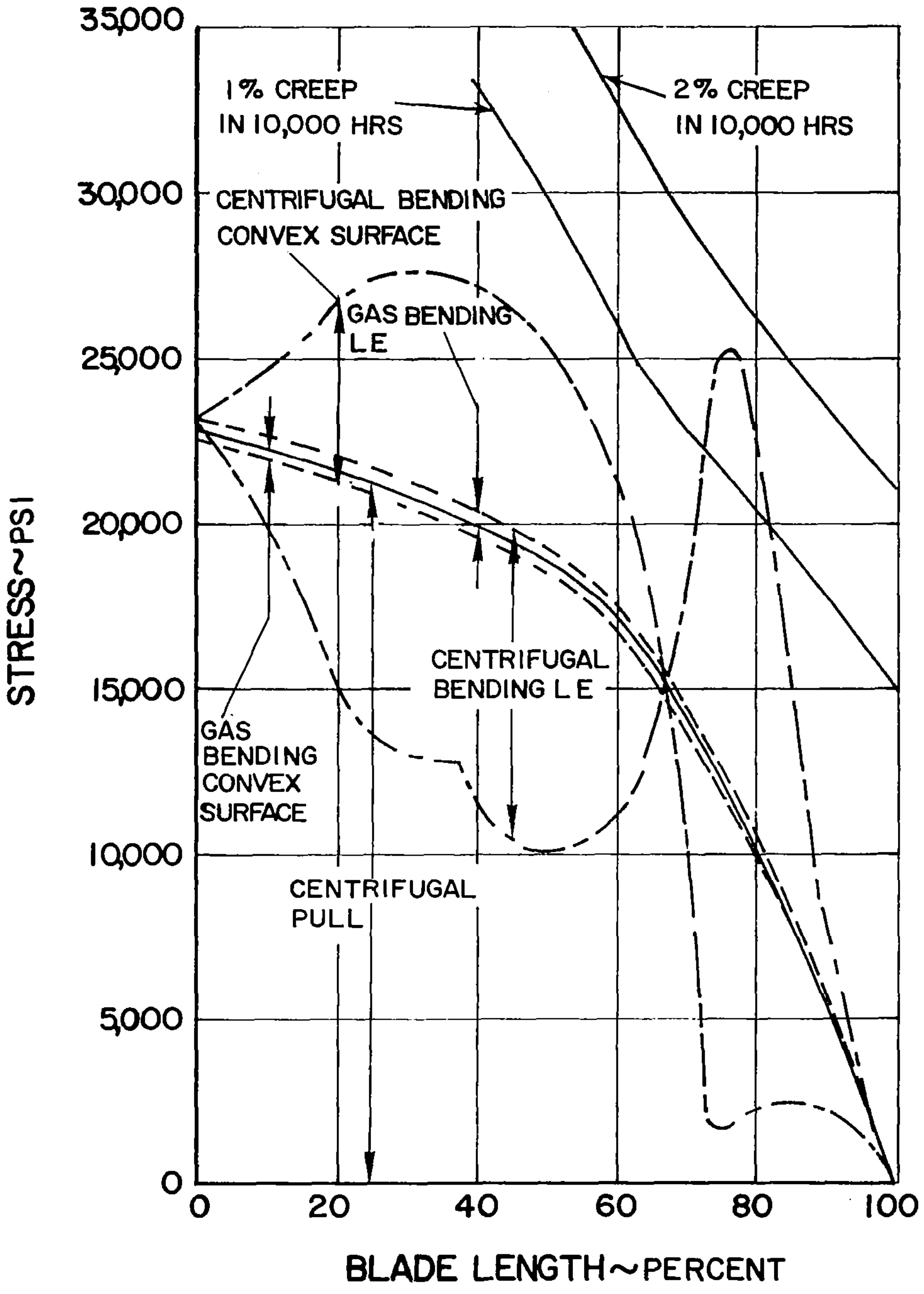

Figure 20 Turbine Blade Stress

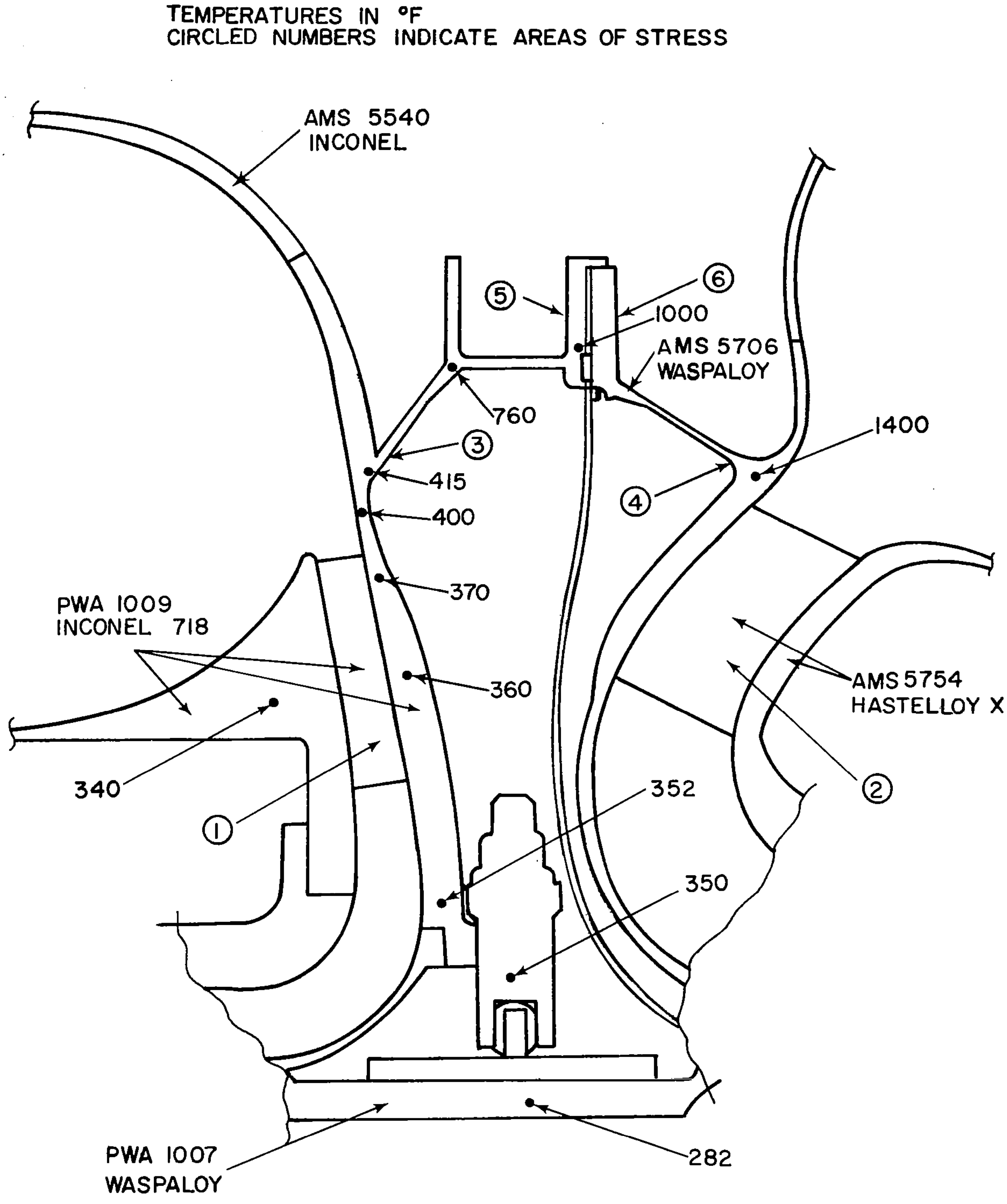
TEMPERATURES IN °F
CIRCLED NUMBERS INDICATE AREAS OF STRESS
AMS 5540
INCONEL
⑤
⑥
1000
AMS 5706
WASPALOY
760
③
1400
415
④
400
370
PWA 1009
INCONEL 718
AMS 5754
HASTELLOY X
360
340
352
①
②
350
PWA 1007
WASPALOY
282

Figure 21 Temperature Map of Scroll Area

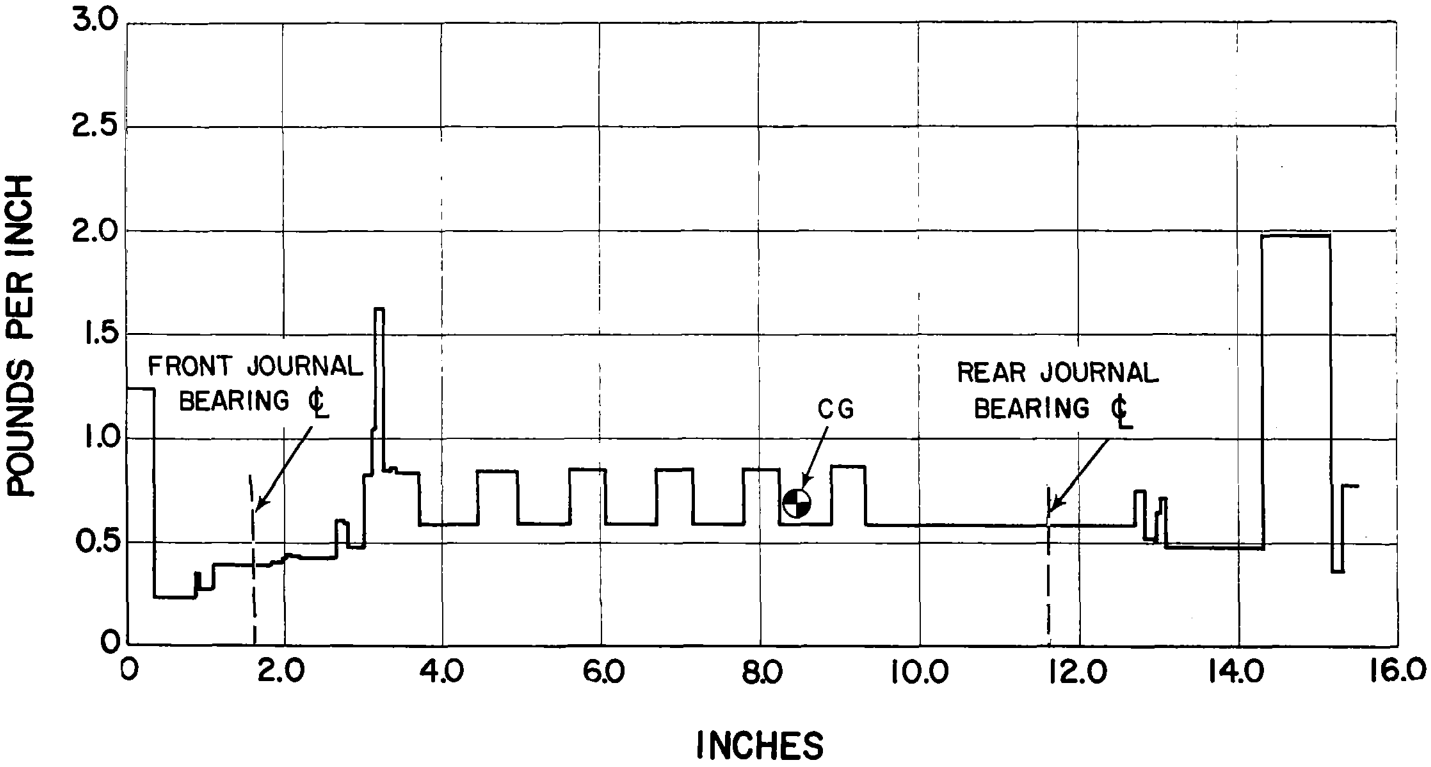

Figure 22 Mass Distribution of Rotor Assembly

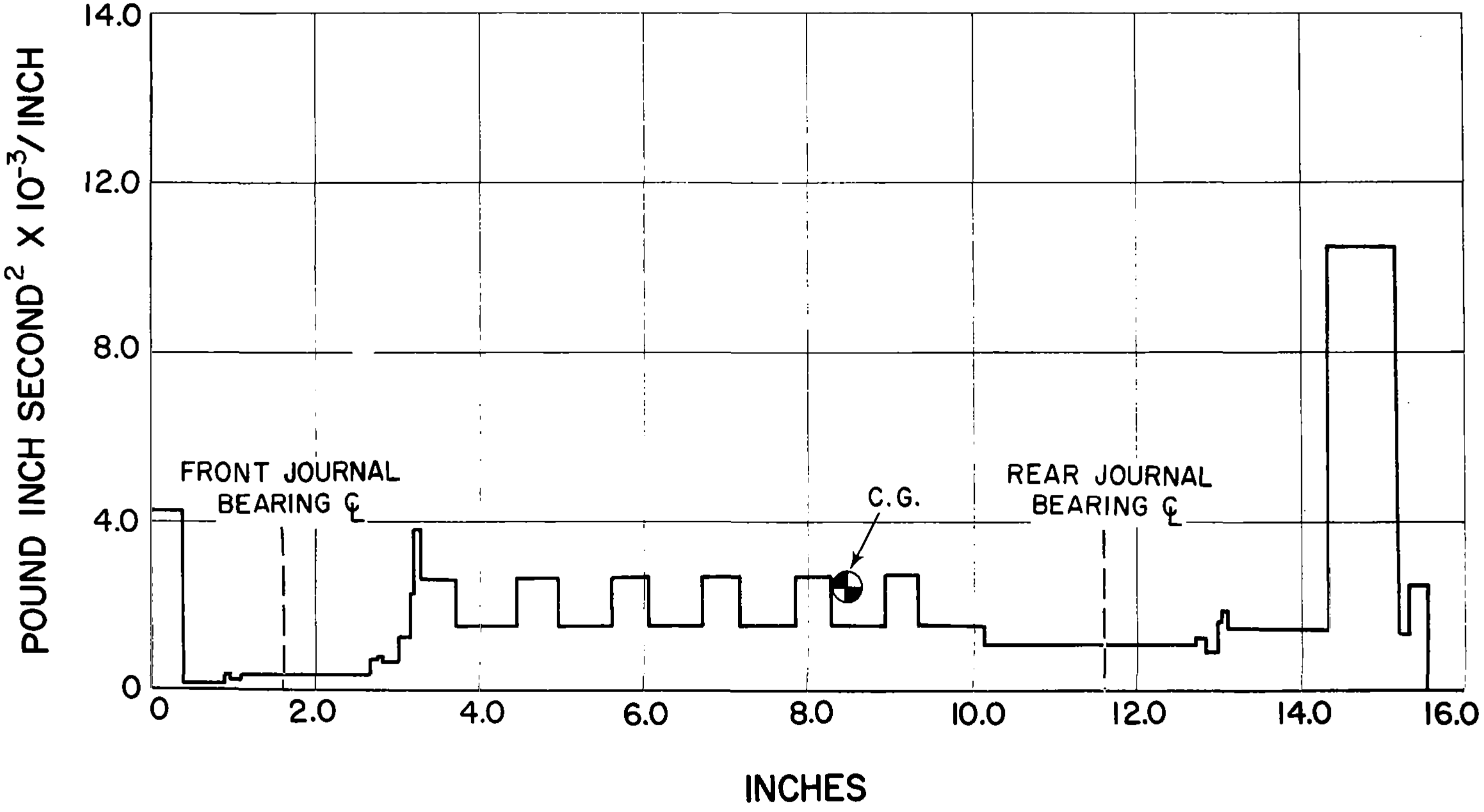

Figure 23 Distribution of Polar Moment of Inertia of Rotor Assembly

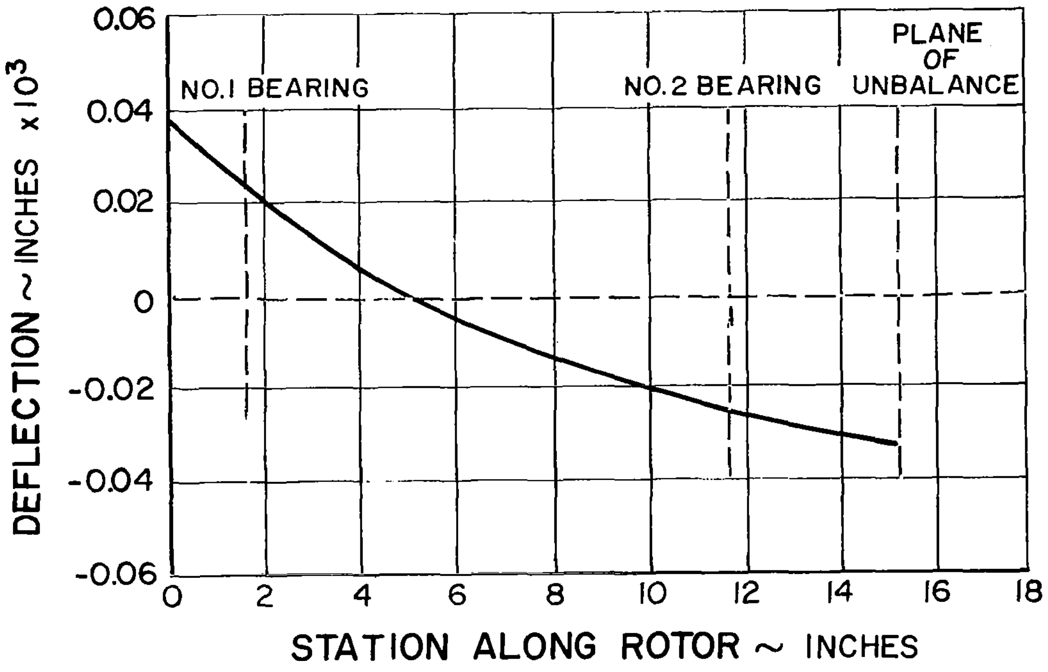

Figure 24 Turbine-Compressor Rotor Response at 50,000 rpm with 0.002 Ounce-Inch of Turbine Unbalance

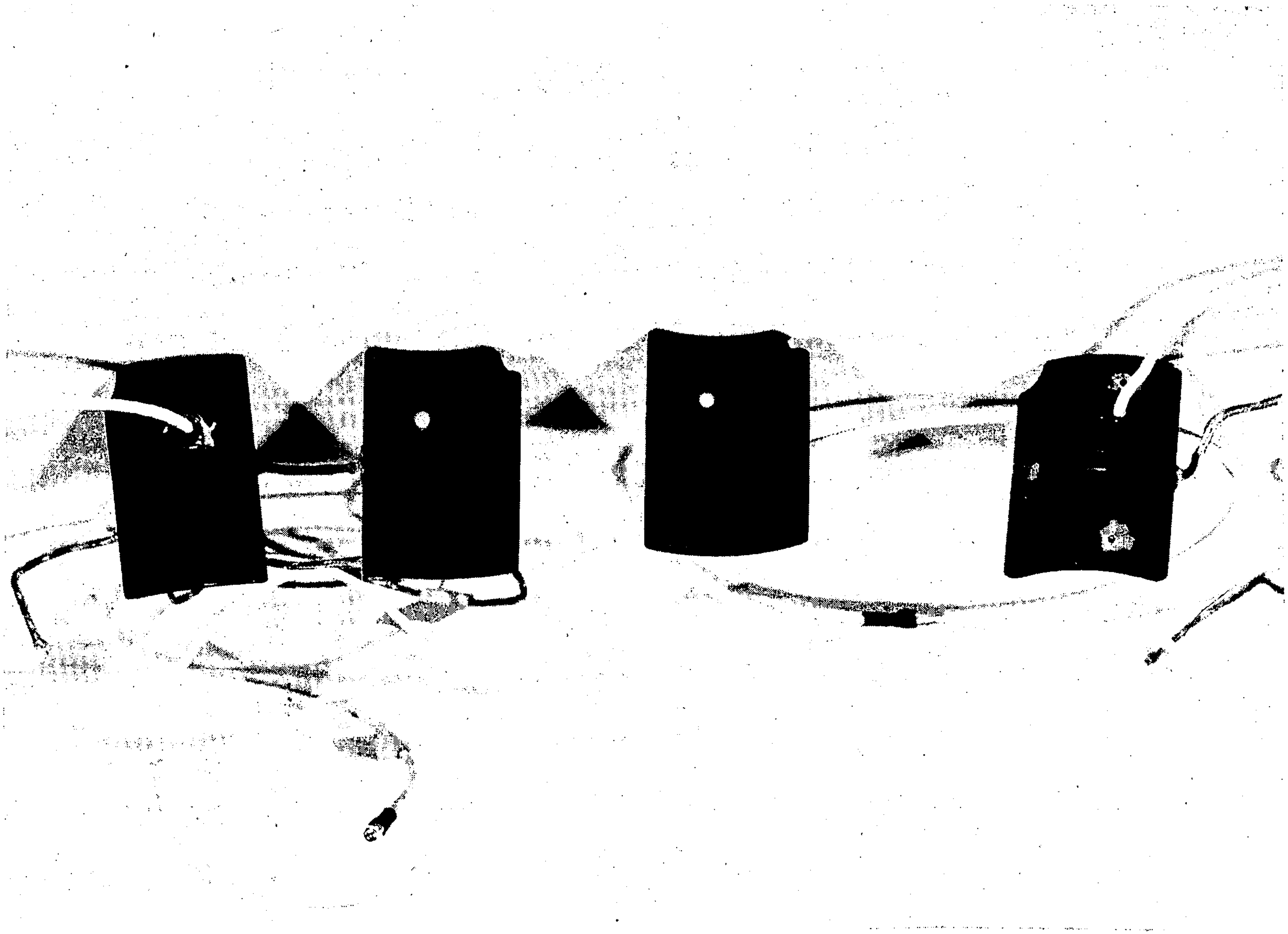

Figure 25 Front Journal Bearing Pads

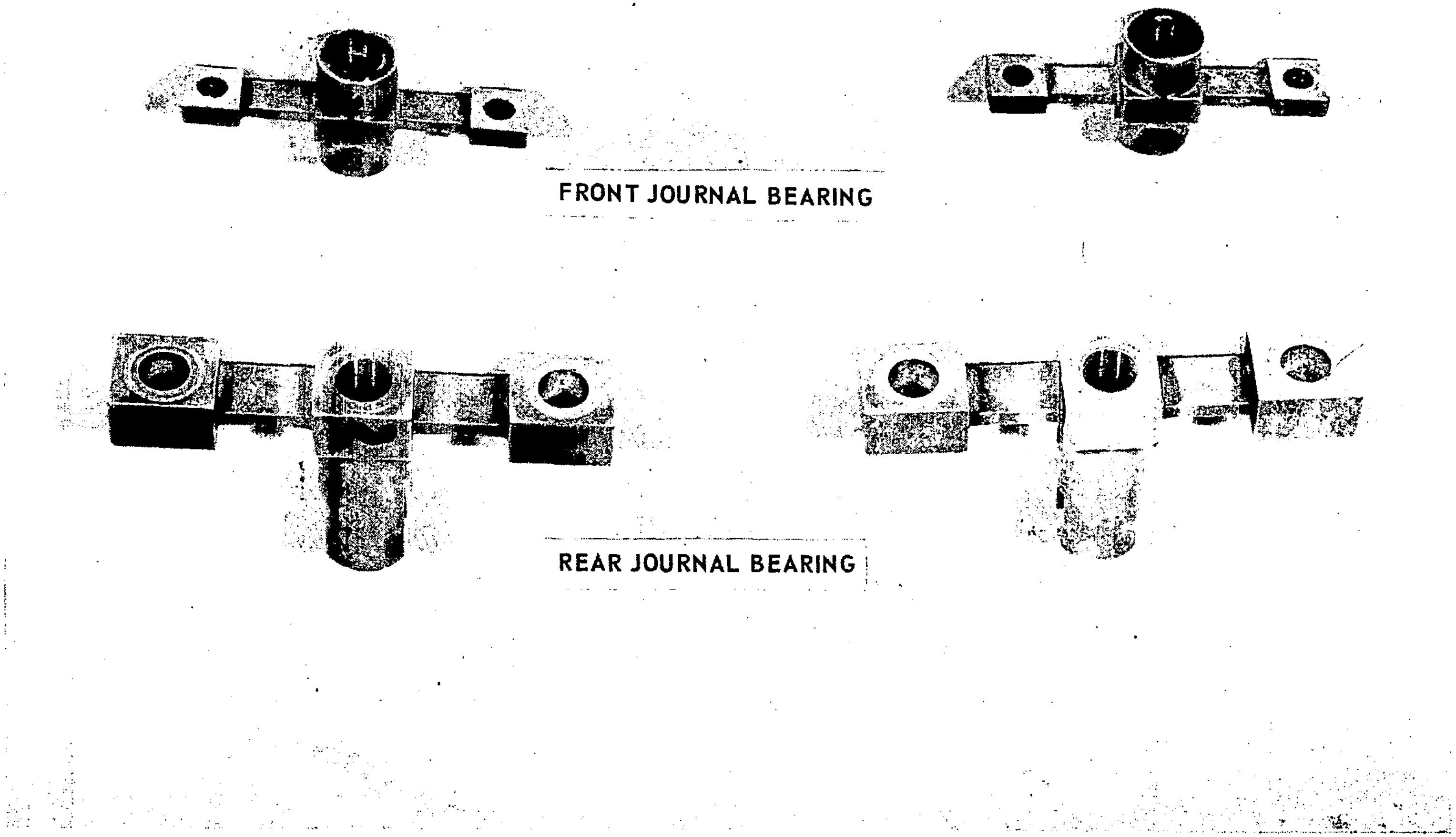
FRONT JOURNAL BEARING
REAR JOURNAL BEARING

Figure 26 High Spring Rate Flexures

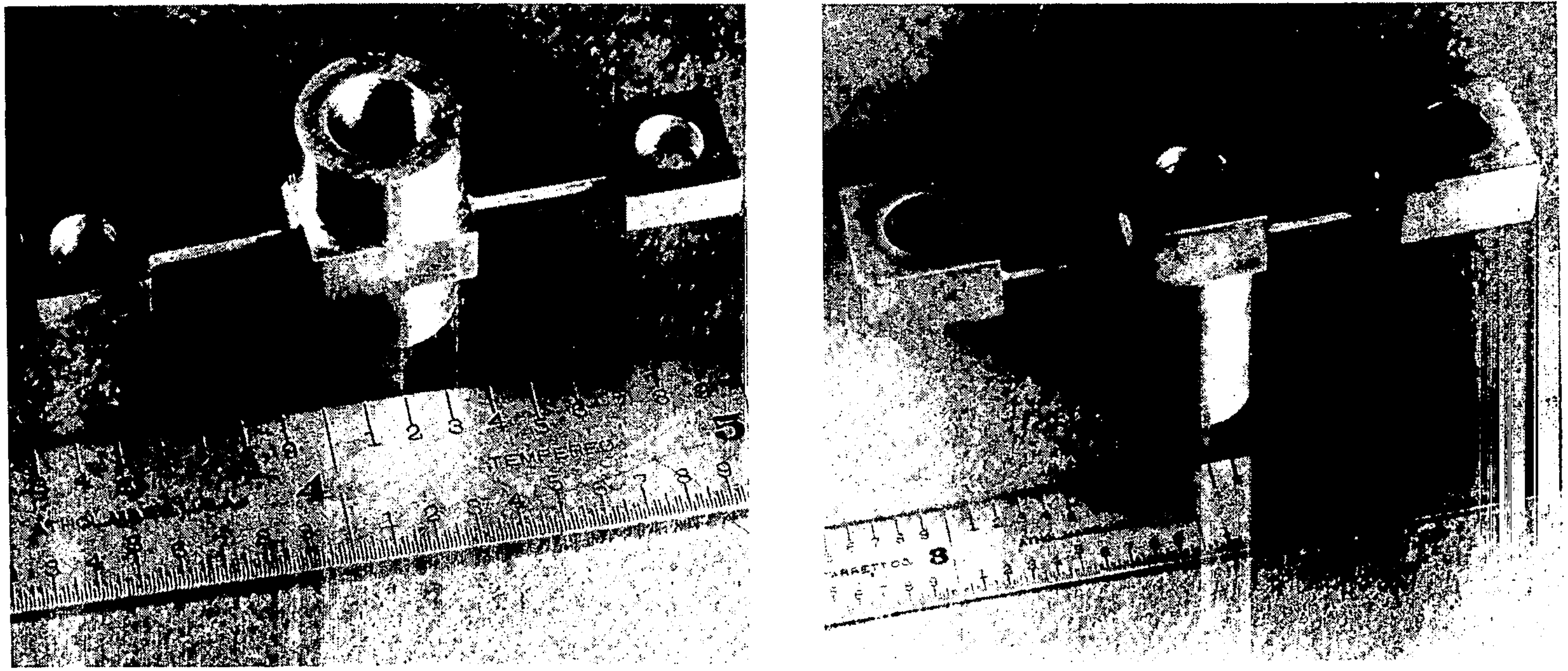

NO. 1 BEARING

NO. 2 BEARING

Figure 27 Low Spring Rate Flexures

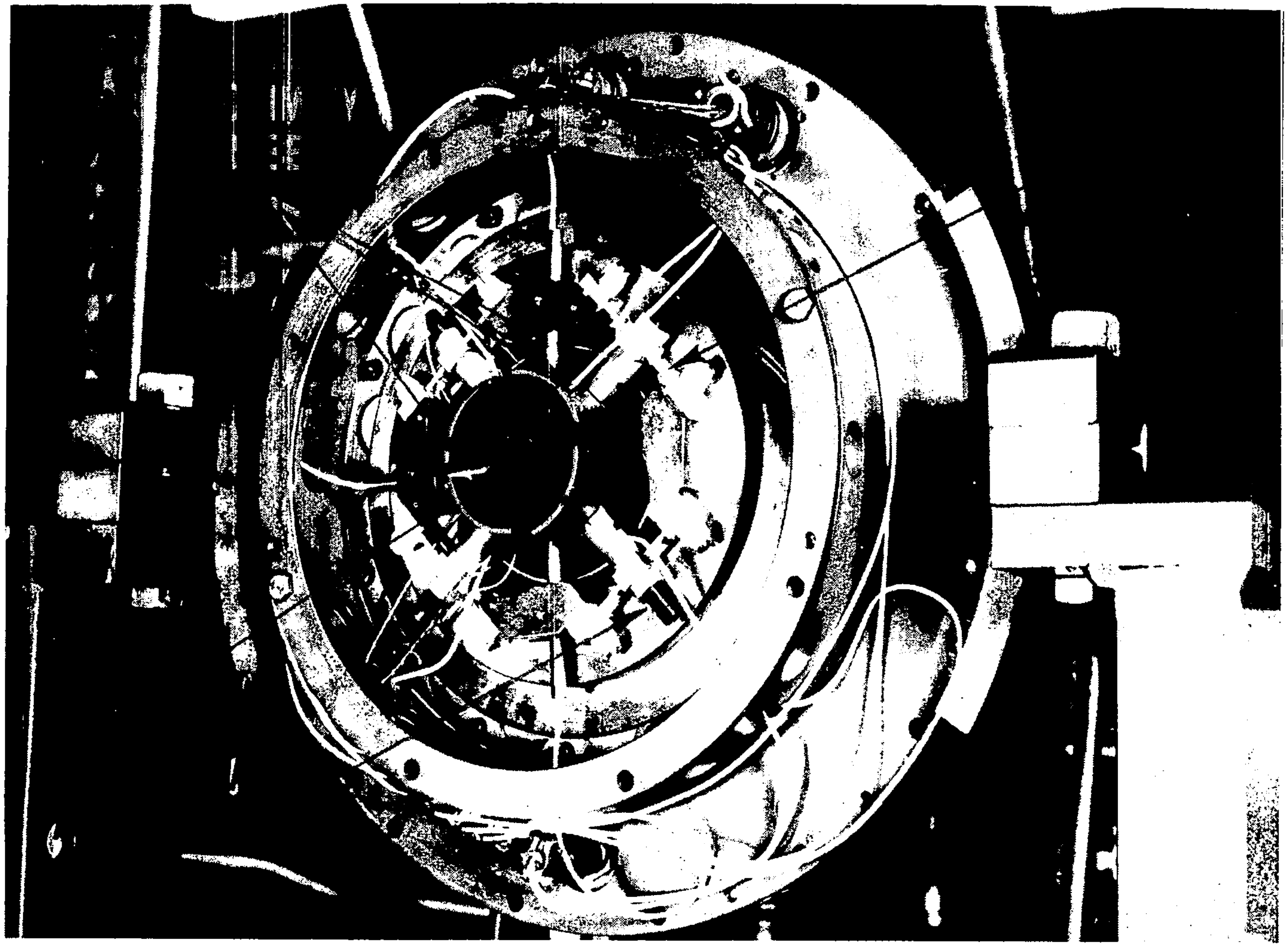

Figure 28 Turbine End of Number 2 Bearing

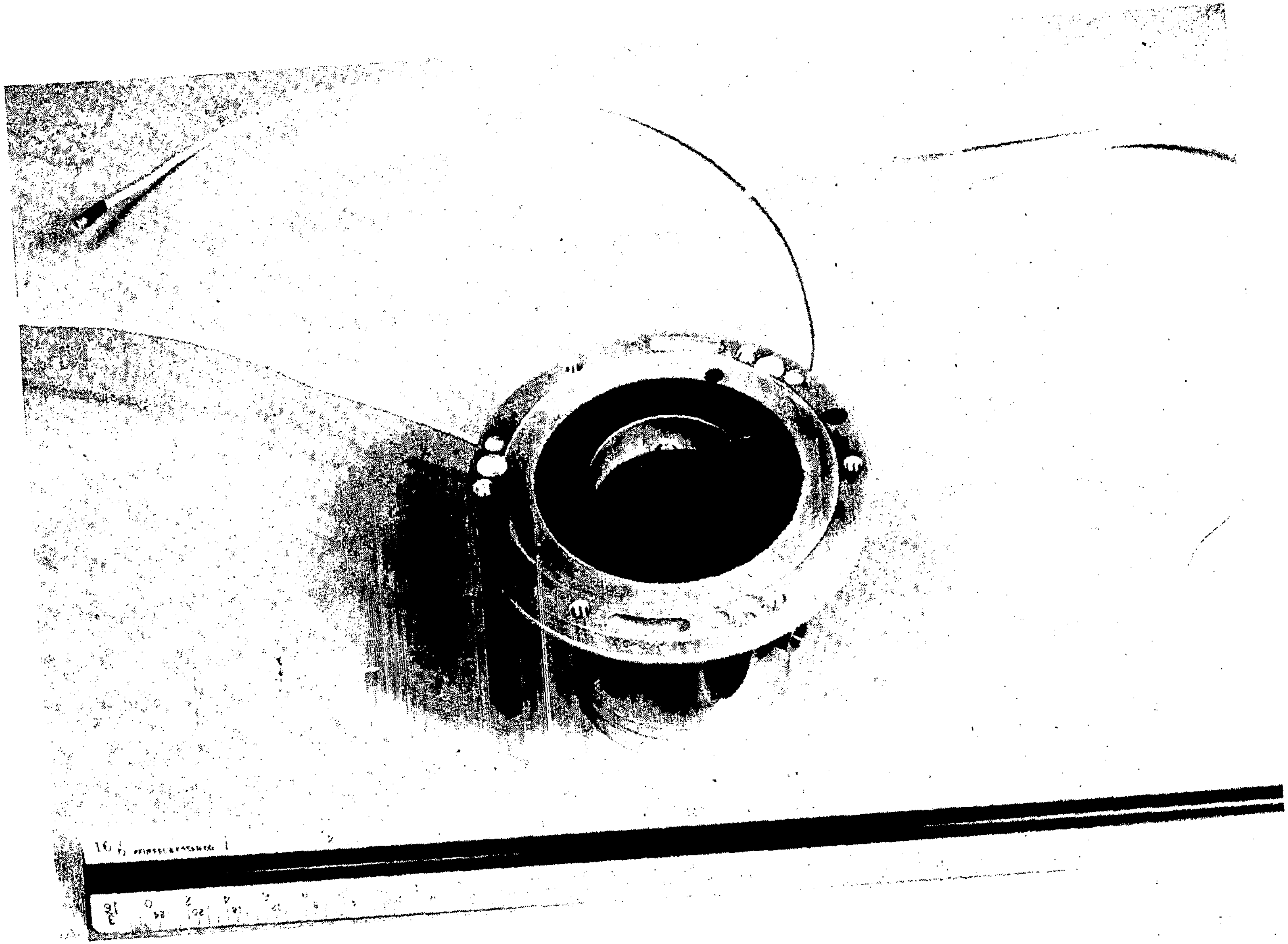

Bearing Support and Rear Thrust Stator

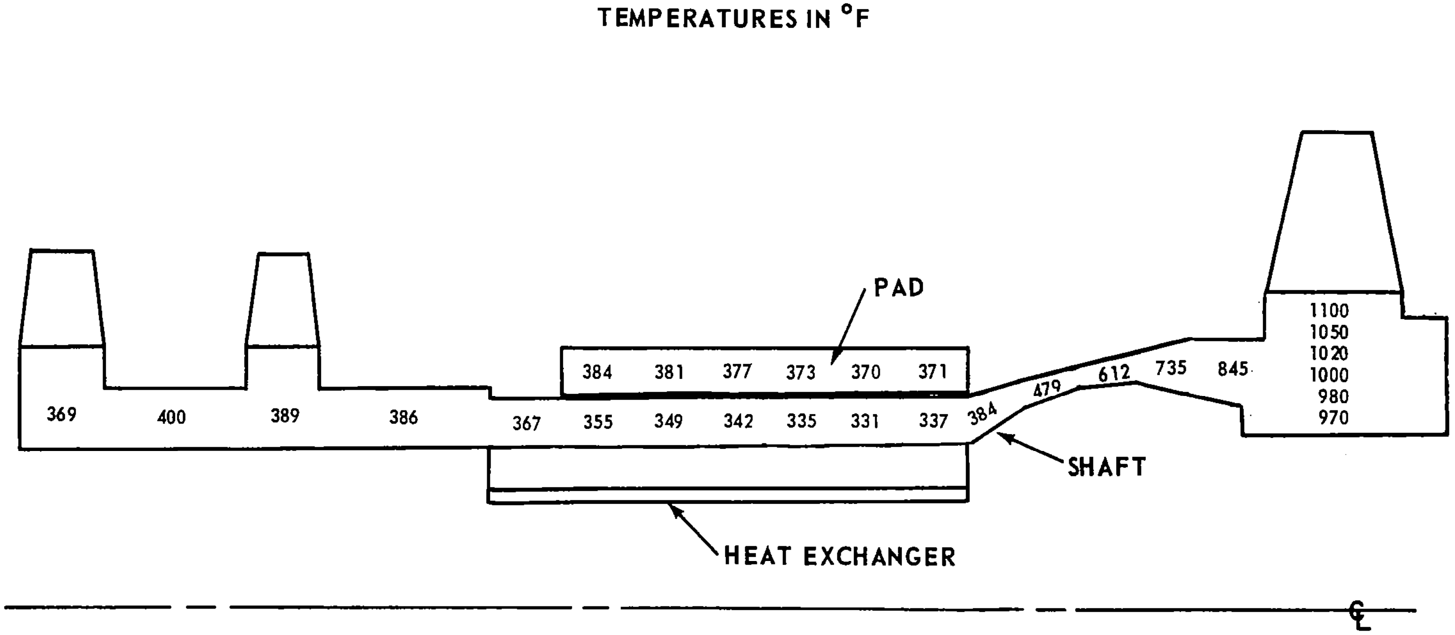
TEMPERATURES IN °F
PAD
384 381 377 373 370 371
369 400 389 386 367 355 349 342 335 331 337 384 479 612 735 845
1100
1050
1020
1000
980
970
SHAFT
HEAT EXCHANGER
℄

Figure 30 Temperature Map of Number 2 Bearing (Initial Design)

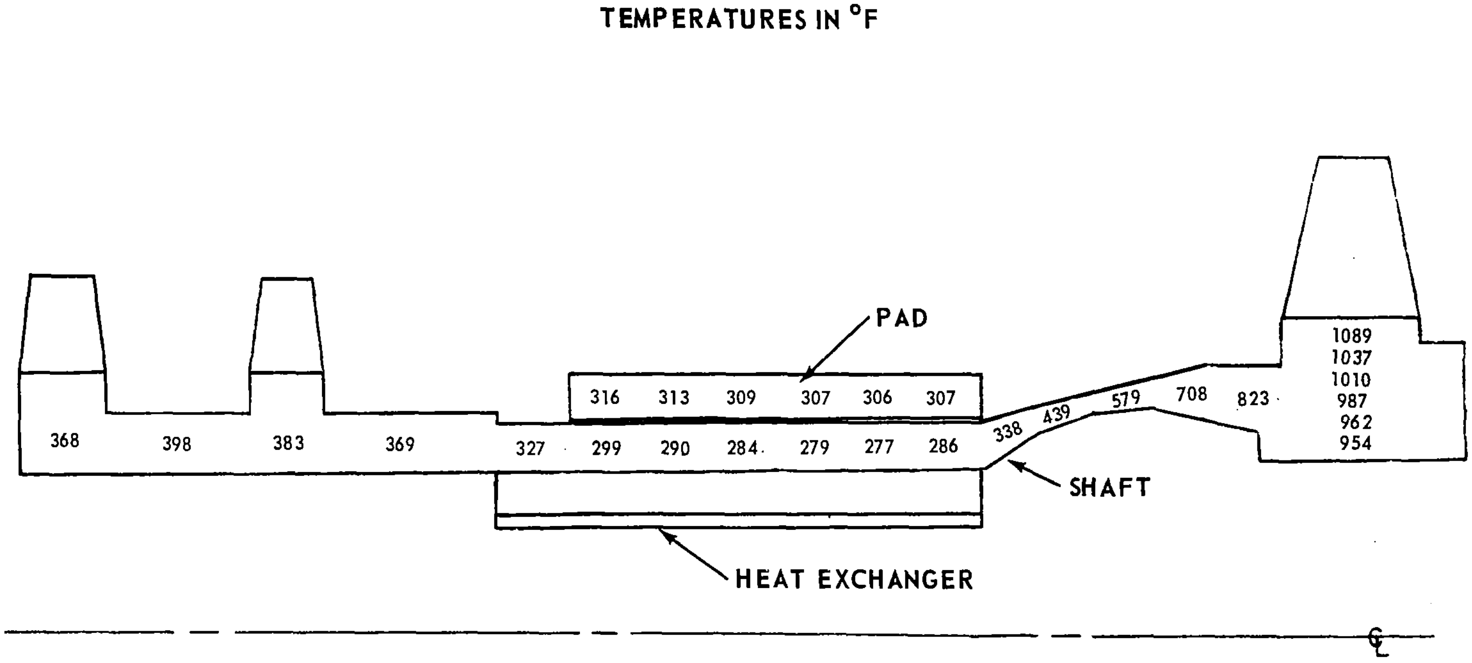
TEMPERATURES IN °F
PAD
316
313
309
307
306
307
368
398
383
369
327
299
290
284
279
277
286
338
439
579
708
823
1089
1037
1010
987
962
954
SHAFT
HEAT EXCHANGER
℄

Figure 31 Temperature Map of Number 2 Bearing (Final Design)

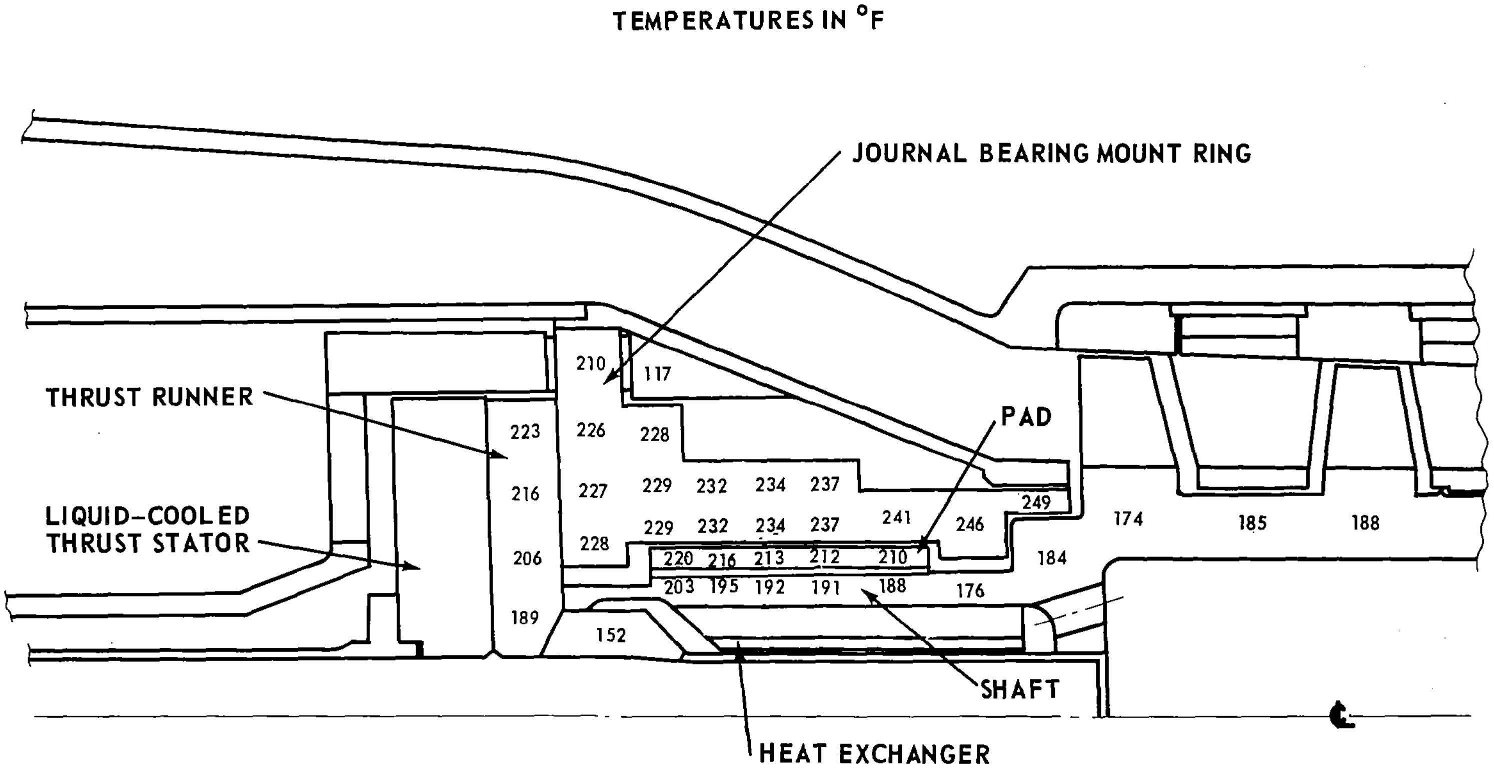
TEMPERATURES IN °F
JOURNAL BEARING MOUNT RING
210
117
THRUST RUNNER
223
226
228
PAD
216
227
229
232
234
237
249
LIQUID-COOLED THRUST STATOR
241
246
174
185
188
229
232
234
237
206
228
184
220
216
213
212
210
203
195
192
191
188
176
189
152
SHAFT
℄
HEAT EXCHANGER

Figure 32 Temperature Map of Number 1 Bearing (Initial Design)

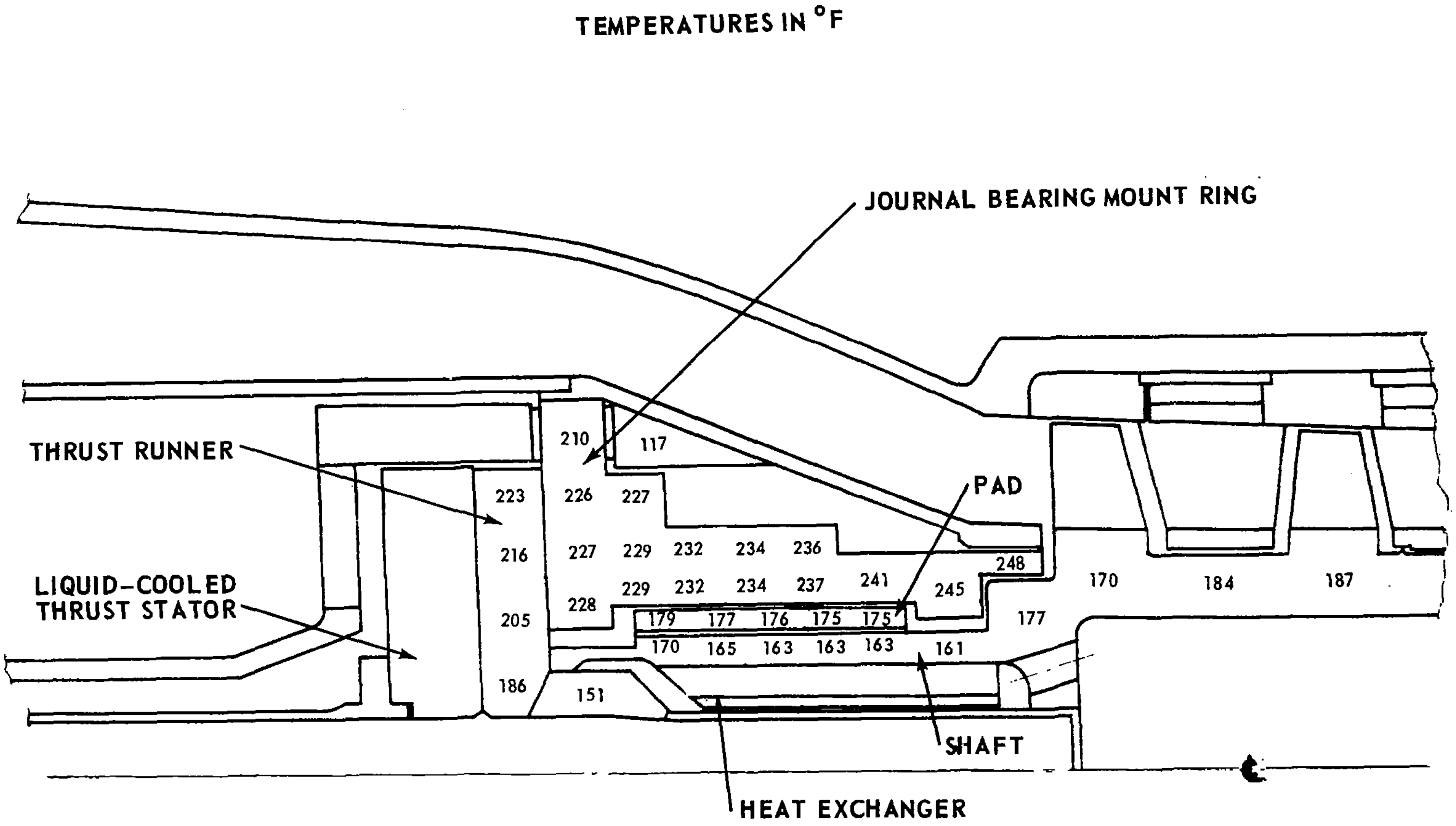
TEMPERATURES IN °F
JOURNAL BEARING MOUNT RING
THRUST RUNNER
PAD
LIQUID-COOLED THRUST STATOR
SHAFT
HEAT EXCHANGER
210
117
223
226
227
216
227
229
232
234
236
205
228
229
232
234
237
241
245
248
170
184
187
179
177
176
175
175
177
170
165
163
163
163
161
186
151
℄

Figure 33 Temperature Map of Number 1 Bearing (Final Design)

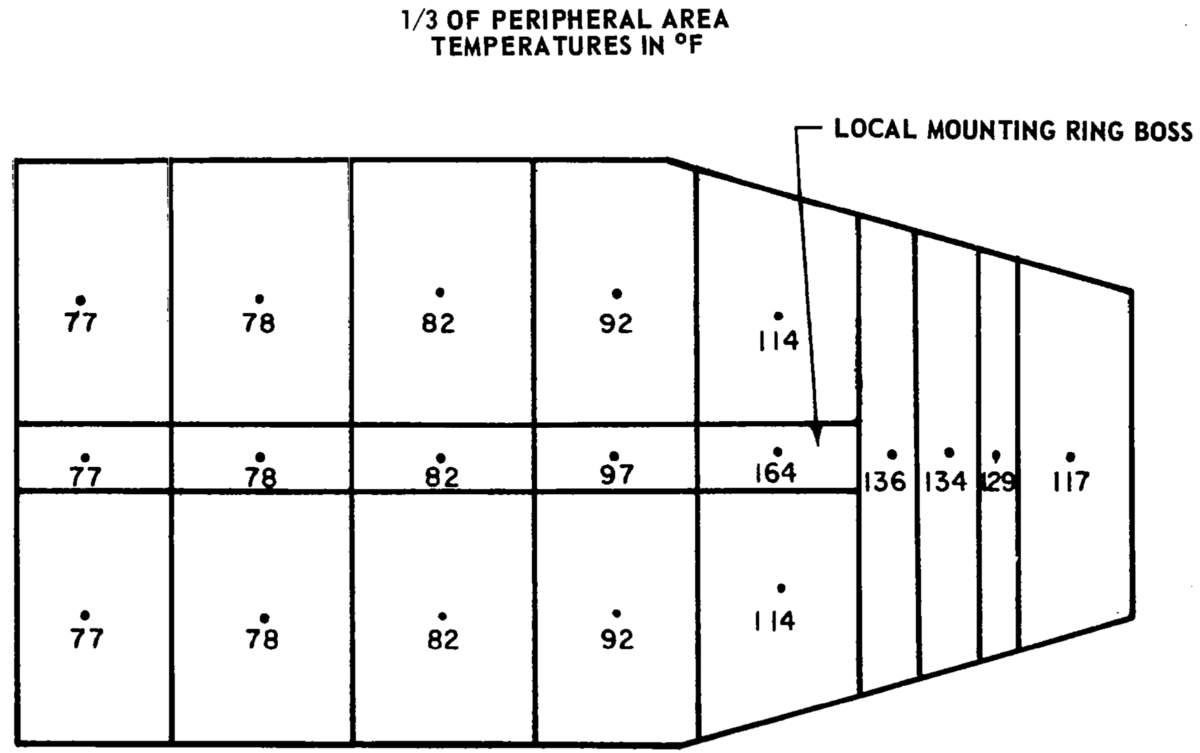
1/3 OF PERIPHERAL AREA
TEMPERATURES IN °F
LOCAL MOUNTING RING BOSS
77
78
82
92
114
77
78
82
97
164
136
134
129
117
77
78
82
92
114

Figure 34 Temperature Map of Turbine-Compressor Inlet Duct

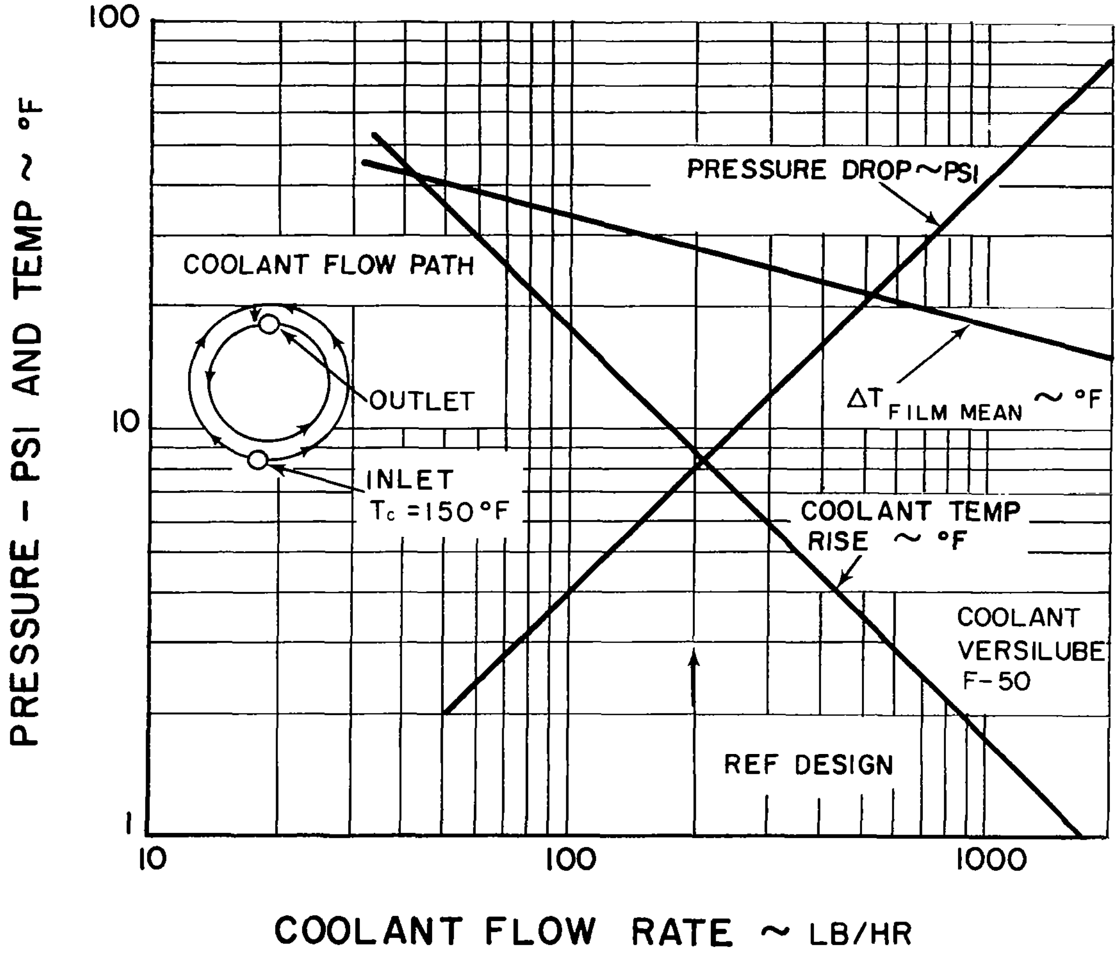

Figure 35 Thrust Bearing Coolant Performance

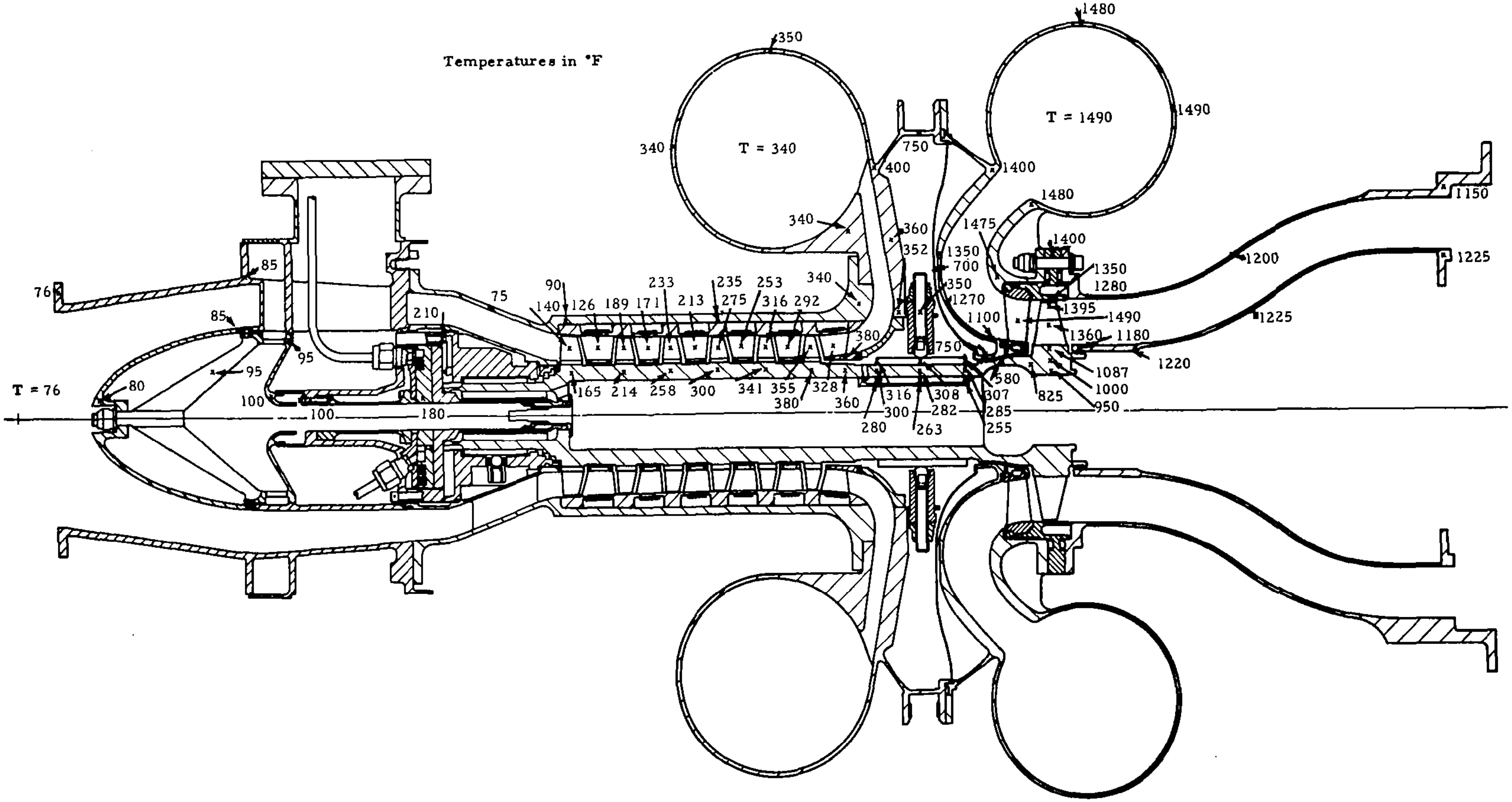
Temperatures in °F
T = 76
76
80
85
85
95
95
100
100
180
210
75
90
140
126
189
171
233
213
235
275
253
316
292
340
165
214
258
300
341
355
380
328
360
380
T = 340
340
340
350
750
400
360
352
1350
700
350
1270
1100
750
316
308
300
282
280
263
307
285
255
T = 1490
1480
1490
1400
1480
1475
1400
1350
1280
1395
1490
1360
1180
580
825
1087
1000
950
1220
1200
1225
1225
1150

Figure 36 Turbine-Compressor Temperature Map

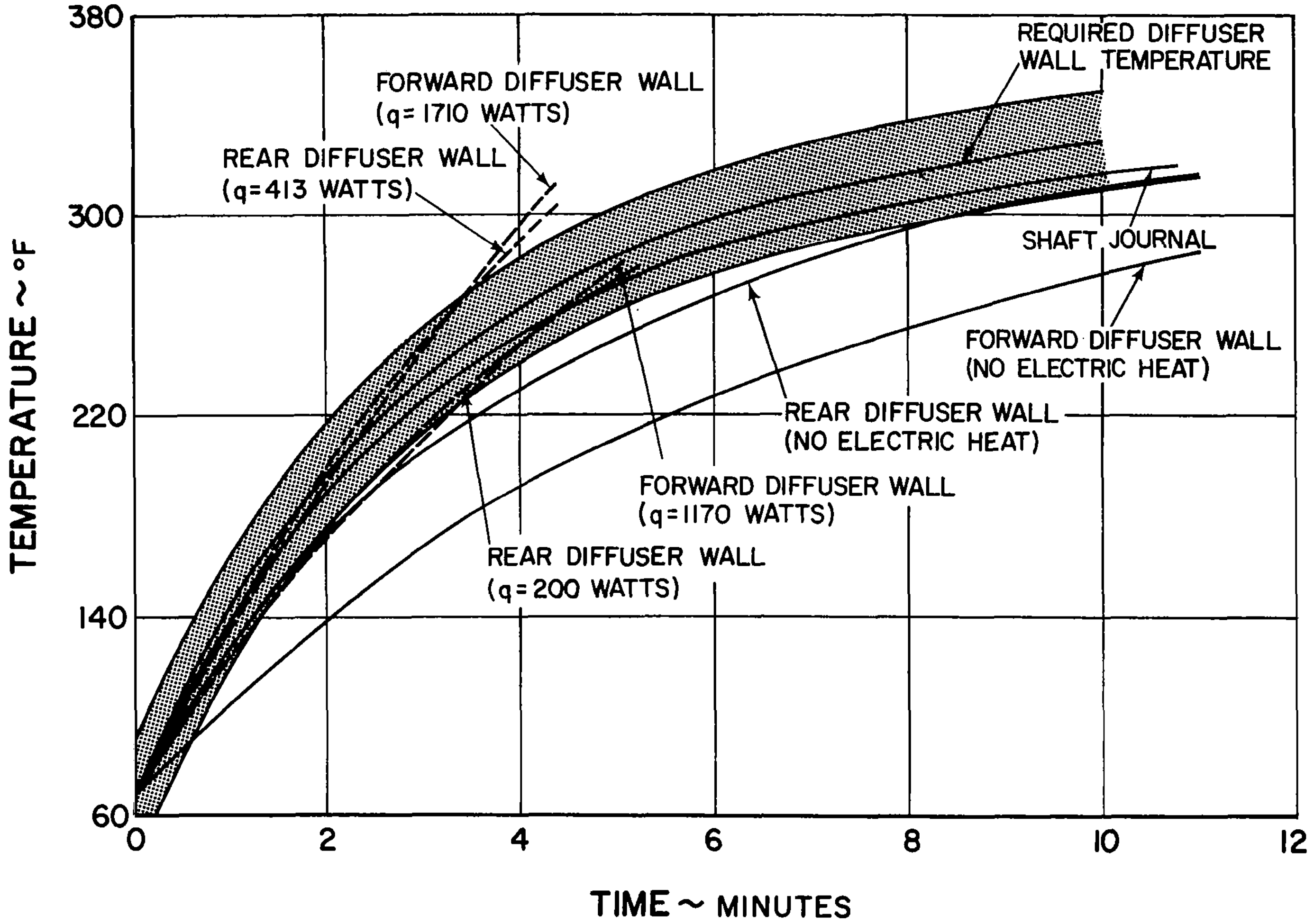

Figure 37 Temperature Transient in Number 2 Bearing (Initial Design)

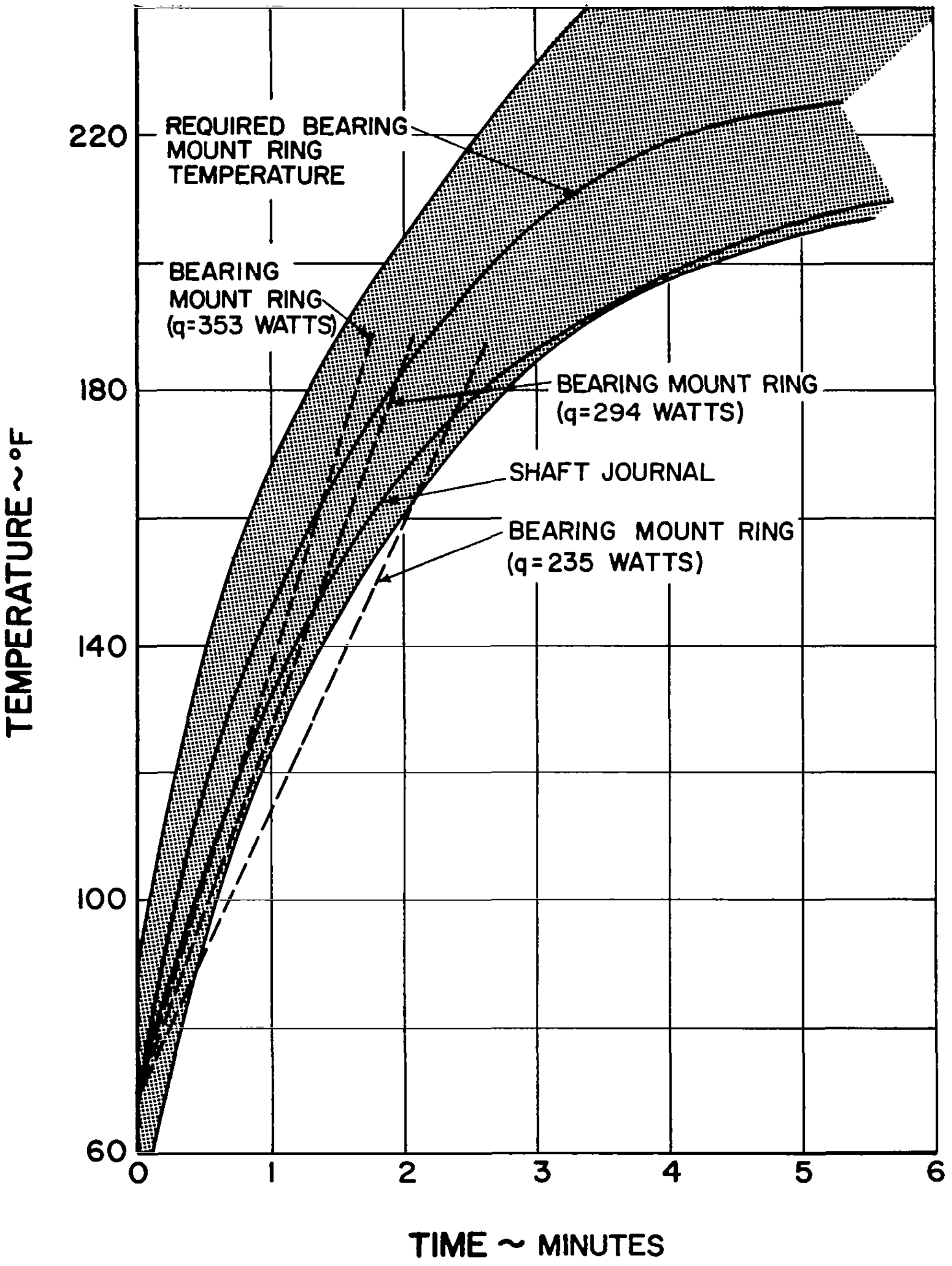

Figure 38 Temperature Transient in Number 1 Bearing (Initial Design)

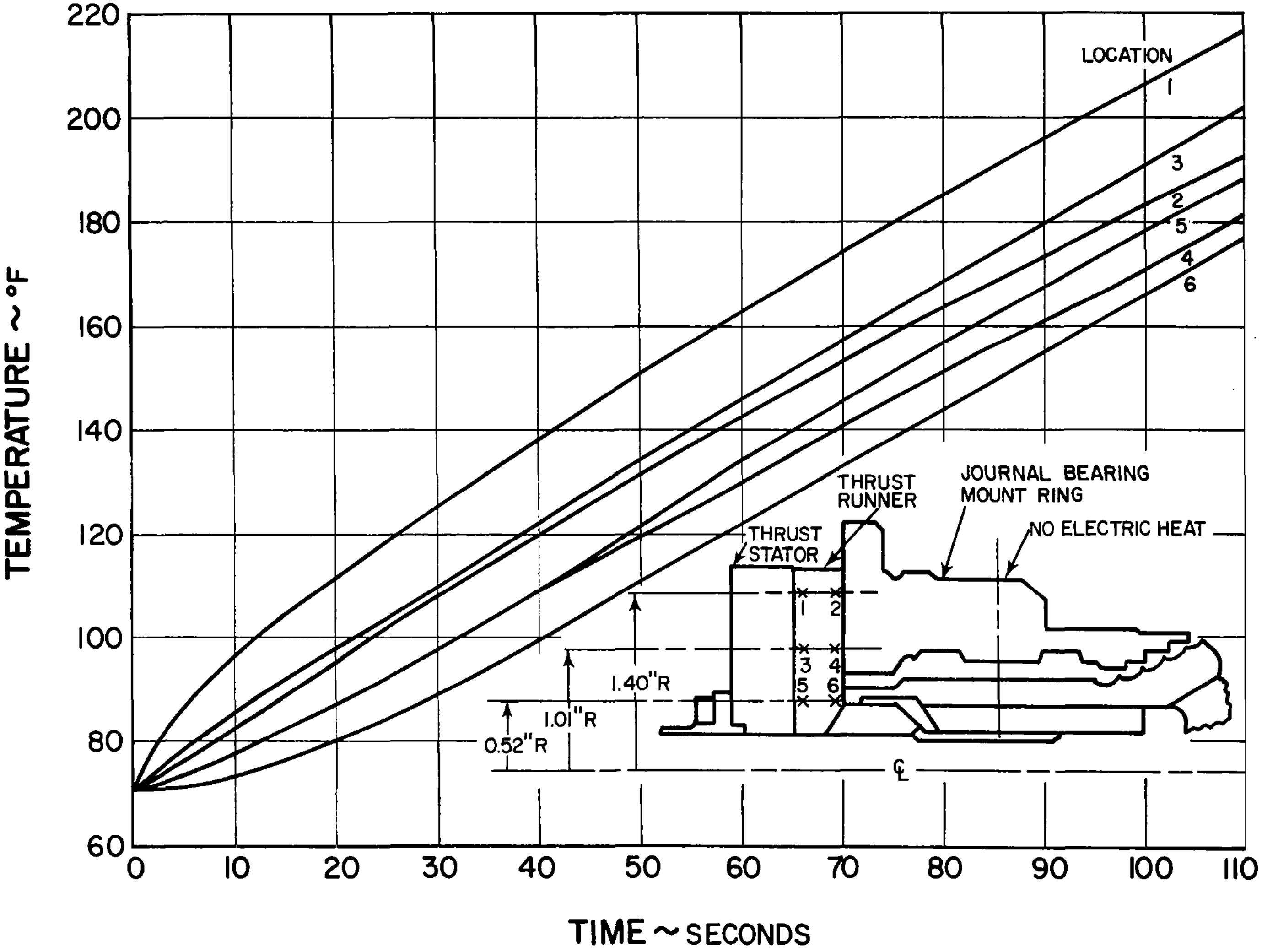

Figure 39 Transient Temperature Response of Thrust Bearing. No Stator Cooling. No Mount Ring Heat

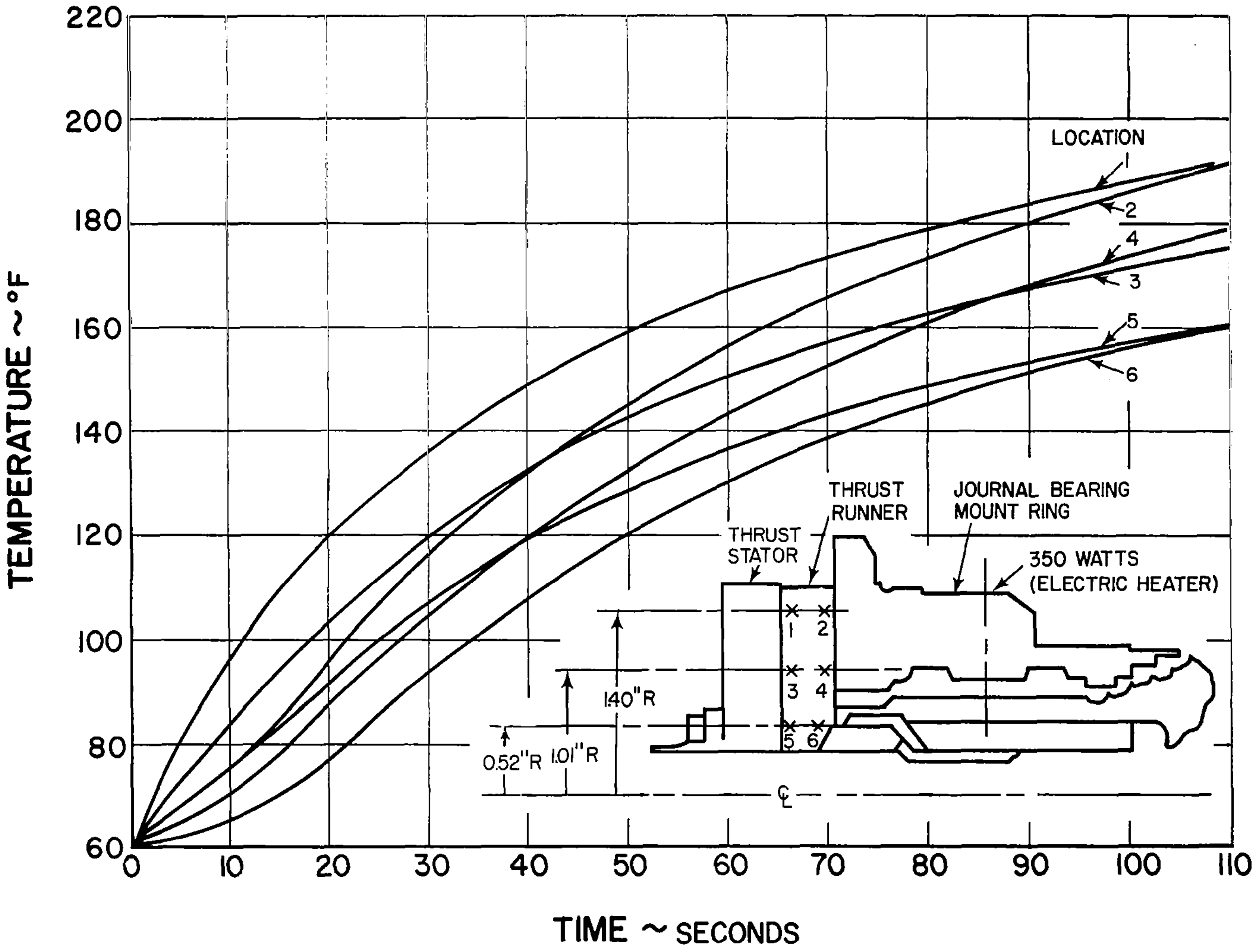

Figure 40 Transient Temperature Response of Thrust Bearing. Stator Cooling at T_c = 150°F. Mount Ring Heated

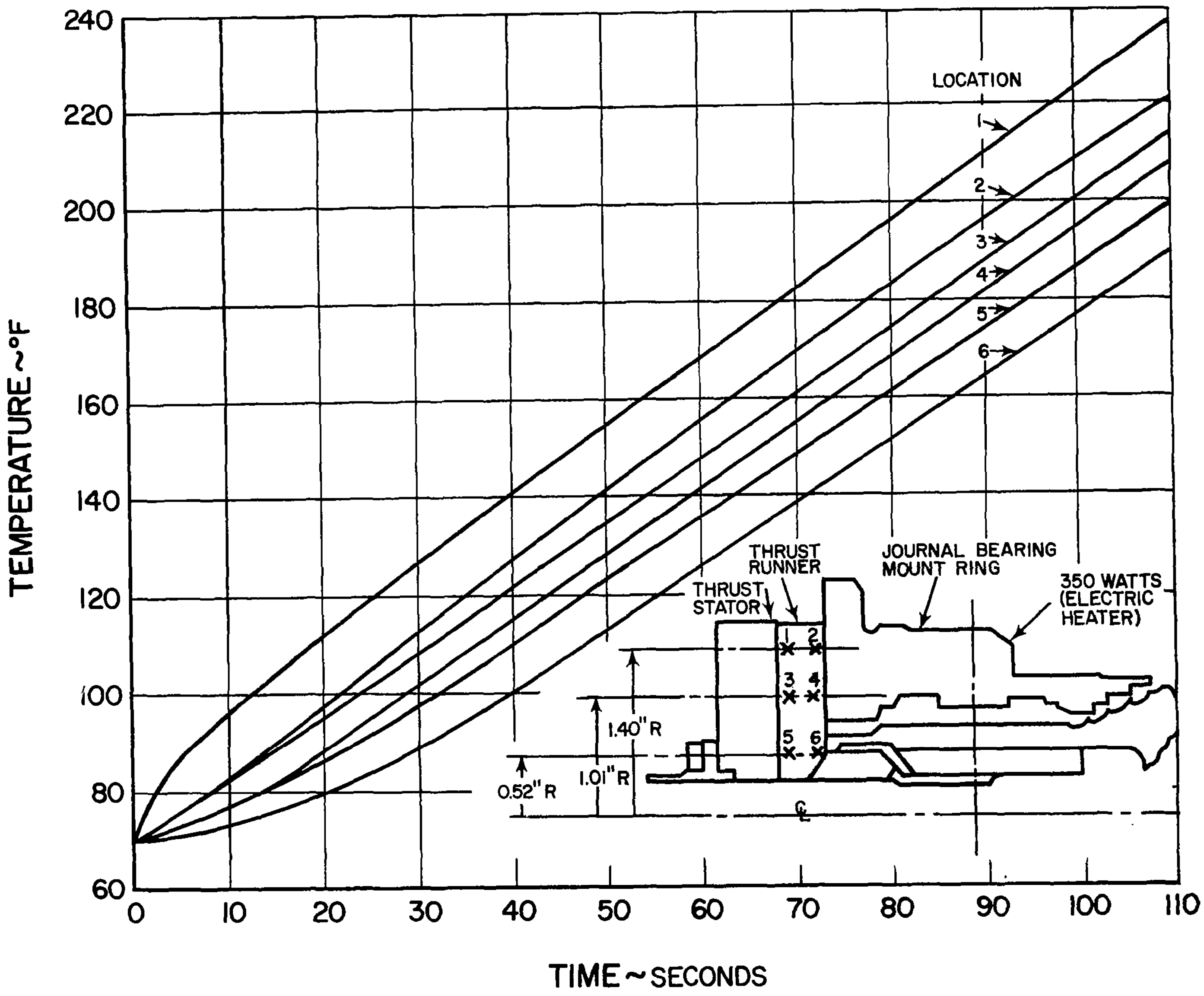

Figure 41 Transient Temperature Response of Thrust Bearing. No Stator Cooling. Mount Ring Heated

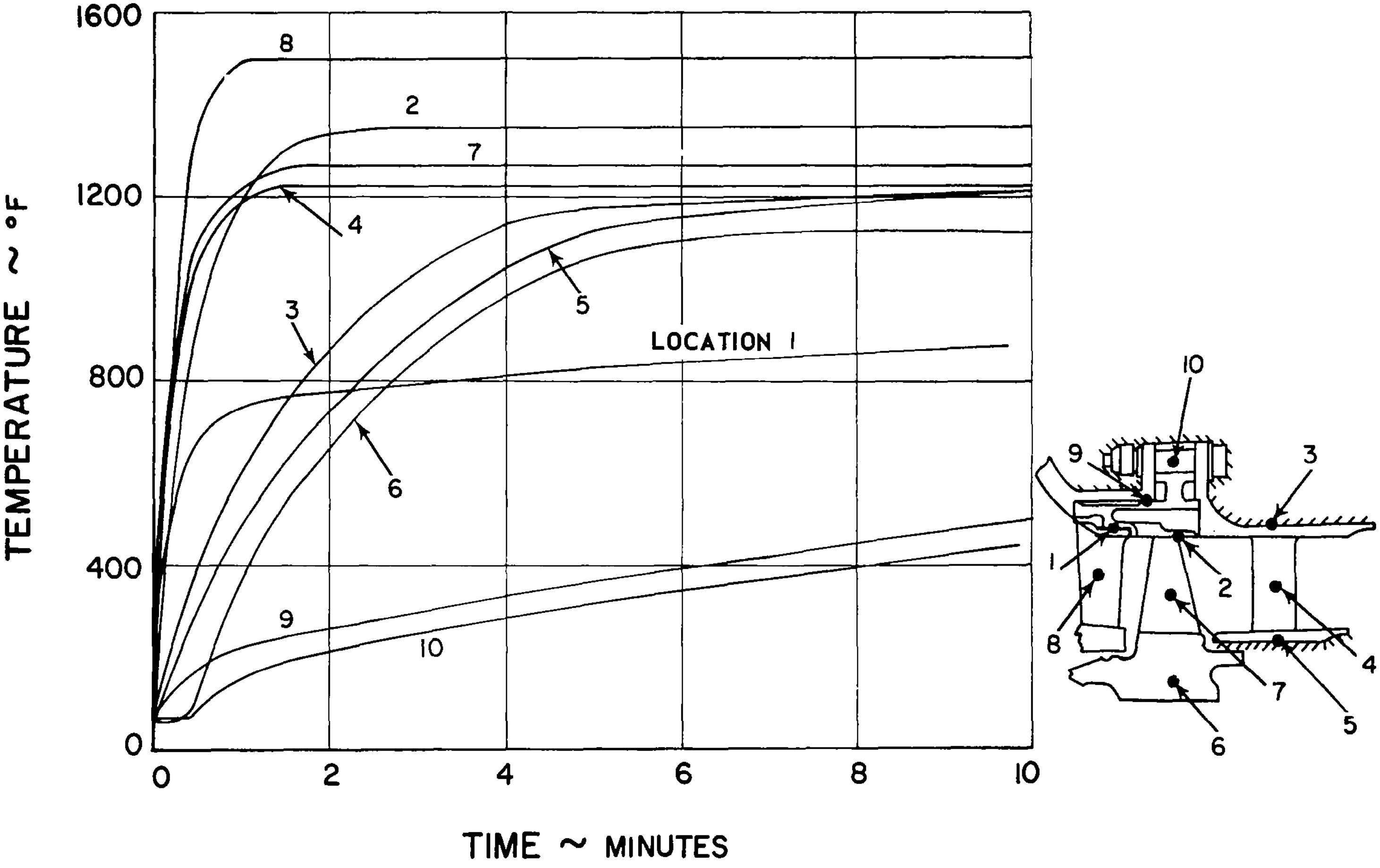

Figure 42 Turbine Thermal Transient

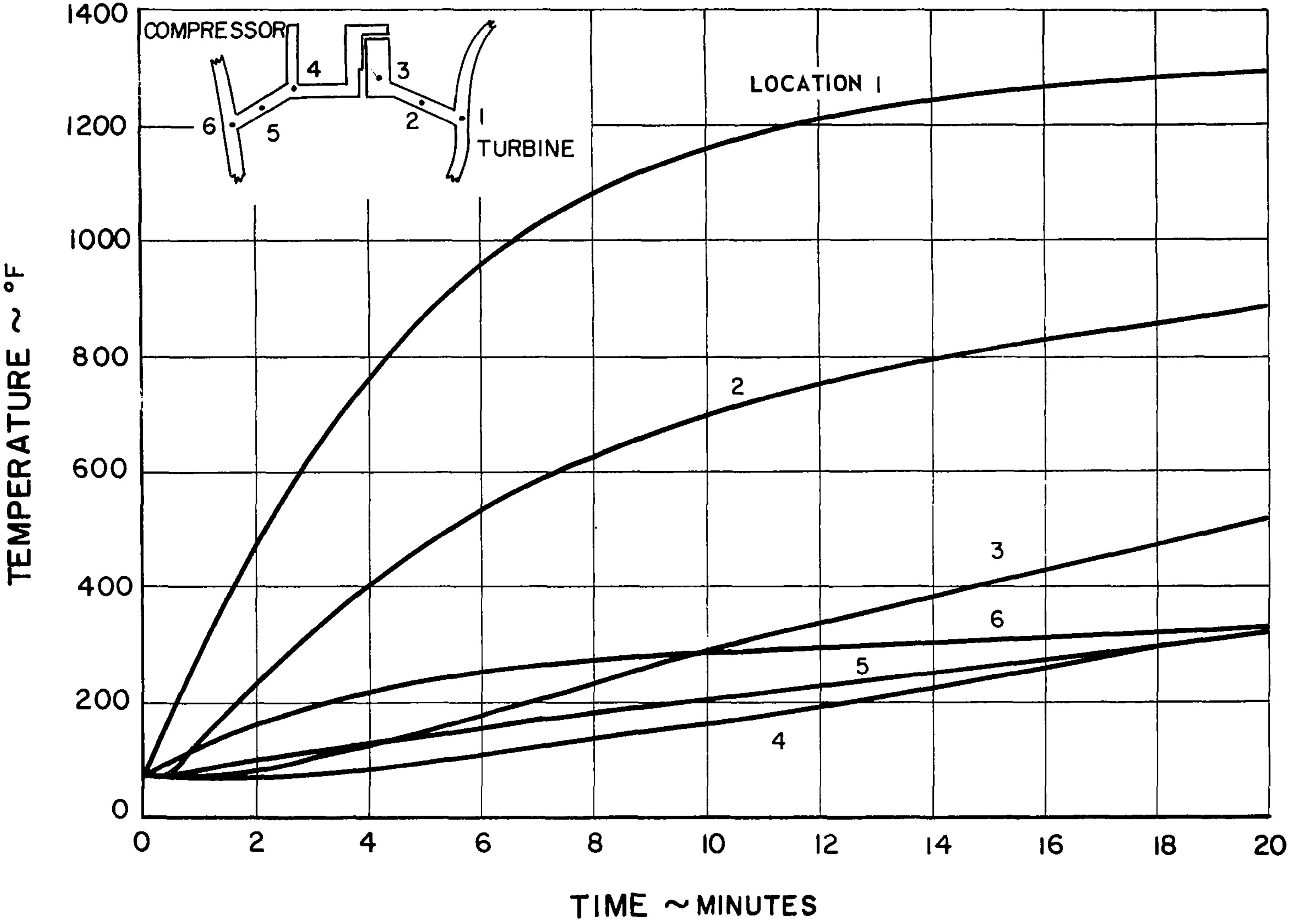

Figure 43 Inter-Scroll Structure Thermal Transient

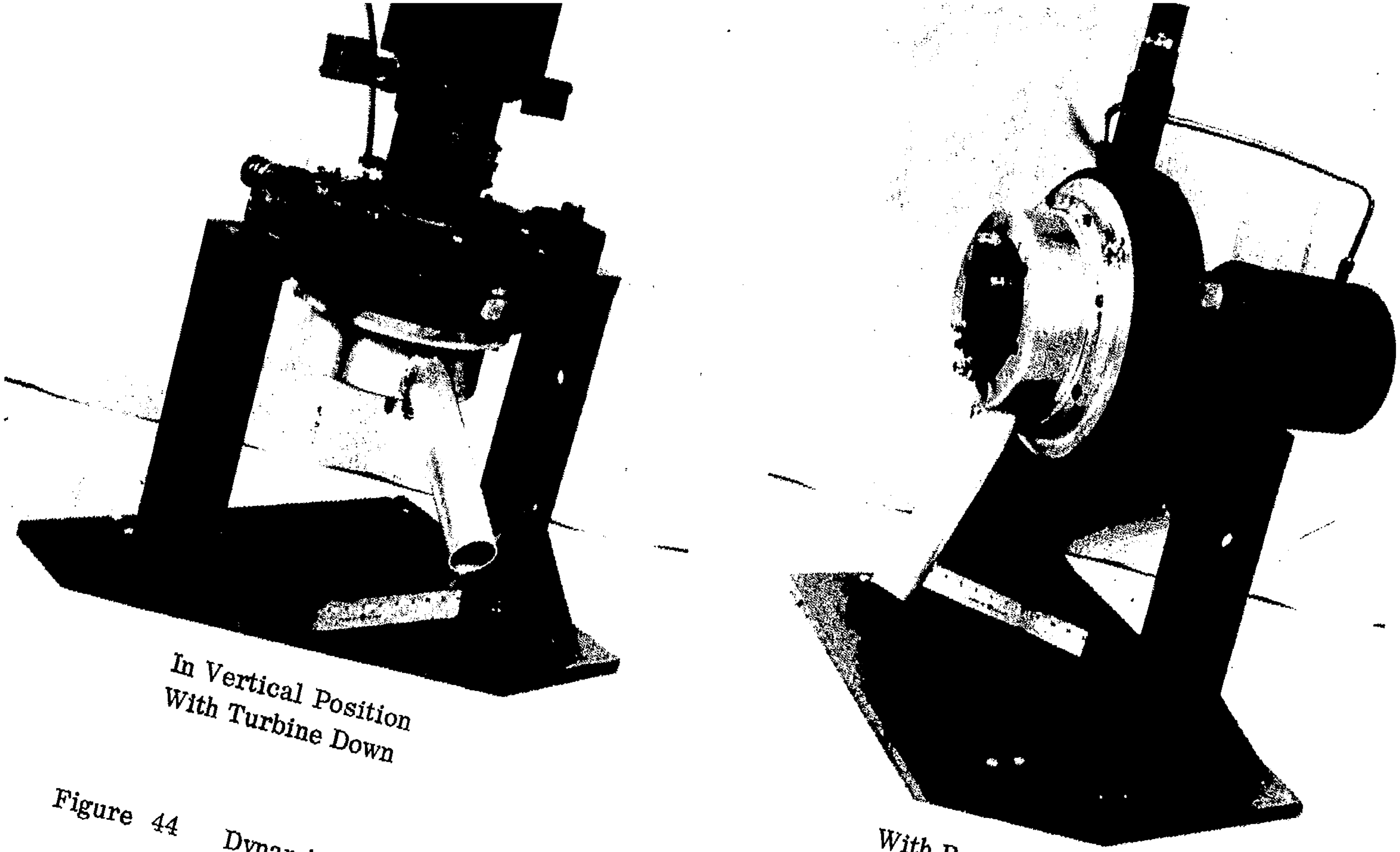

In Vertical Position
With Turbine Down

With Rotor In
Horizontal Position

Figure 44 Dynamic Simulator of Turbine-Compressor Gas Bearing System

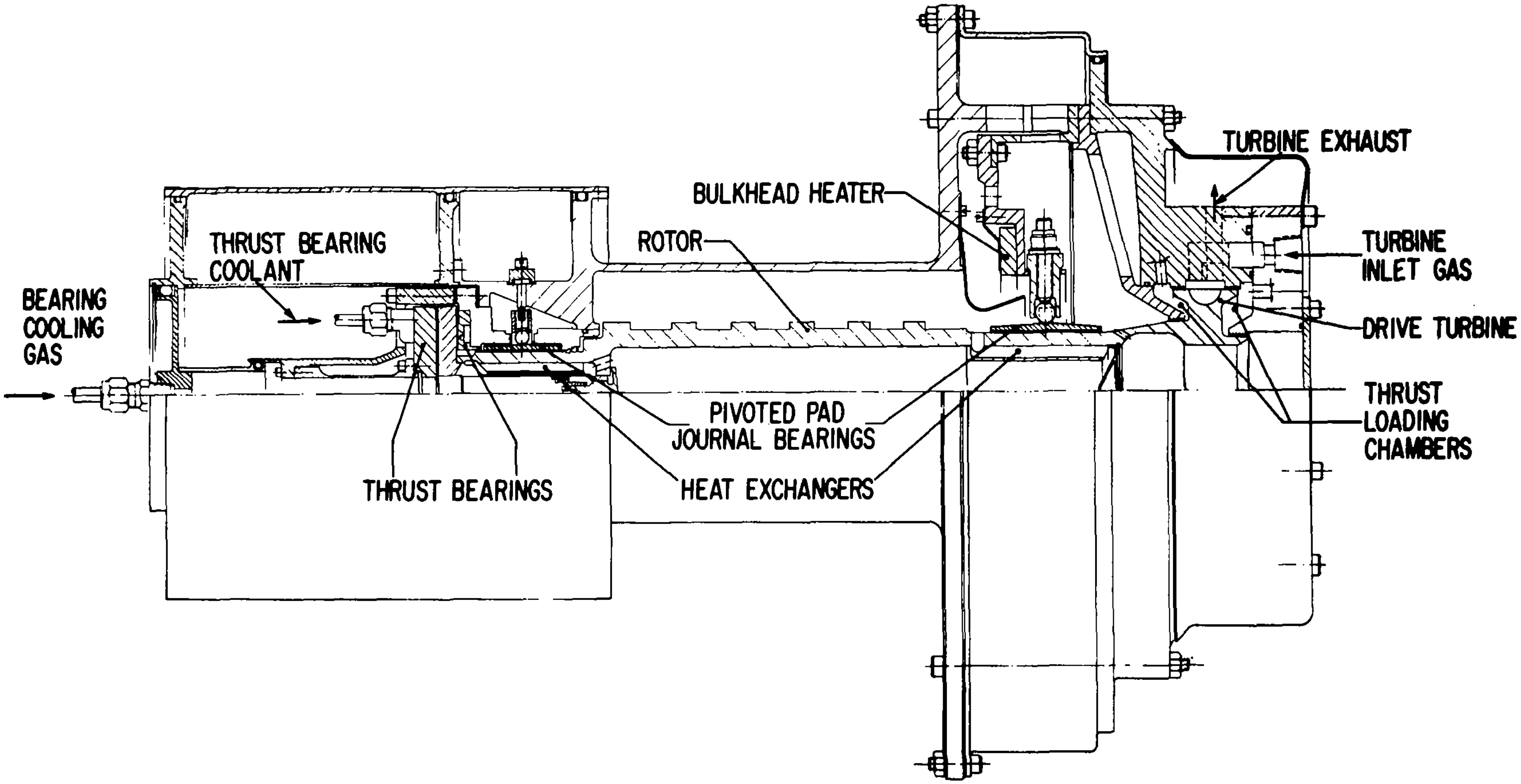
TURBINE EXHAUST
BULKHEAD HEATER
ROTOR
THRUST BEARING COOLANT
BEARING COOLING GAS
TURBINE INLET GAS
DRIVE TURBINE
PIVOTED PAD JOURNAL BEARINGS
THRUST LOADING CHAMBERS
THRUST BEARINGS
HEAT EXCHANGERS

Figure 45 Cross-Section of Dynamic Simulator

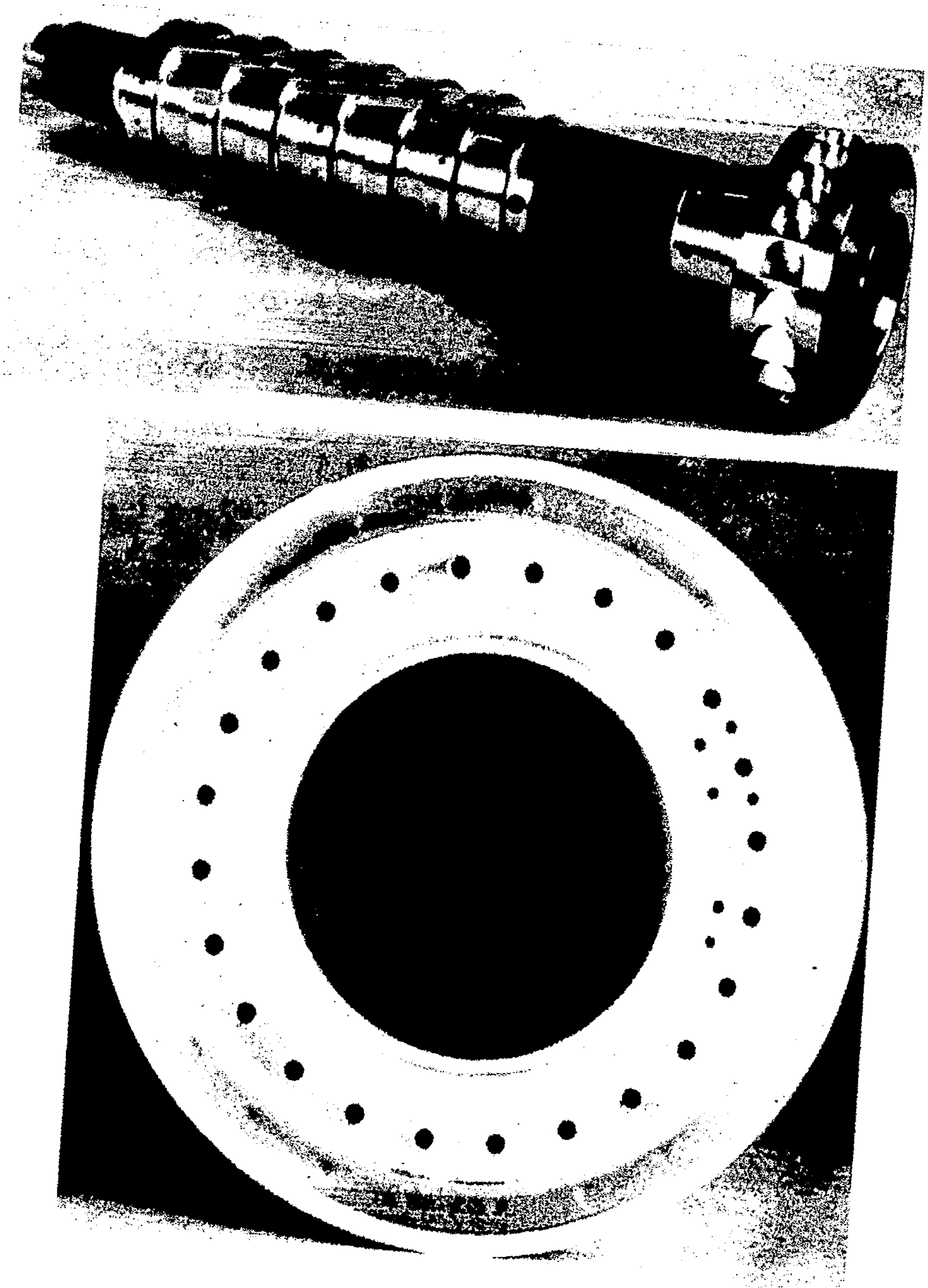

Figure 46 Shaft of Dynamic Simulator and Turbine-End View Showing Heat Exchanger Brazed Inside Journal Bearing

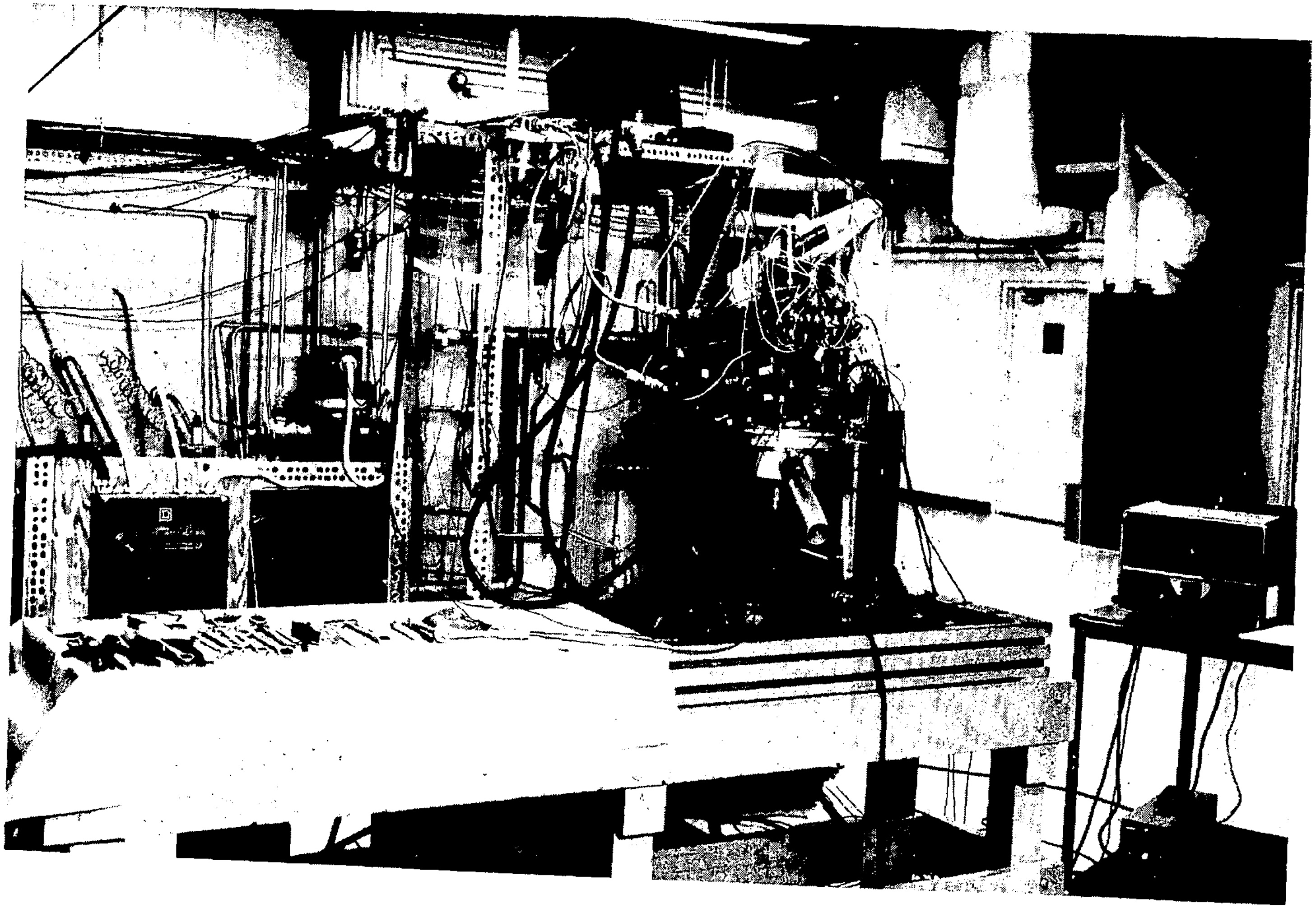

Figure 47 Dynamic Simulator Installed in Vertical Position with Compressor Inlet up

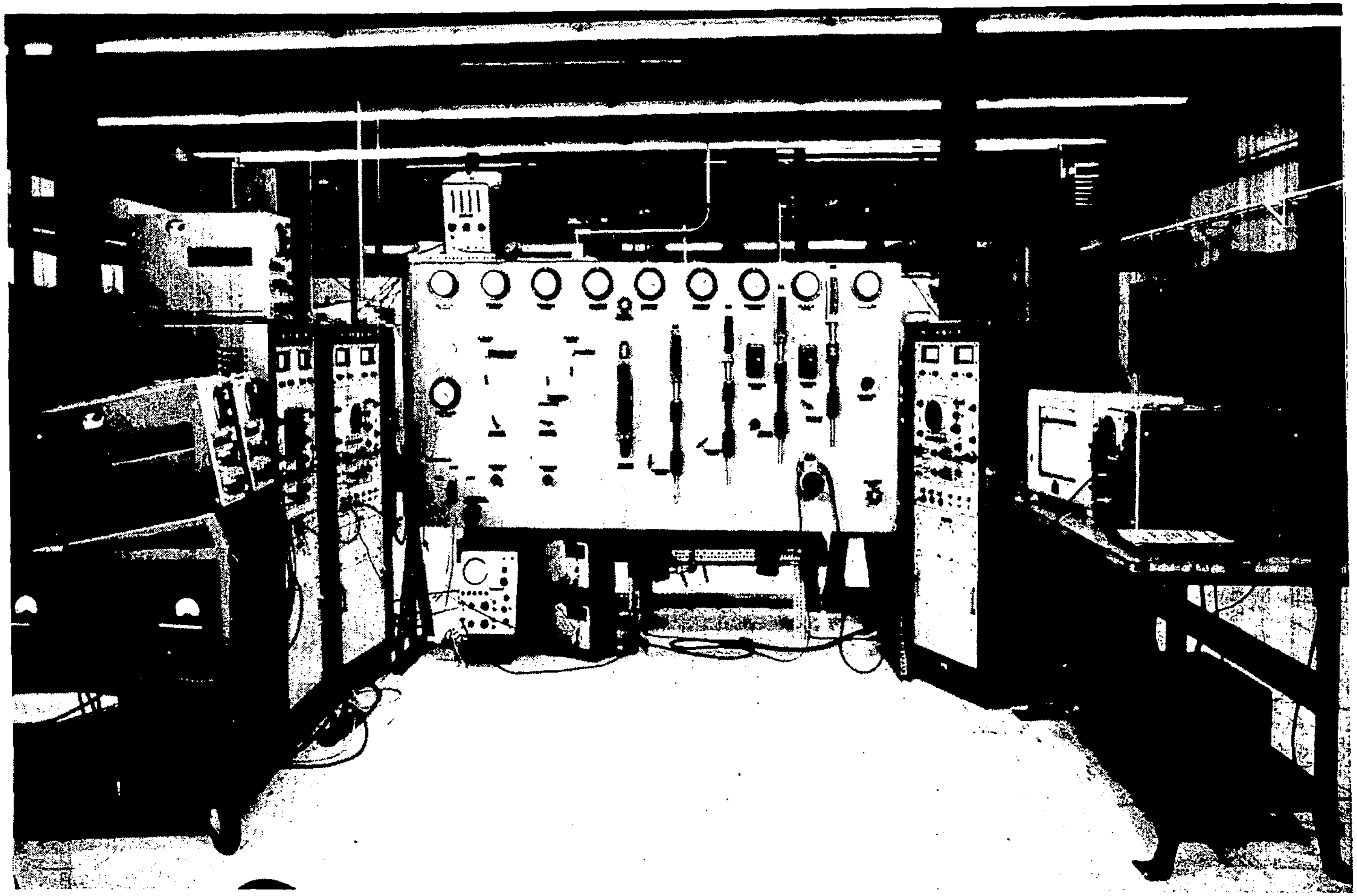

Figure 48 Control Panel and Instrumentation Readout Equipment for Dynamic Simulator

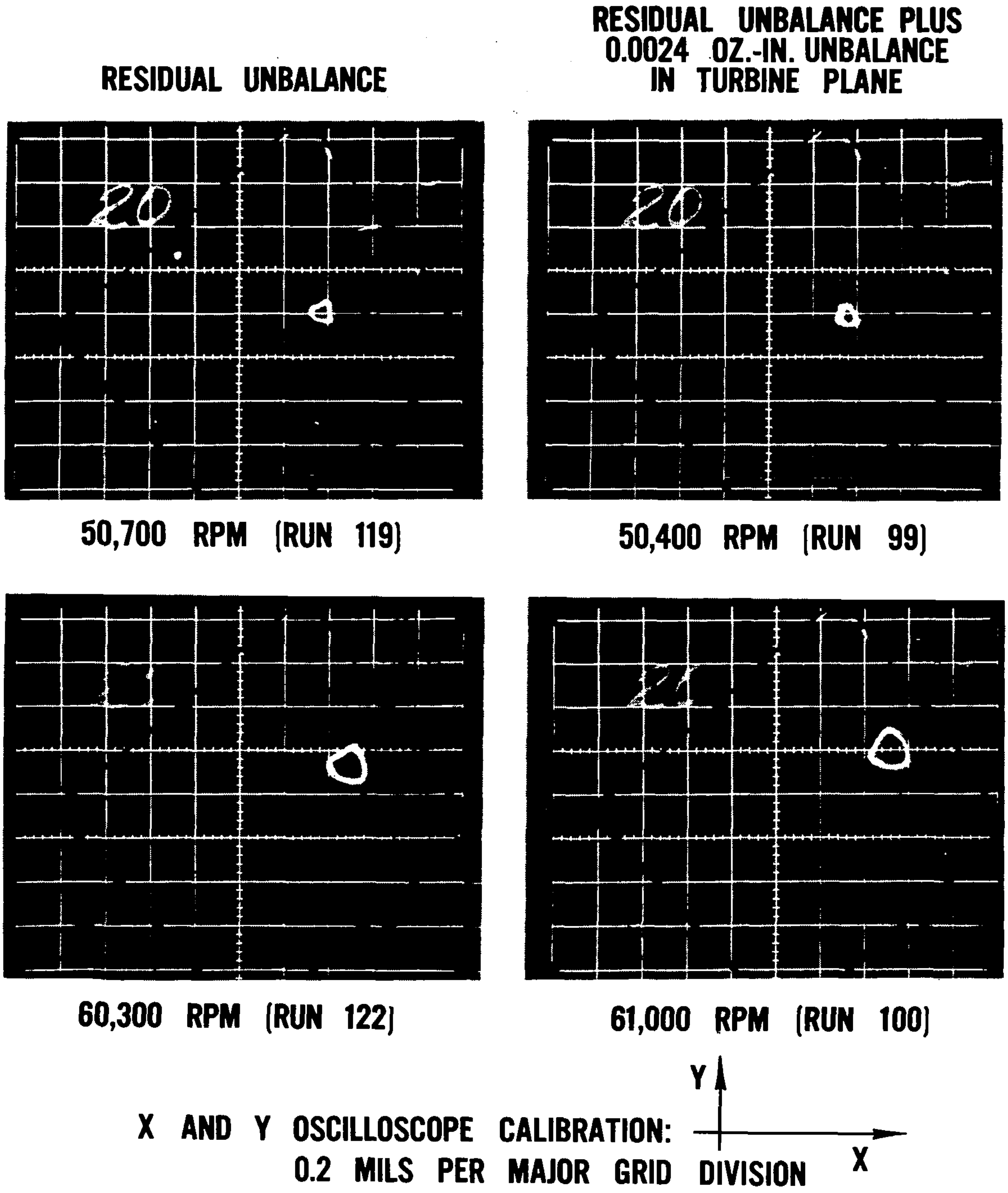

RESIDUAL UNBALANCE

RESIDUAL UNBALANCE PLUS 0.0024 OZ.-IN. UNBALANCE IN TURBINE PLANE

50,700 RPM (RUN 119)

50,400 RPM (RUN 99)

60,300 RPM (RUN 122)

61,000 RPM (RUN 100)

X AND Y OSCILLOSCOPE CALIBRATION: 0.2 MILS PER MAJOR GRID DIVISION

Figure 49 Dynamic Simulator Test Results. Traces of Number 2 Journal Bearing (Initial Design)

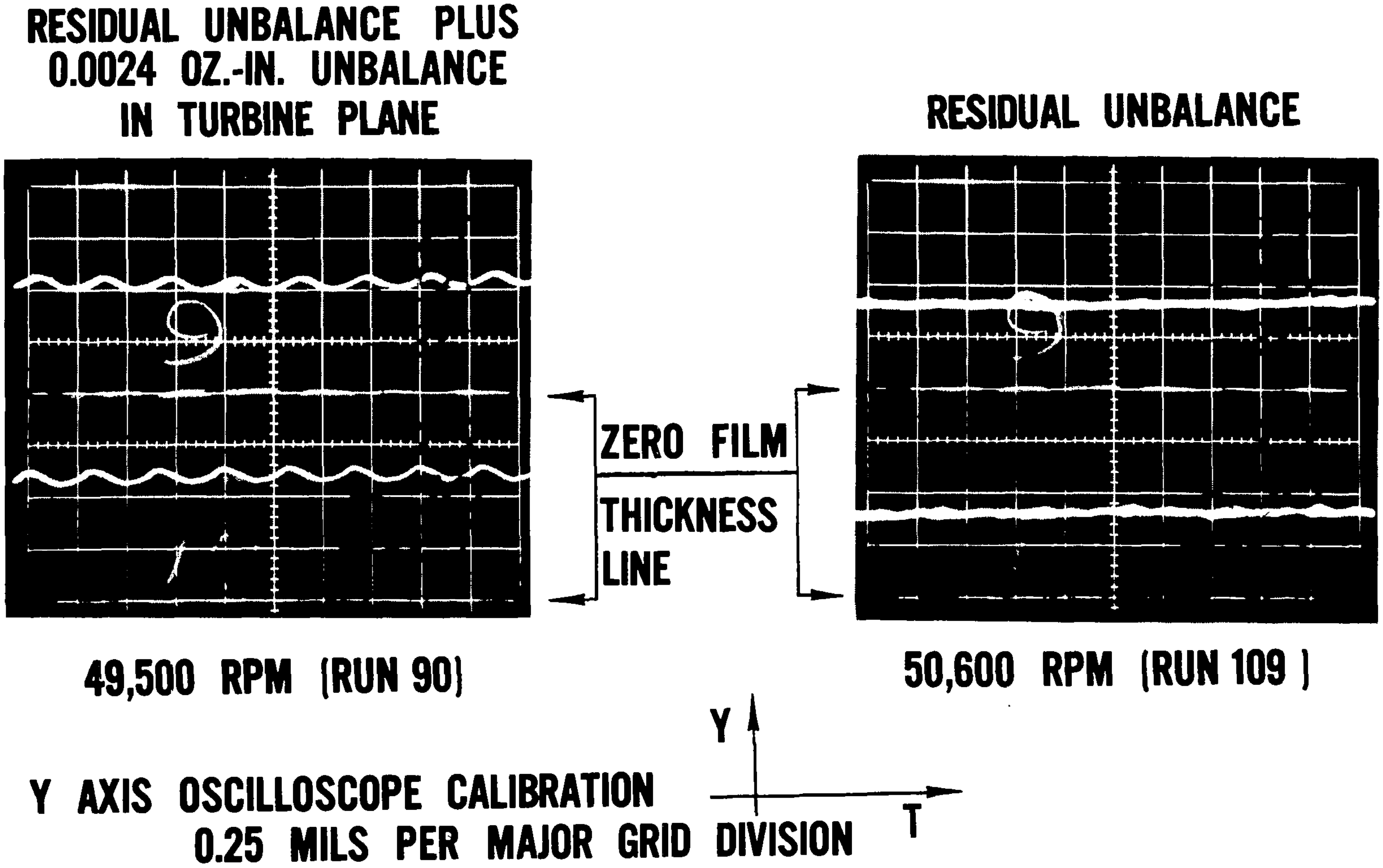

Figure 50 Dynamic Simulator Test Results. Pad-to-Shaft Film Thickness of Number 1 Journal Bearing (Initial Design)

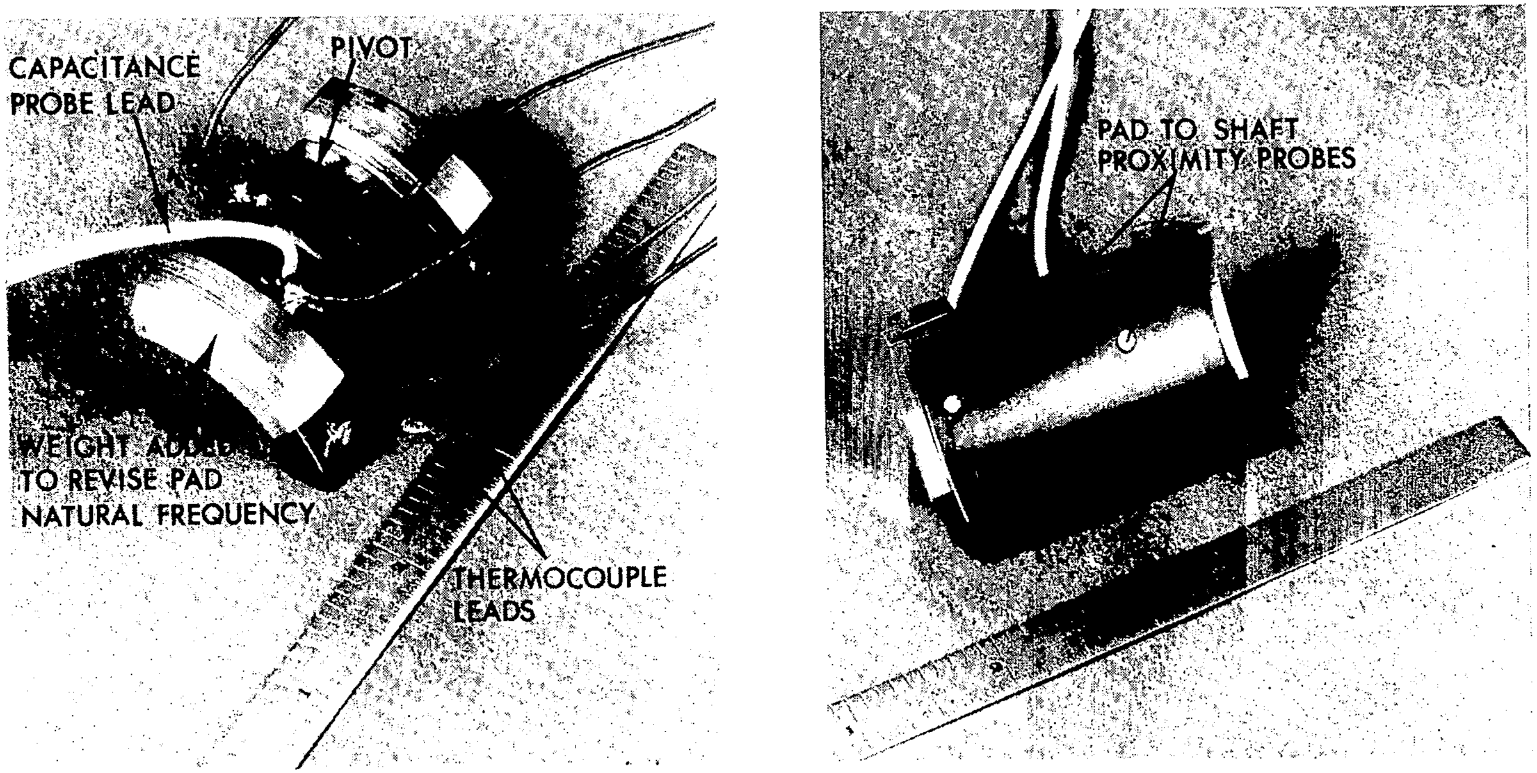
CAPACITANCE PROBE LEAD
PIVOT
WEIGHT ADDED TO REVISE PAD NATURAL FREQUENCY
THERMOCOUPLE LEADS
PAD TO SHAFT PROXIMITY PROBES

Figure 51 Modified Configuration of Number 2 Journal Bearing Pads

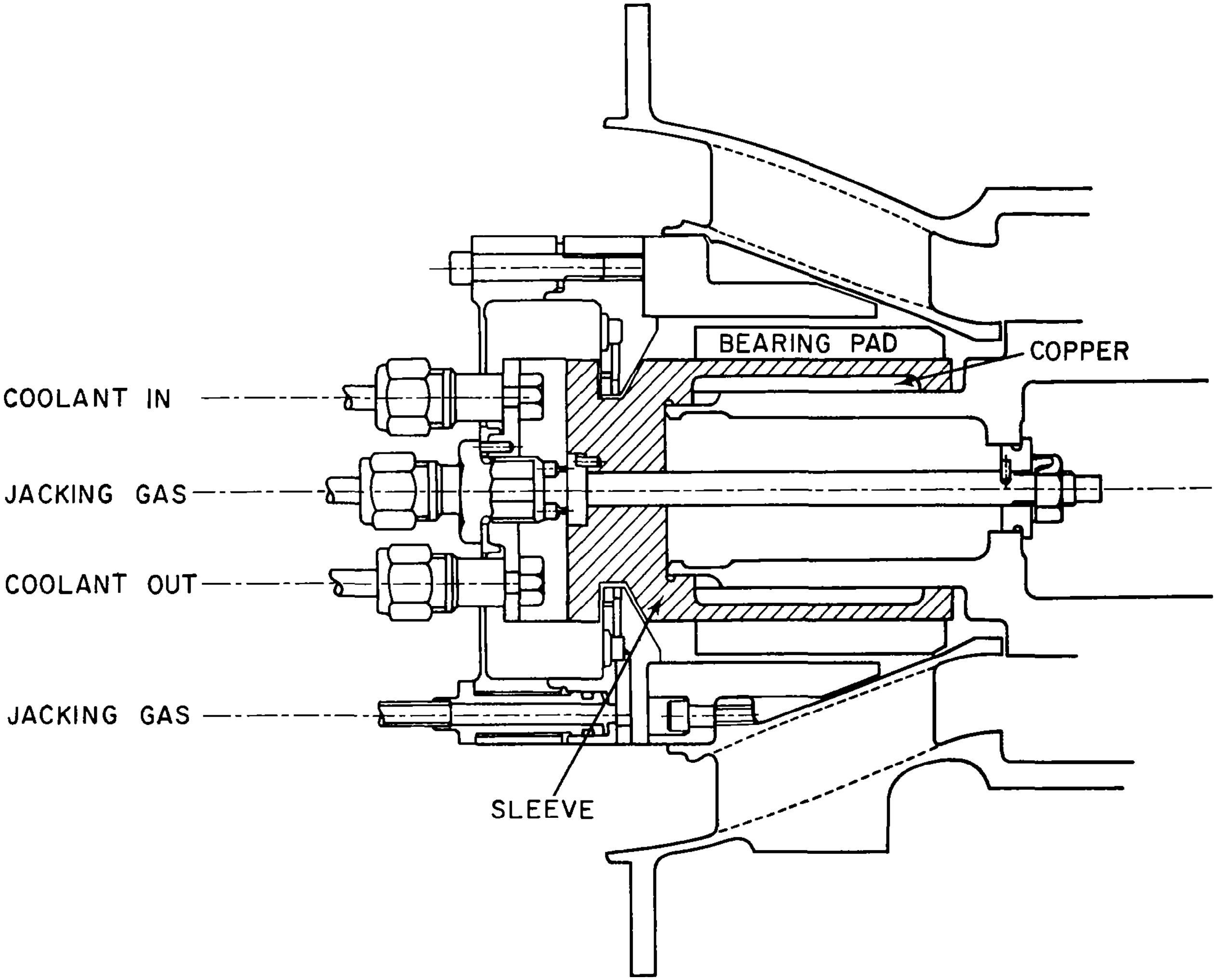
BEARING PAD
COPPER
COOLANT IN
JACKING GAS
COOLANT OUT
JACKING GAS
SLEEVE

Figure 52 Number 1 Bearing Area with Sleeve Concept

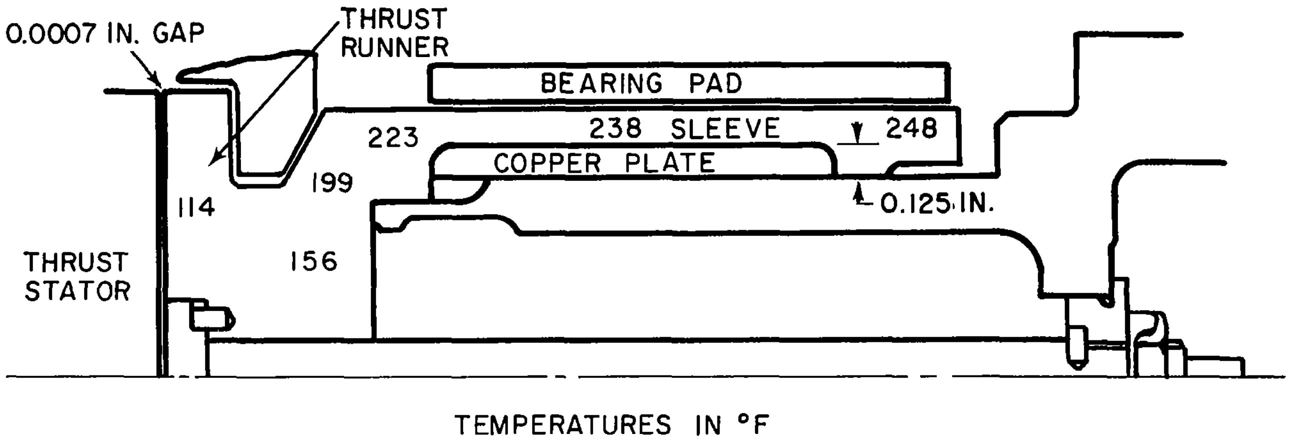
0.0007 IN. GAP
THRUST RUNNER
BEARING PAD
223
238 SLEEVE
248
COPPER PLATE
199
114
0.125 IN.
THRUST STATOR
156
TEMPERATURES IN °F

Figure 53 Temperature Map of Number 1 Bearing with Sleeve Concept

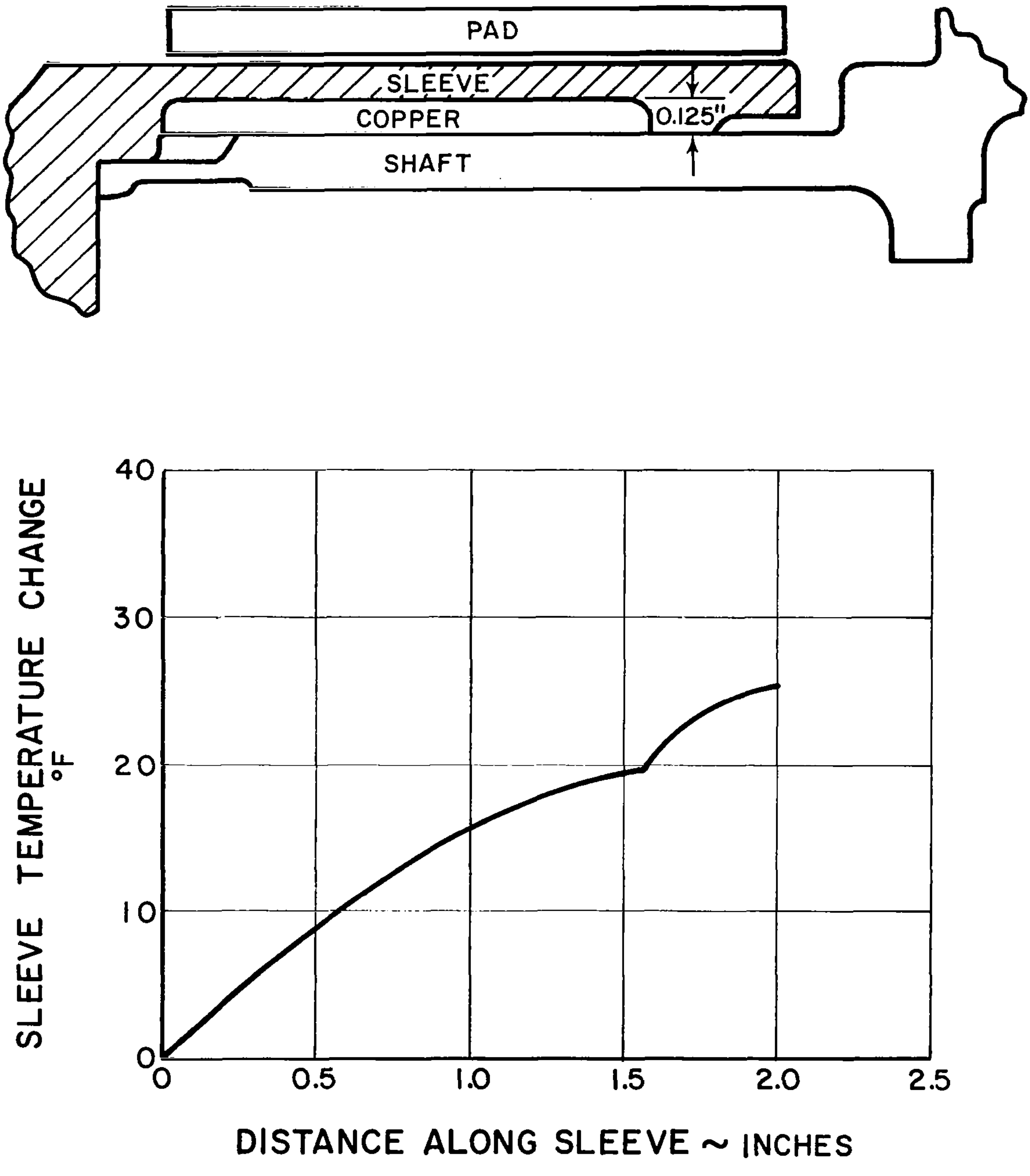

Figure 54 Shaft Temperature vs Length of Number 1 Bearing with Sleeve Concept

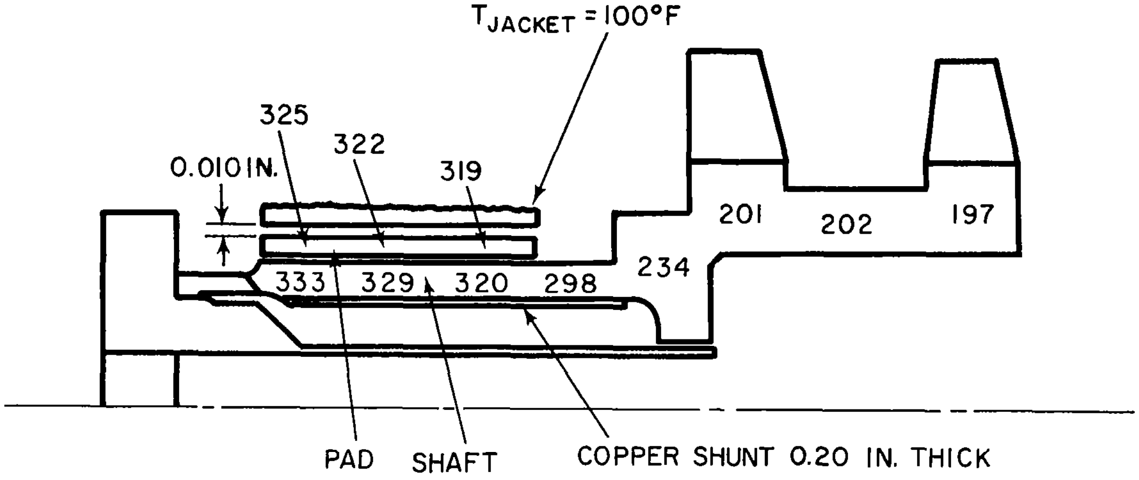
T_{JACKET} = 100°F
325
322
319
0.010 IN.
333
329
320
298
234
201
202
197
PAD
SHAFT
COPPER SHUNT 0.20 IN. THICK

TEMPERATURES IN °F

Figure 55 Temperature Map of Number 1 Bearing with Cooling Jacket Concept

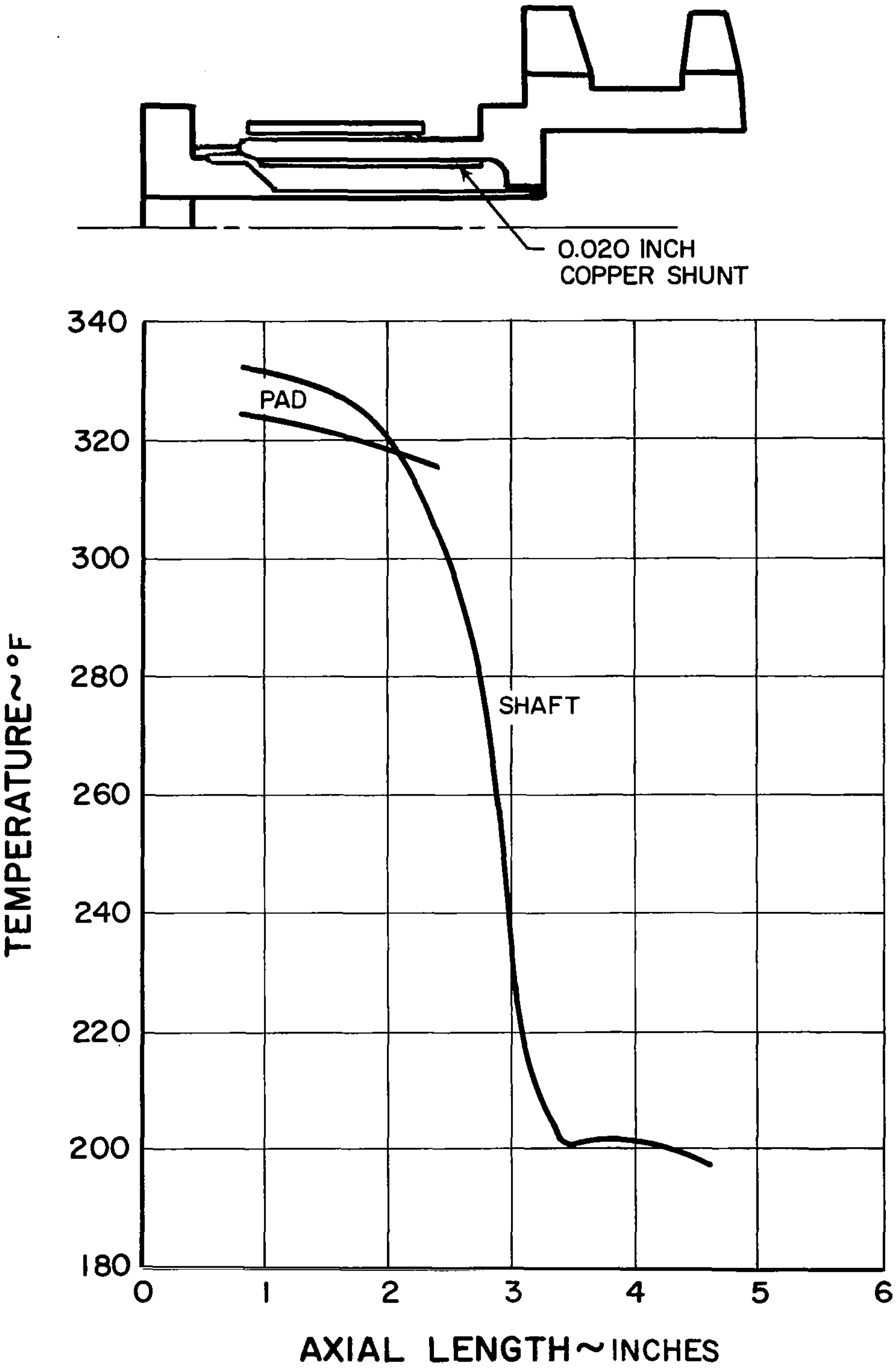

Figure 56 Shaft Temperature vs Length at Number 1 Bearing with Cooling Jacket Concept

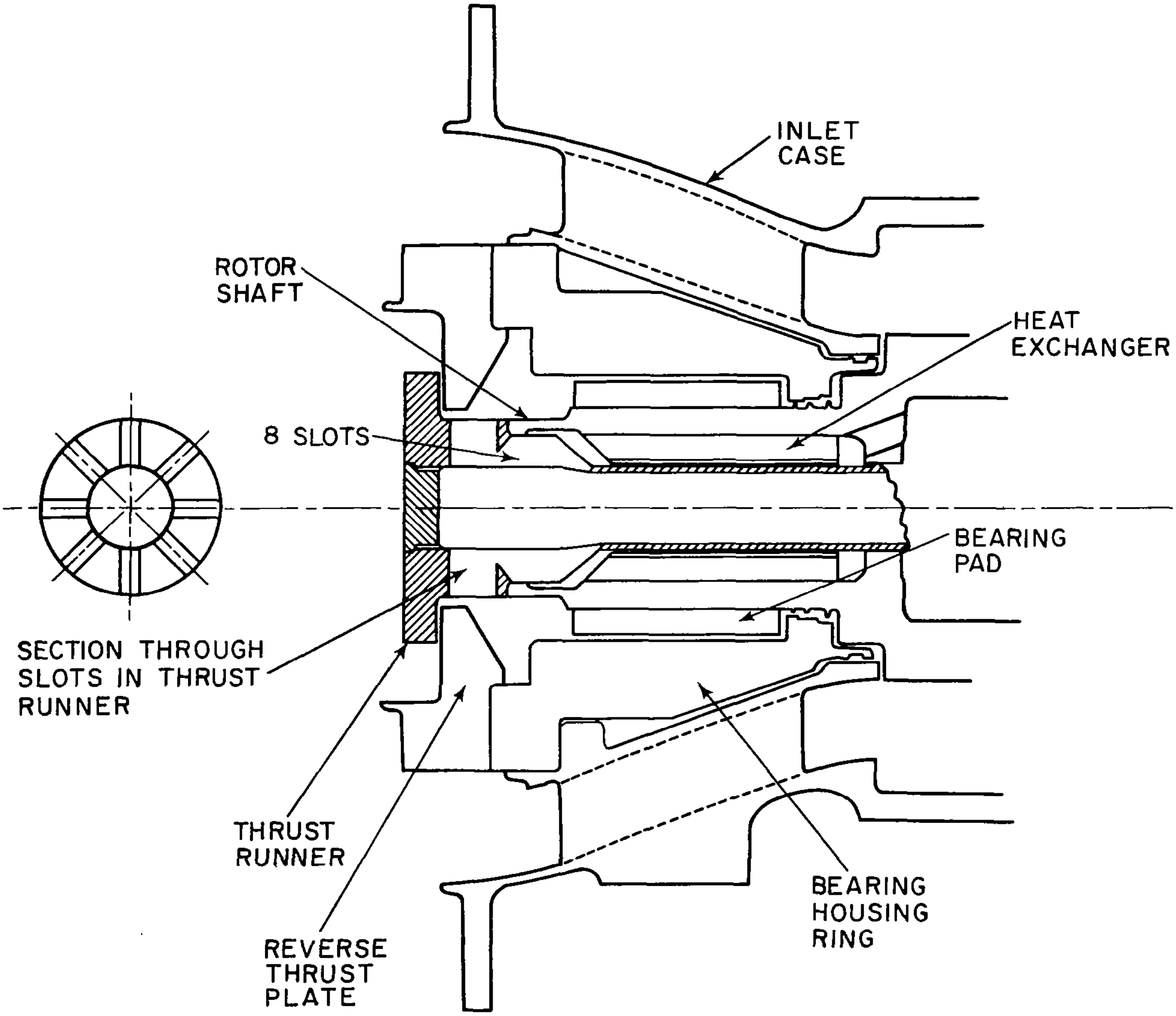
INLET CASE
ROTOR SHAFT
HEAT EXCHANGER
8 SLOTS
BEARING PAD
SECTION THROUGH SLOTS IN THRUST RUNNER
THRUST RUNNER
REVERSE THRUST PLATE
BEARING HOUSING RING

Figure 57 Number 1 Bearing Area with Gas Cooling

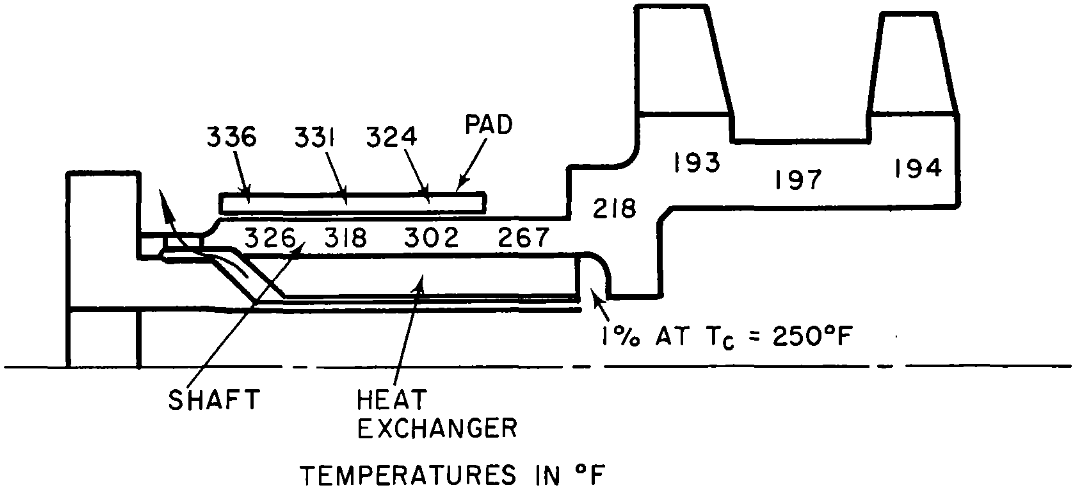
336
331
324
PAD
326
318
302
267
218
193
197
194
1% AT T_C = 250°F
SHAFT
HEAT EXCHANGER
TEMPERATURES IN °F

Figure 58 Temperature Map of Number 1 Bearing with Gas Cooling Concept No. 1

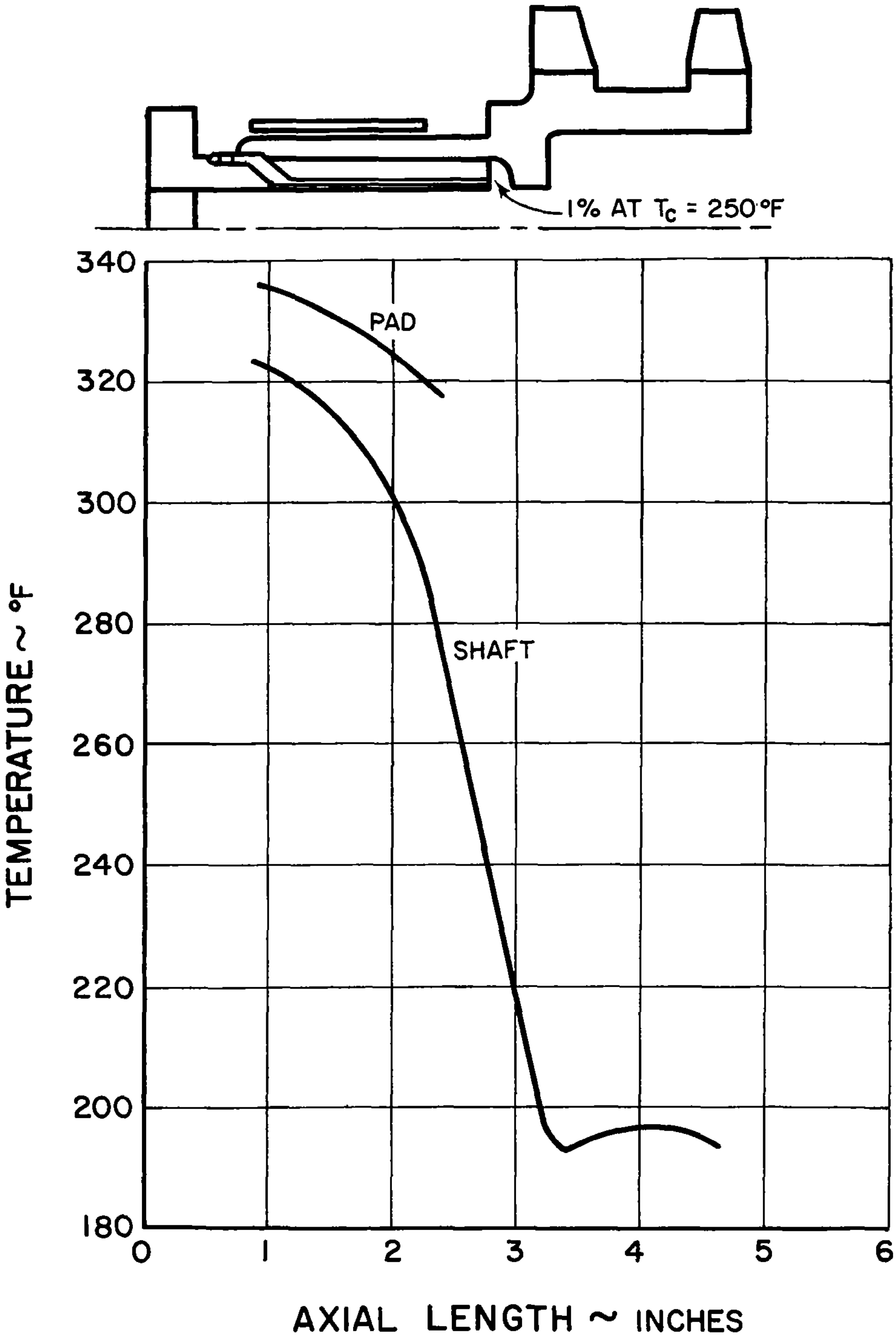

Figure 59 Shaft Temperature vs Length at Number 1 Bearing with Gas Cooling Concept No. 1

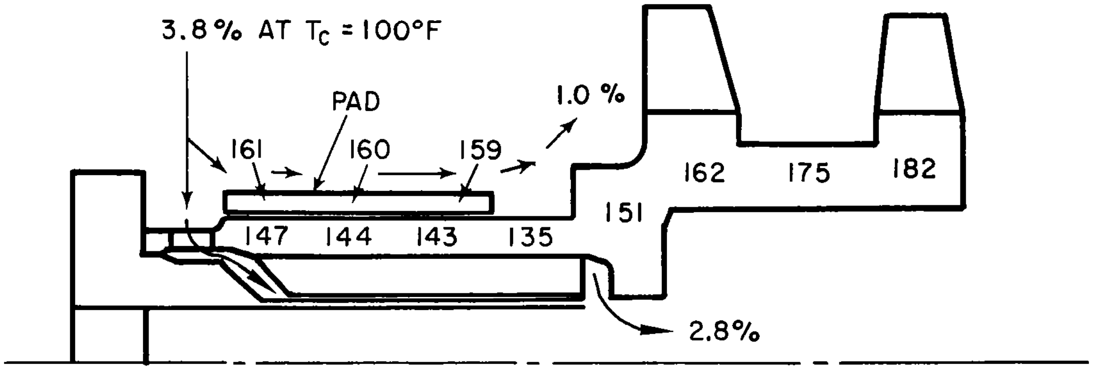
3.8 % AT T_C = 100°F
PAD
1.0 %
161
160
159
147
144
143
135
151
162
175
182
2.8%

TEMPERATURES IN °F

Figure 60 Temperature Map of Number 1 Bearing with Gas Cooling Concept No. 2

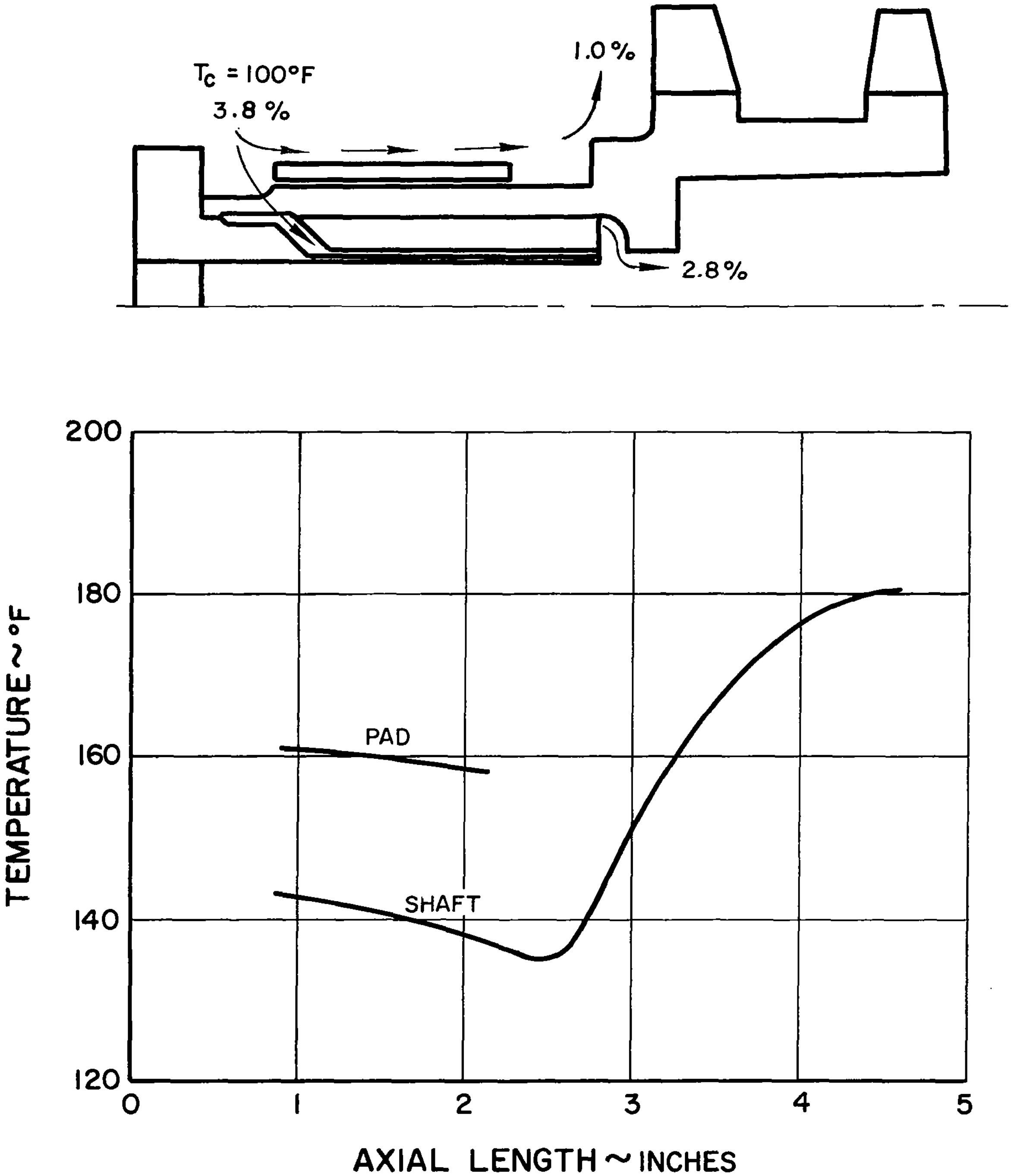

Figure 61 Shaft Temperature vs Length at Number 1 Bearing with Gas Cooling Concept No. 2

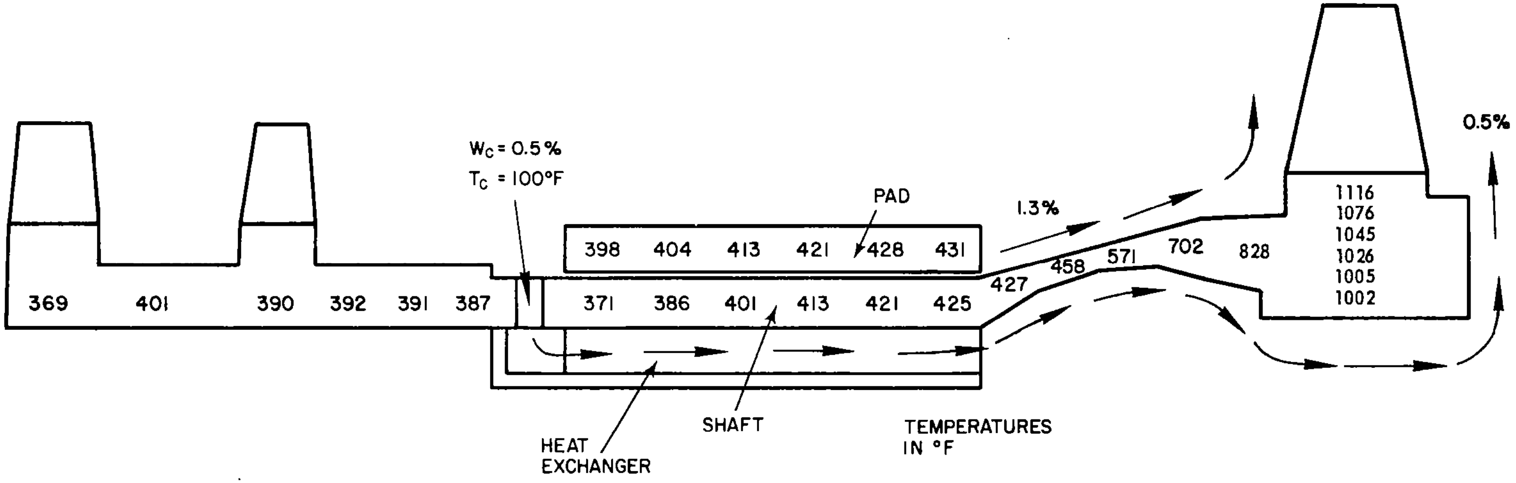
W$_C$ = 0.5%
T$_C$ = 100°F
PAD
1.3%
0.5%
398
404
413
421
428
431
369
401
390
392
391
387
371
386
401
413
421
425
427
458
571
702
828
1116
1076
1045
1026
1005
1002
HEAT EXCHANGER
SHAFT
TEMPERATURES IN °F

Figure 62 Temperature Map of Number 2 Bearing with Gas Cooling Concept No. 1 (0.5% Gas Flow)

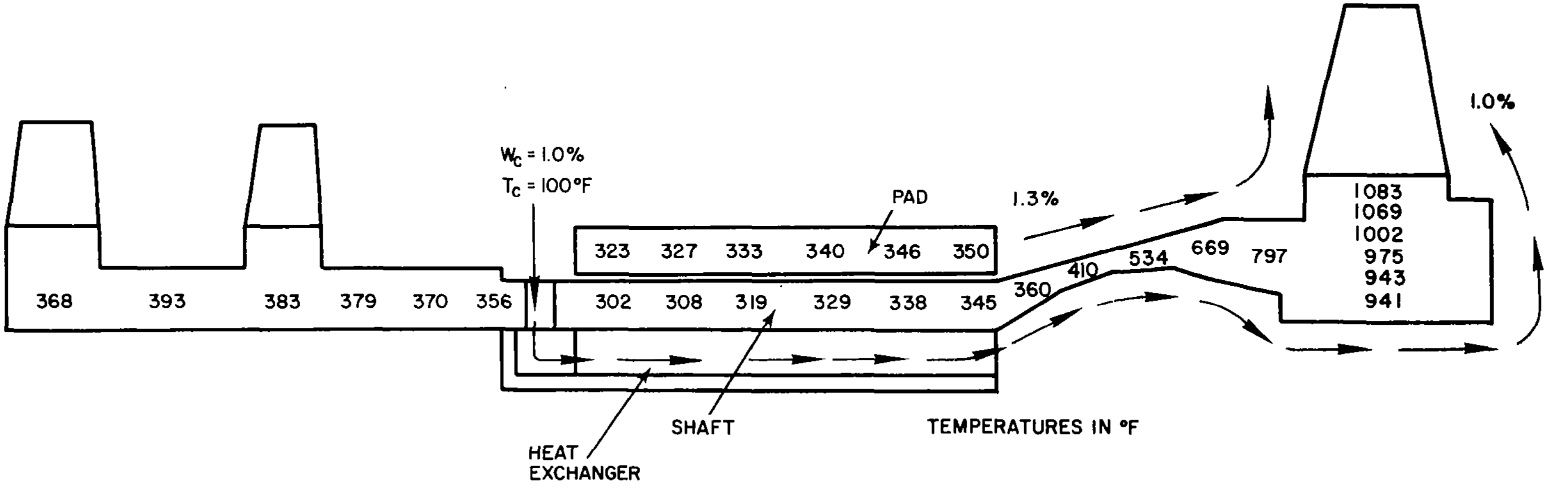
W_C = 1.0%
T_C = 100°F
PAD
1.3%
1.0%
323 327 333 340 346 350
368 393 383 379 370 356
302 308 319 329 338 345
360 410 534 669 797
1083
1069
1002
975
943
941
SHAFT
HEAT EXCHANGER
TEMPERATURES IN °F

Figure 63 Temperature Map of Number 2 Bearing with Gas Cooling Concept No. 1 (1. 0% Gas Flow)

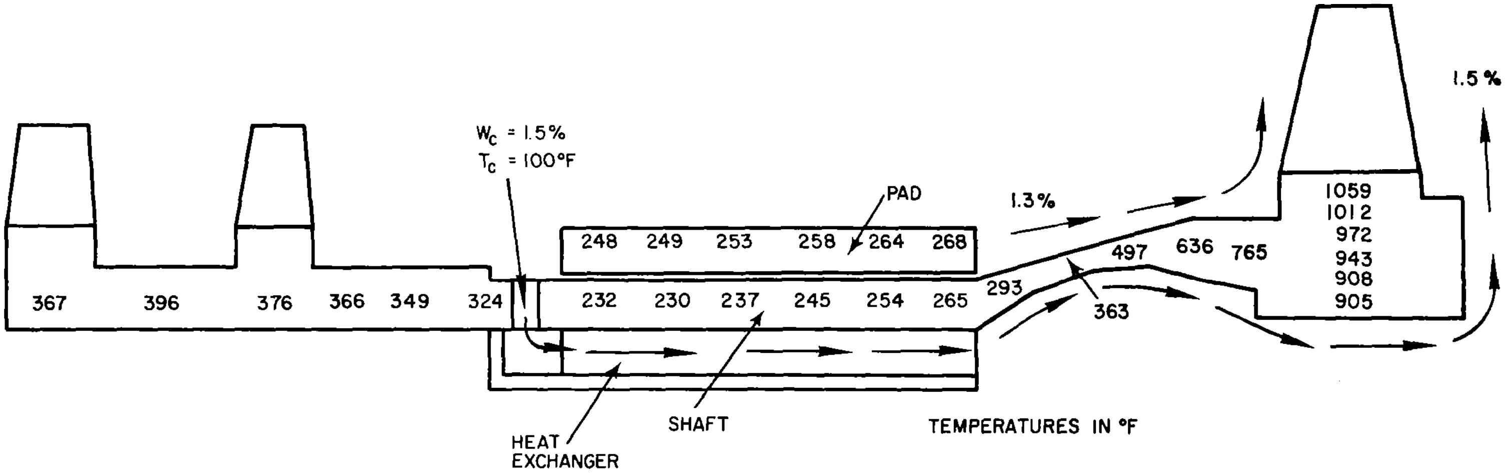

W_C = 1.5%
T_C = 100°F
PAD
1.3%
1.5%
248
249
253
258
264
268
367
396
376
366
349
324
232
230
237
245
254
265
293
497
636
765
363
1059
1012
972
943
908
905
HEAT EXCHANGER
SHAFT
TEMPERATURES IN °F

Figure 64 Temperature Map of Number 2 Bearing with Gas Cooling Concept No. 1
(1.5% Gas Flow)

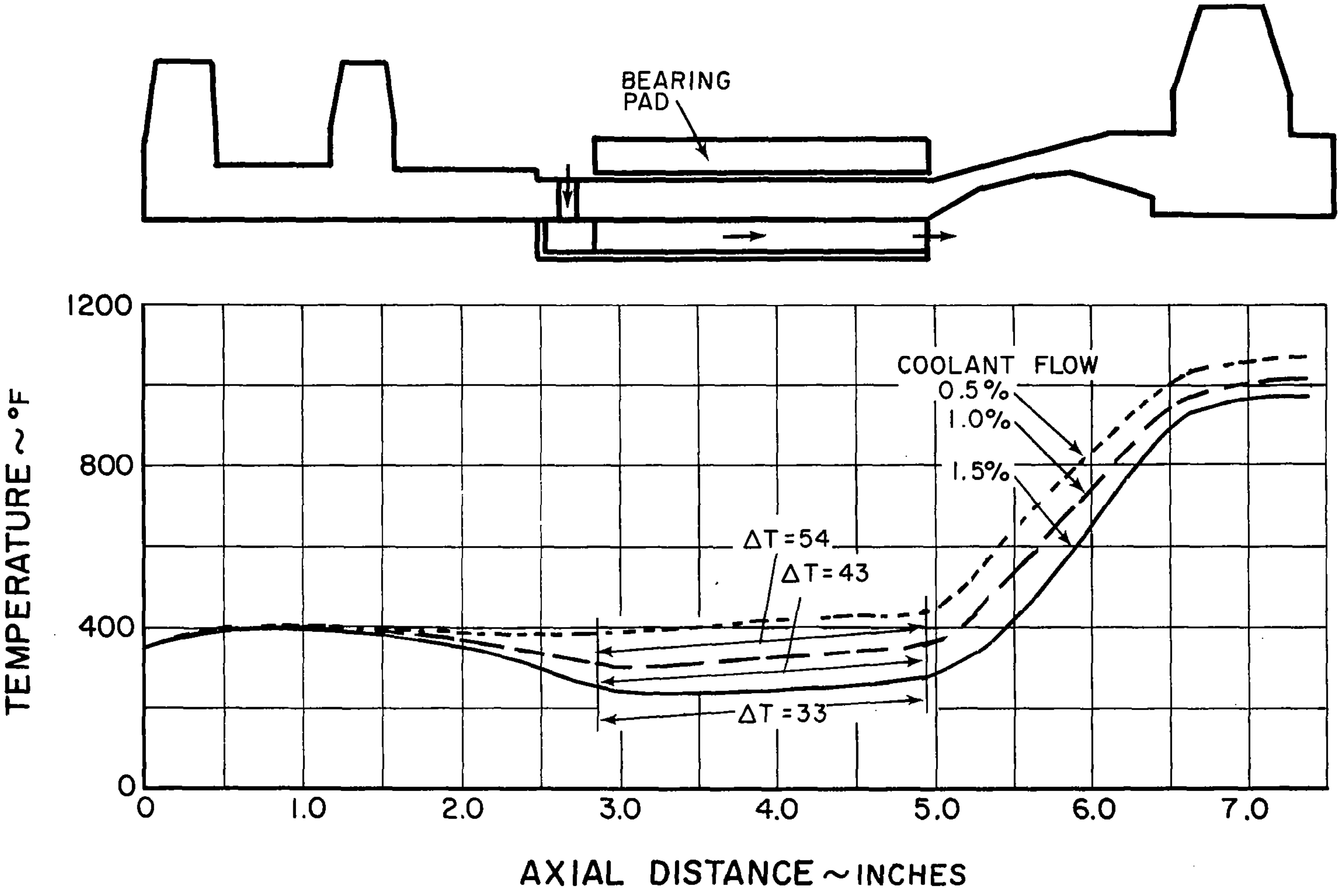

Figure 65 Temperature vs Axial Distance at Number 2 Bearing with Gas Cooling Concept No. 1

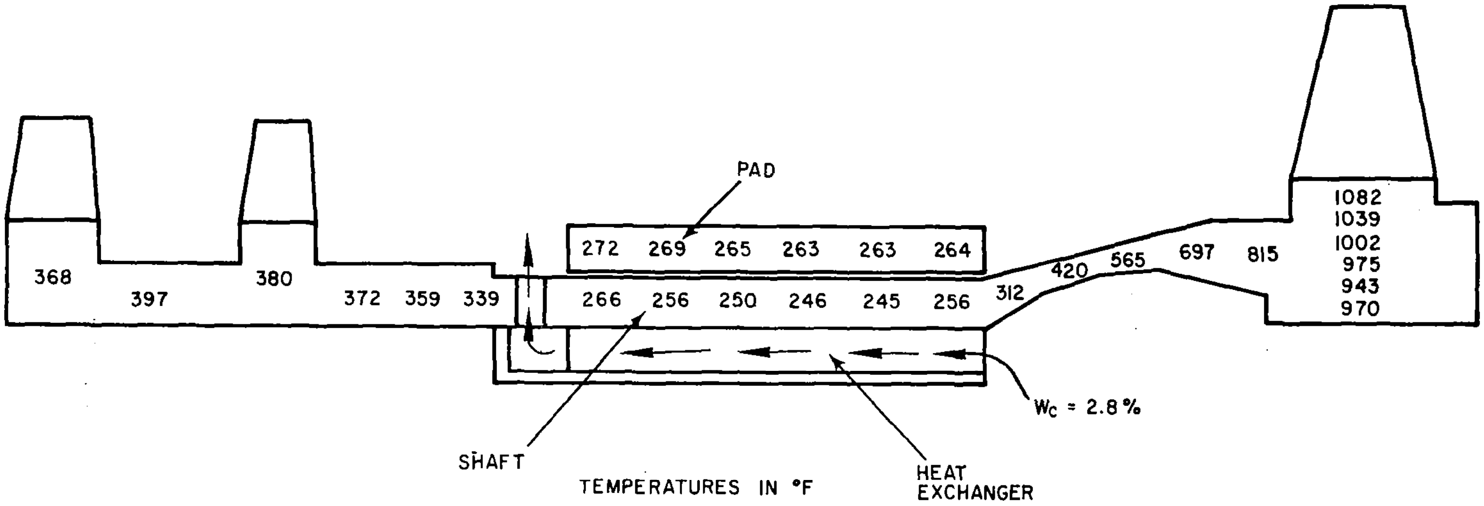
PAD
272 269 265 263 263 264
1082
1039
1002
975
943
970
368
397
380
372 359 339
266 256 250 246 245 256
312
420
565
697
815
Wc = 2.8 %
SHAFT
TEMPERATURES IN °F
HEAT EXCHANGER

Figure 66 Temperature Map of Number 2 Bearing

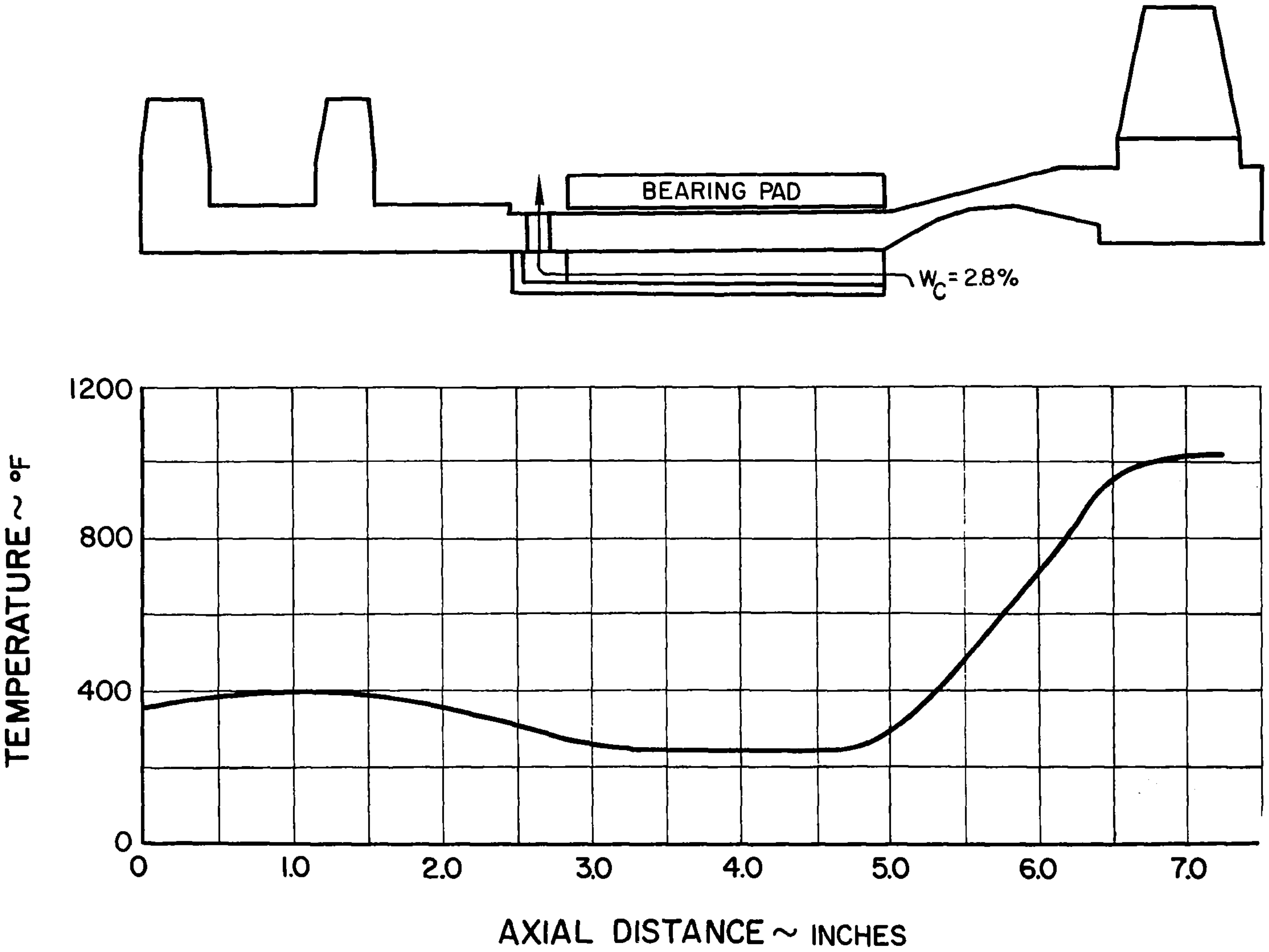

Figure 67 Temperature vs Axial Distance at Number 2 Bearing

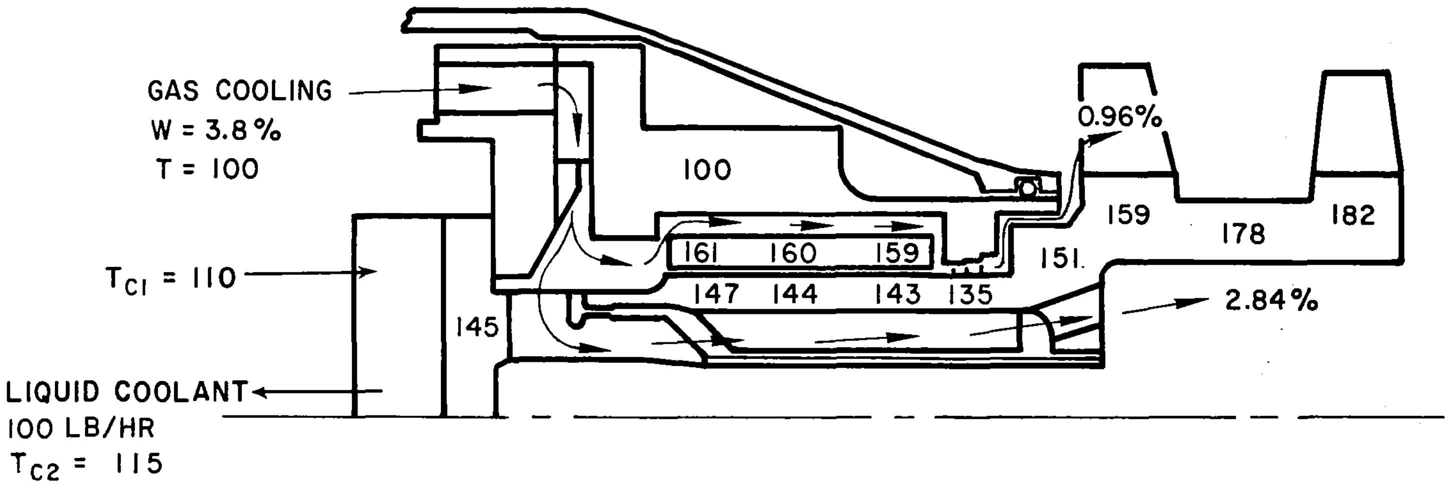
GAS COOLING
W = 3.8 %
T = 100
T_{C1} = 110
LIQUID COOLANT
100 LB/HR
T_{C2} = 115
100
161
160
159
147
144
143
135
145
151
0.96%
159
178
182
2.84%

TEMPERATURES IN °F

Figure 68 Temperature Map of Number 1 Bearing and Thrust Bearing

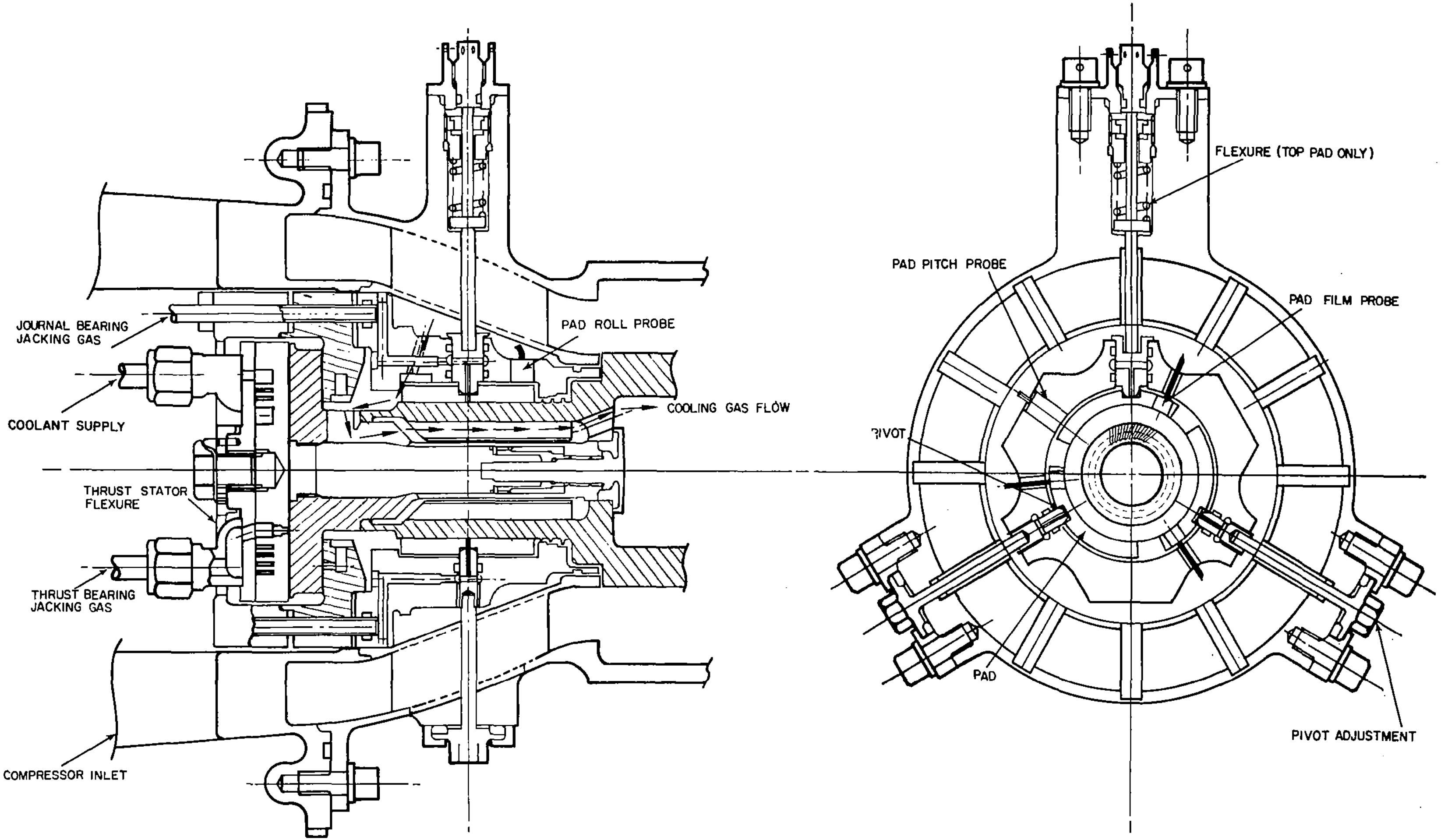
JOURNAL BEARING JACKING GAS
COOLANT SUPPLY
THRUST STATOR FLEXURE
THRUST BEARING JACKING GAS
COMPRESSOR INLET
PAD ROLL PROBE
COOLING GAS FLOW
FLEXURE (TOP PAD ONLY)
PAD PITCH PROBE
PAD FILM PROBE
PIVOT
PAD
PIVOT ADJUSTMENT

Figure 69 Turbine-Compressor Backup Gas Bearing Design. Thrust Bearing and No. 1 Journal Bearing

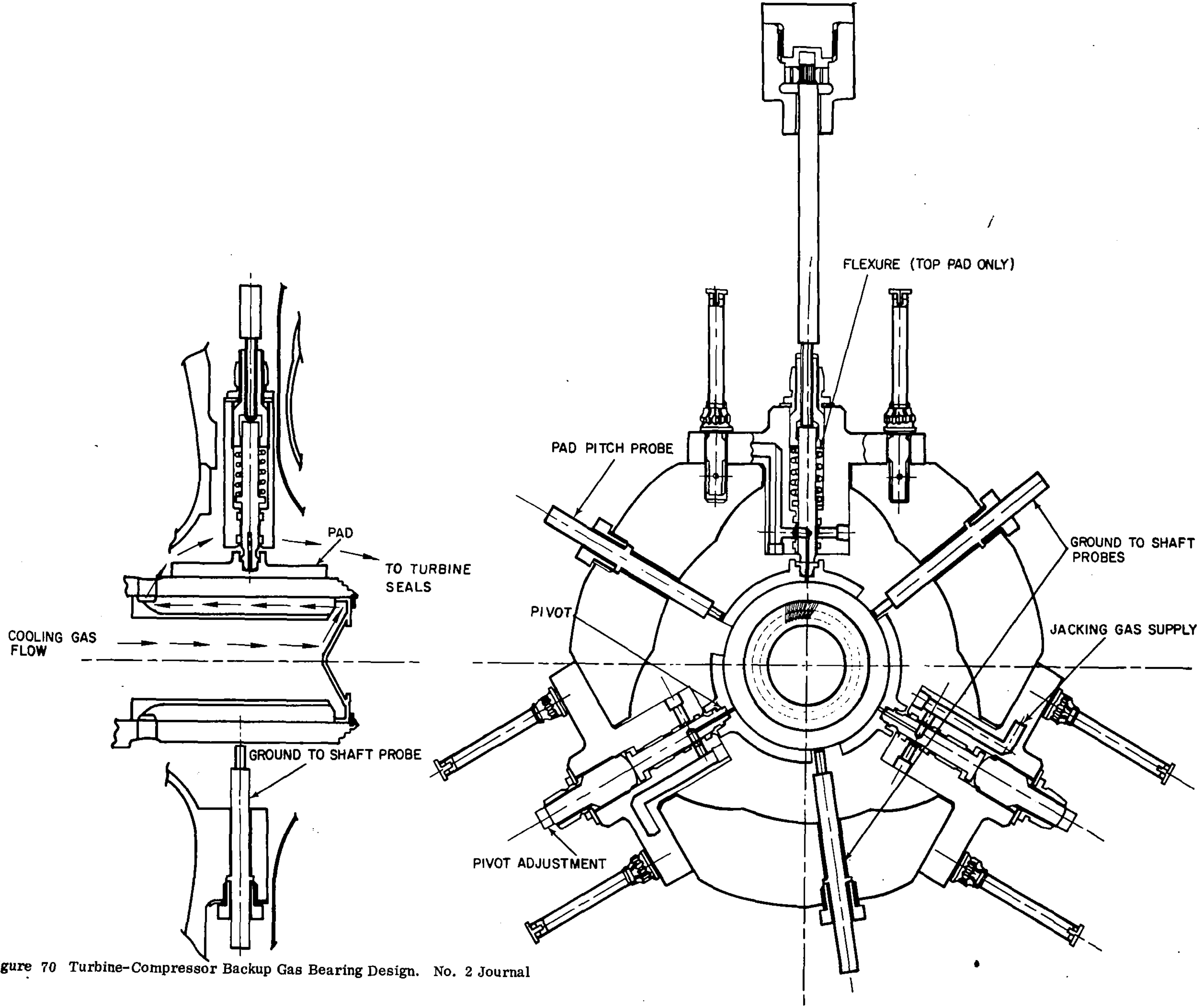
FLEXURE (TOP PAD ONLY)
PAD PITCH PROBE
PAD
TO TURBINE SEALS
GROUND TO SHAFT PROBES
PIVOT
JACKING GAS SUPPLY
COOLING GAS FLOW
GROUND TO SHAFT PROBE
PIVOT ADJUSTMENT

Figure 70 Turbine-Compressor Backup Gas Bearing Design. No. 2 Journal

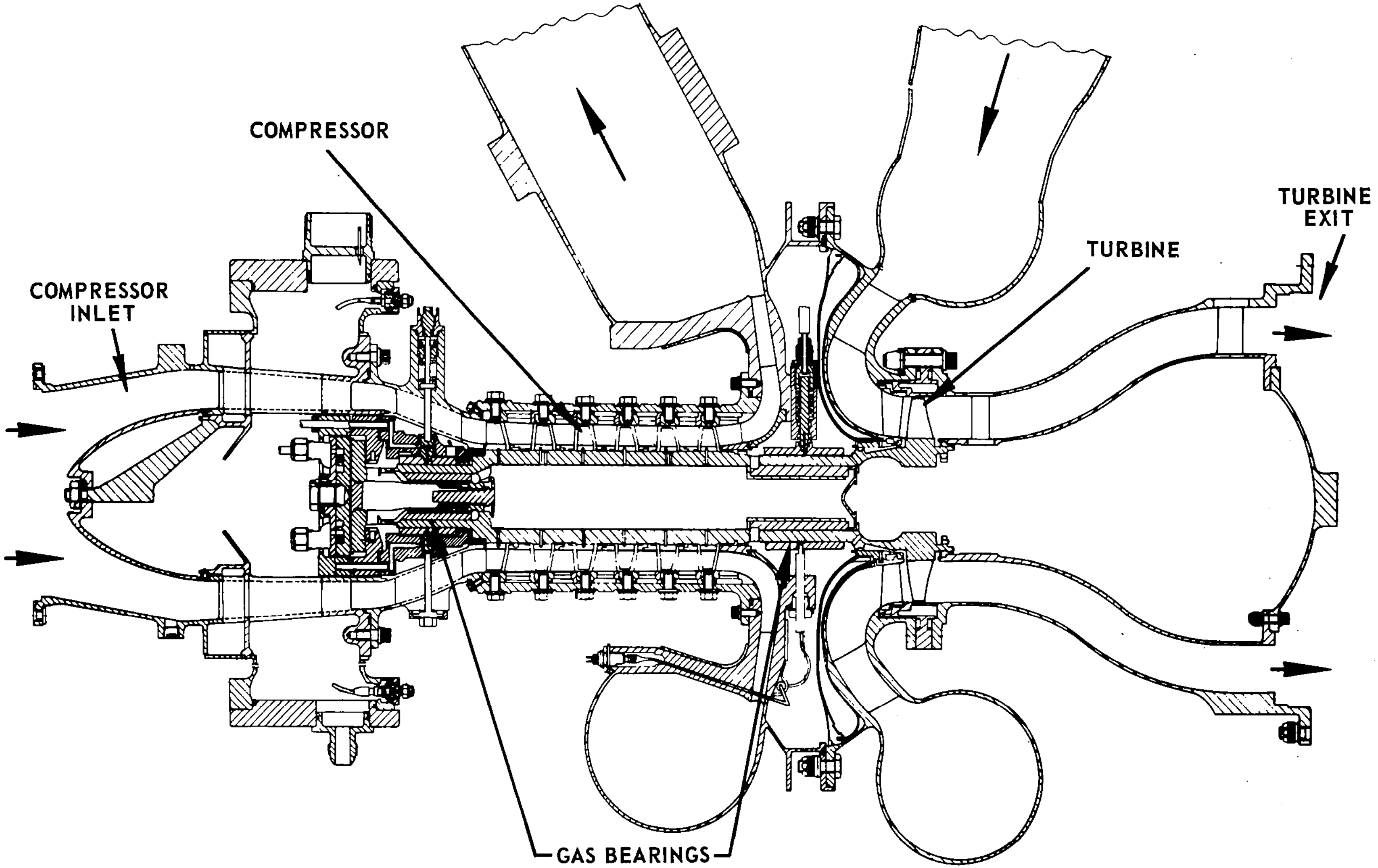
COMPRESSOR
COMPRESSOR INLET
TURBINE EXIT
TURBINE
GAS BEARINGS

Figure 71 Turbine-Compressor with Backup Gas Bearings

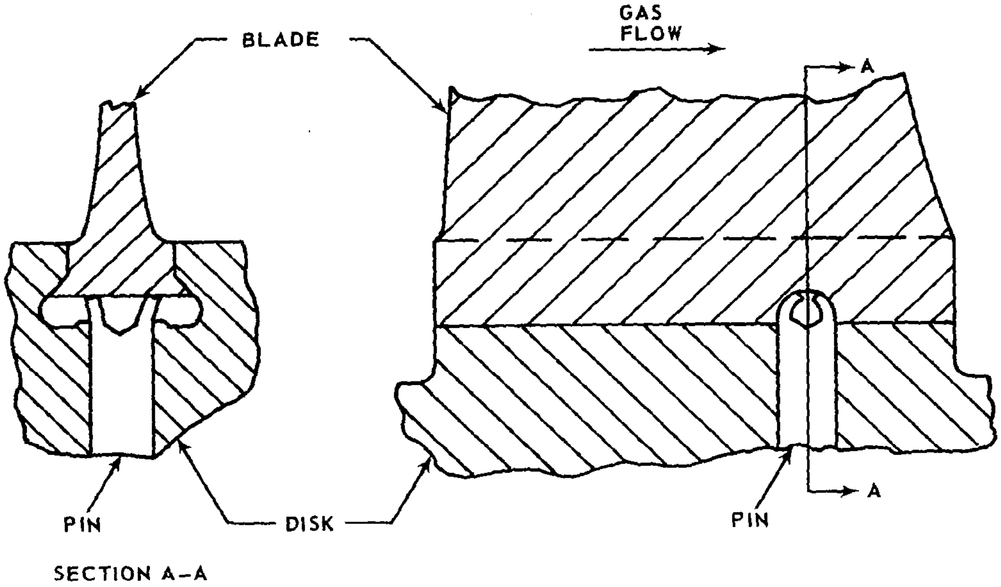
BLADE
GAS FLOW
A
A
PIN
DISK
PIN
SECTION A-A

Figure 72 Compressor Blade-Locking Pin Installed

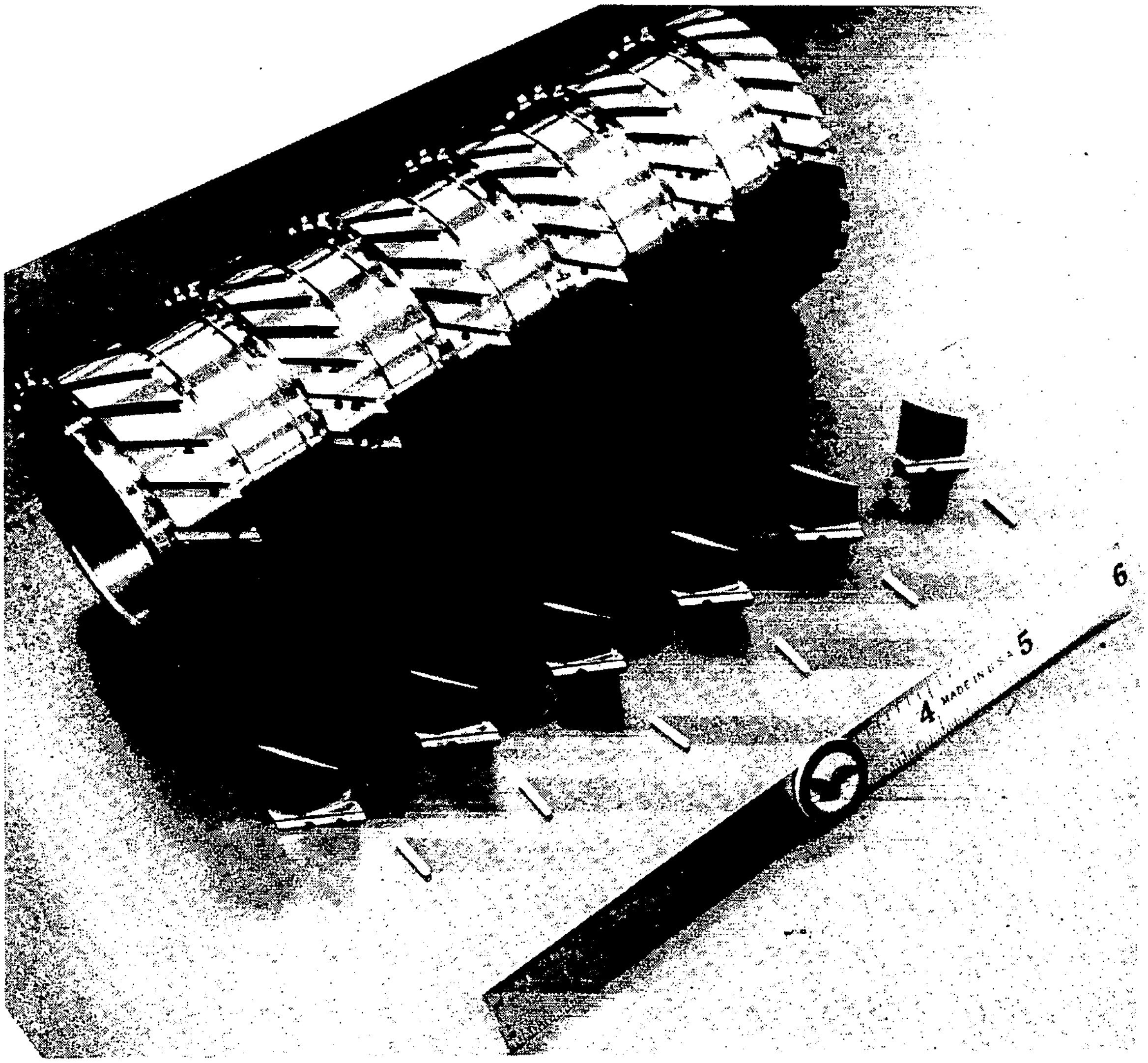
4
MADE IN U.S.A.
5
6

Figure 73 Compressor Research Package Disk, Blades, and Lock Pins

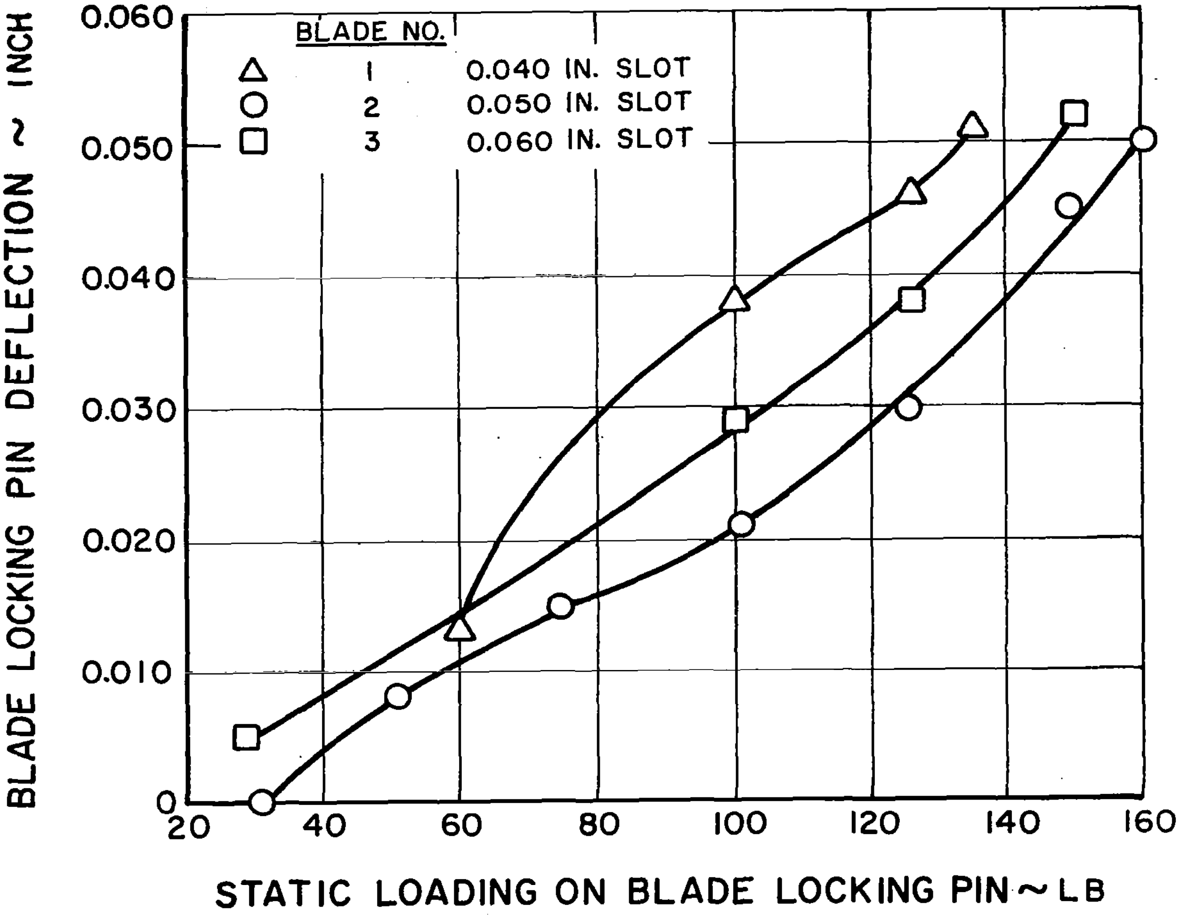

Figure 74 Aluminum Blade Locking Pin Test Results

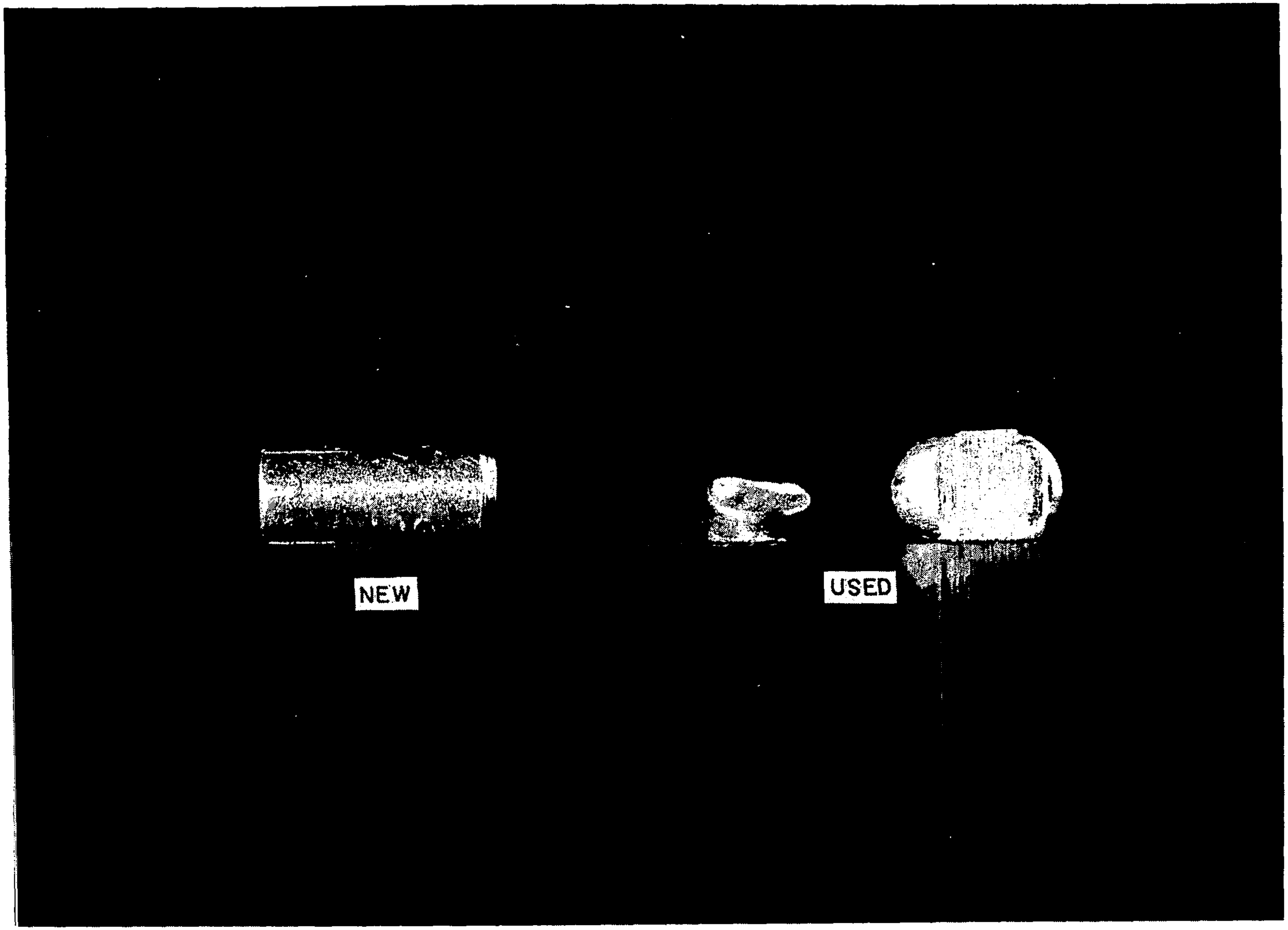

Figure 75 Aluminum Blade Locking Pins

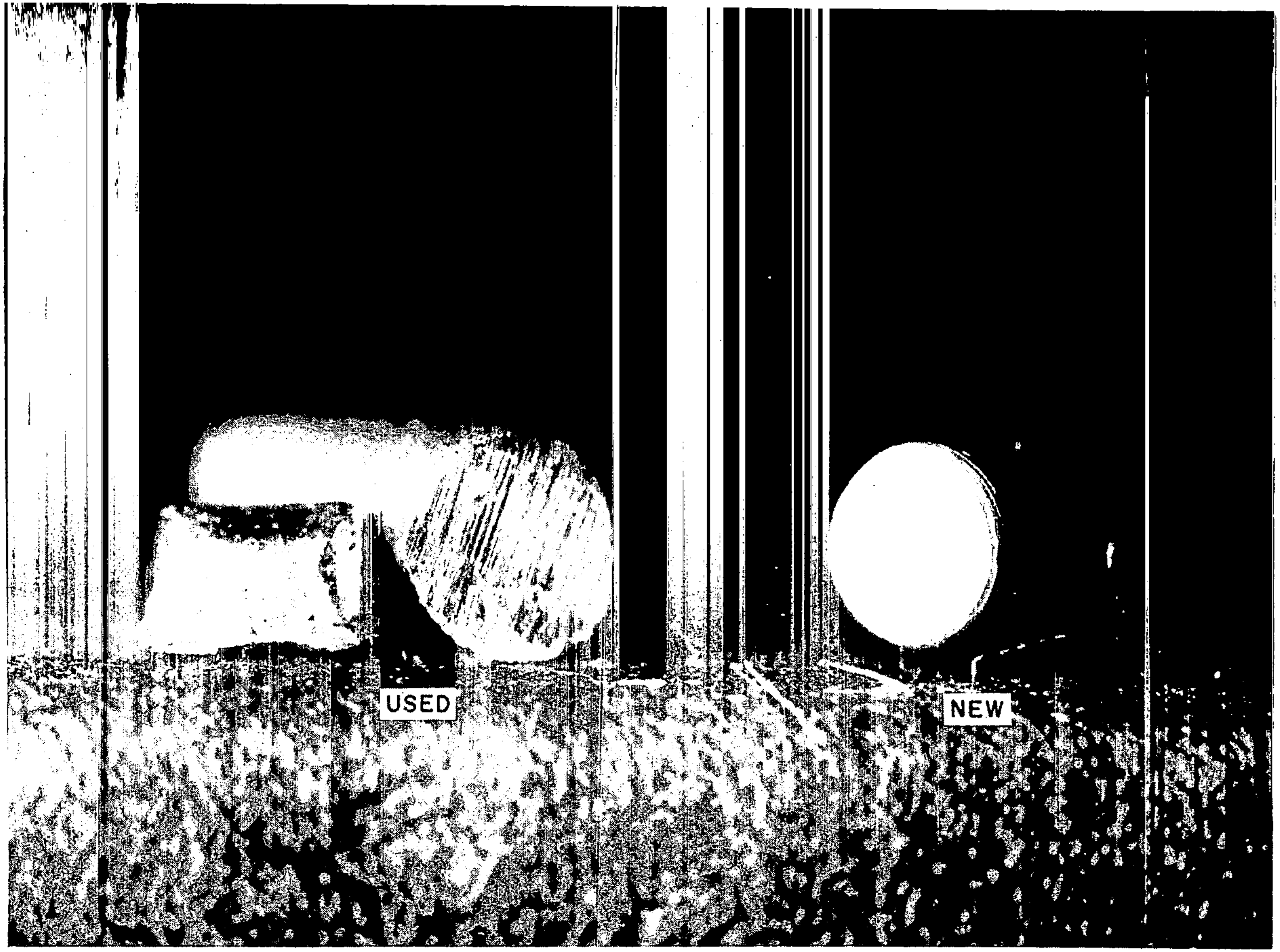

Figure 76 Silver-Plated Copper Blade Locking Pins

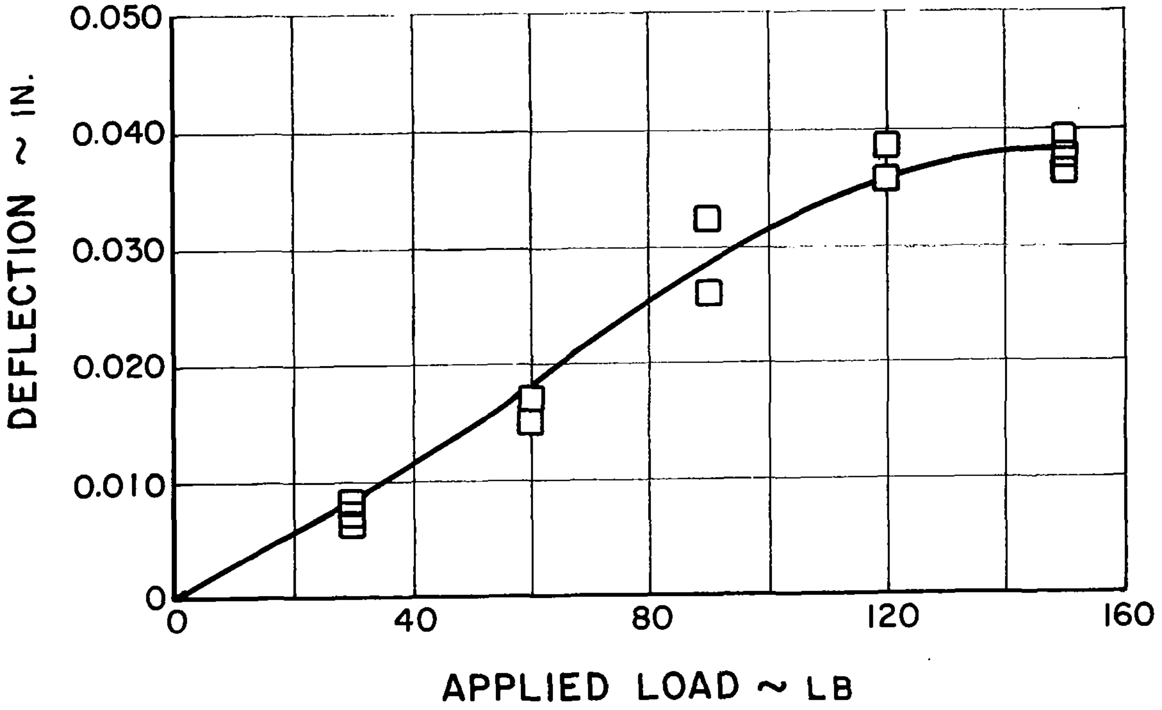

Figure 77 Solid Copper Pin Deformation Test Results

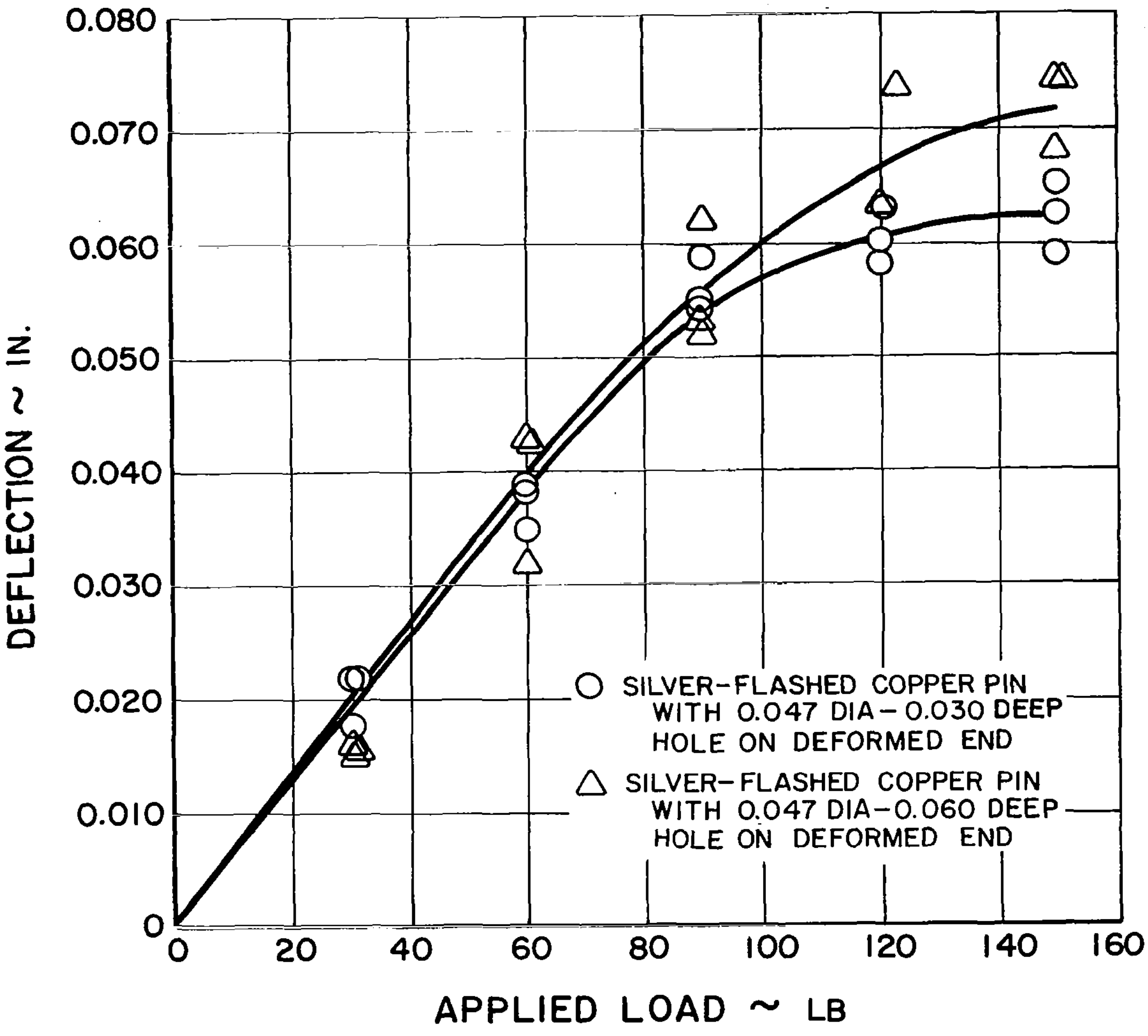

Figure 78 Relieved Copper Pin Deformation Test Results

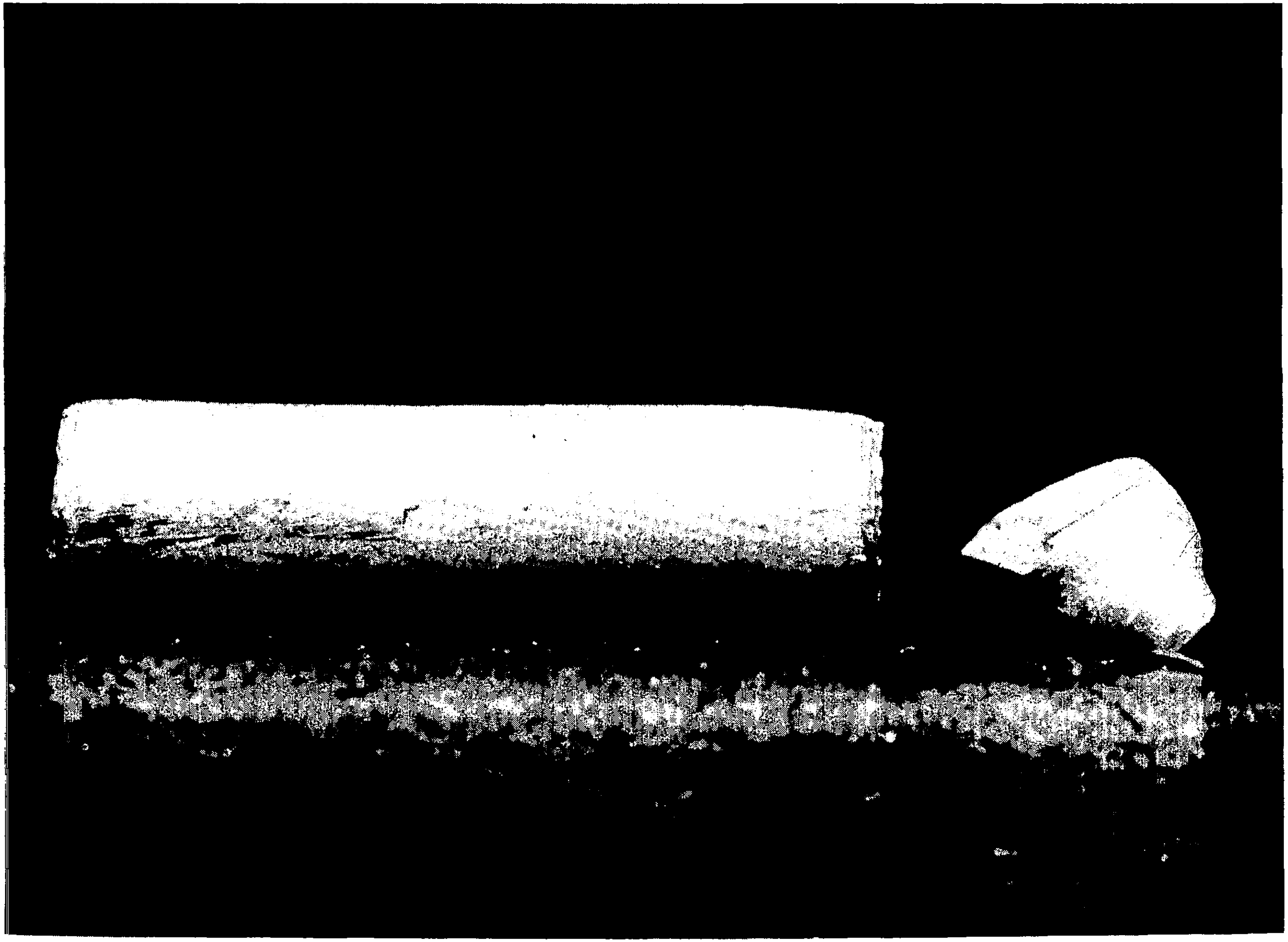

Figure 79 Drilled Copper Blade Locking Pin Showing Deformed Head Sheared Off after Blade Removal

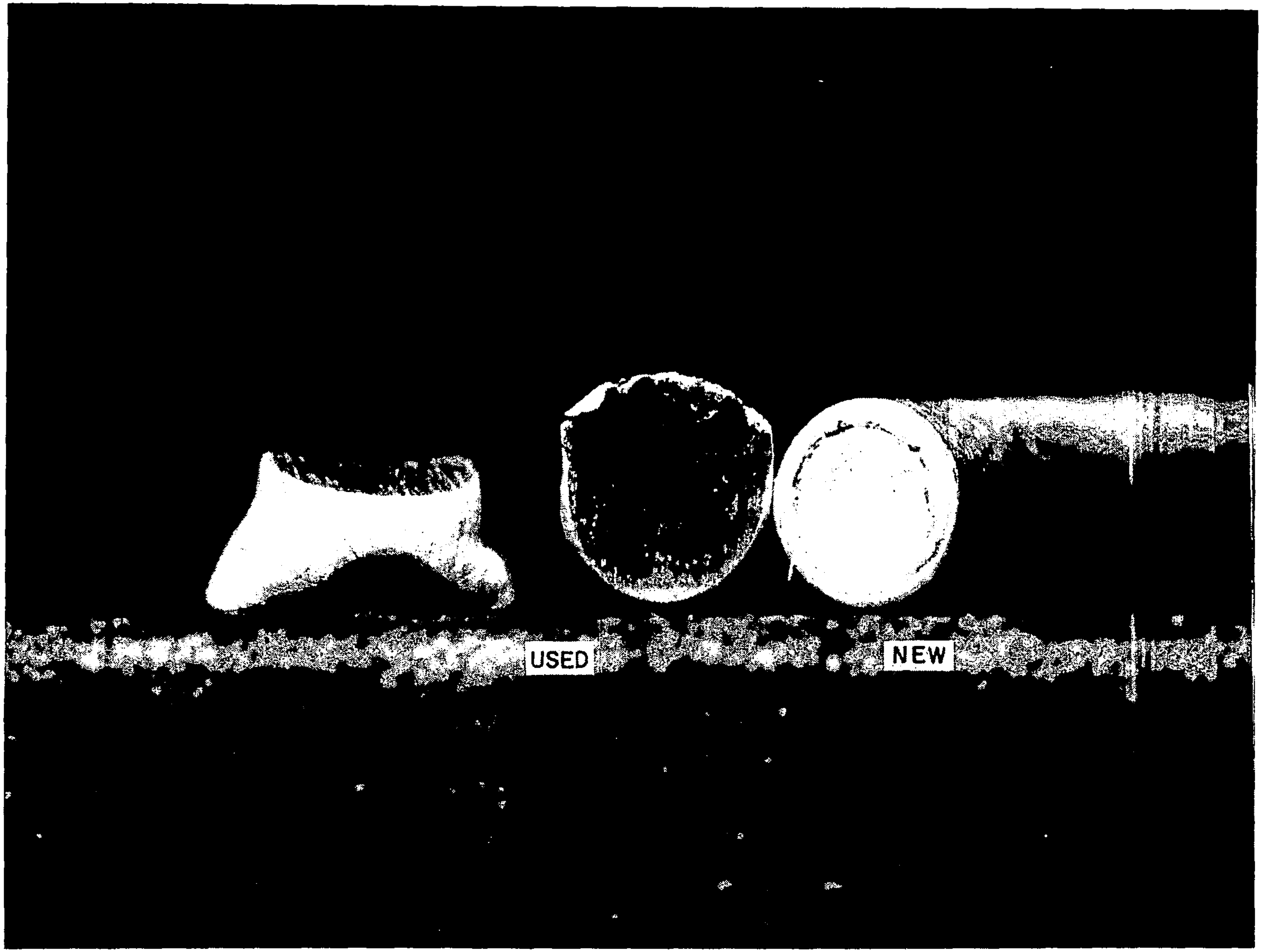

Figure 80 Drilled Copper Blade Locking Pins

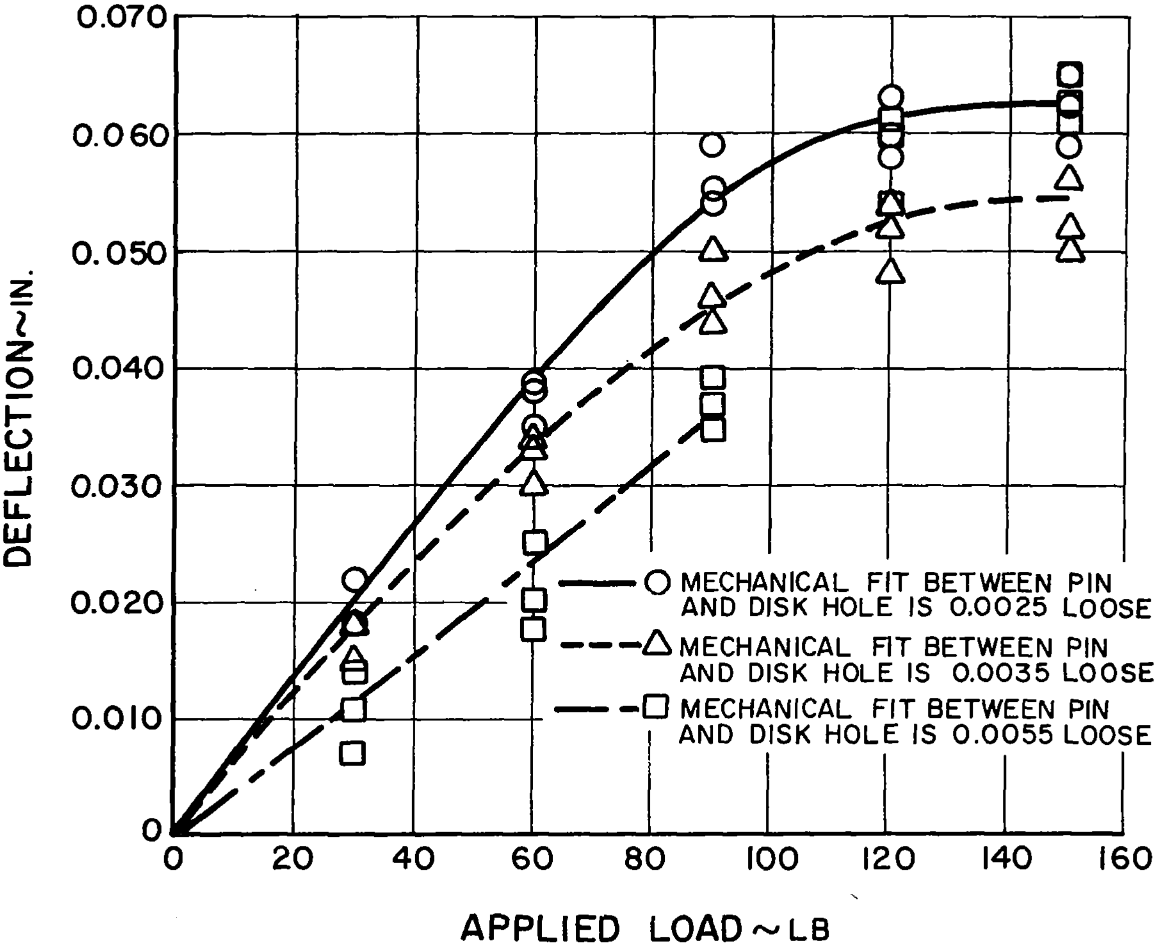

Figure 81 Relieved Copper Pin Deformation Test Results

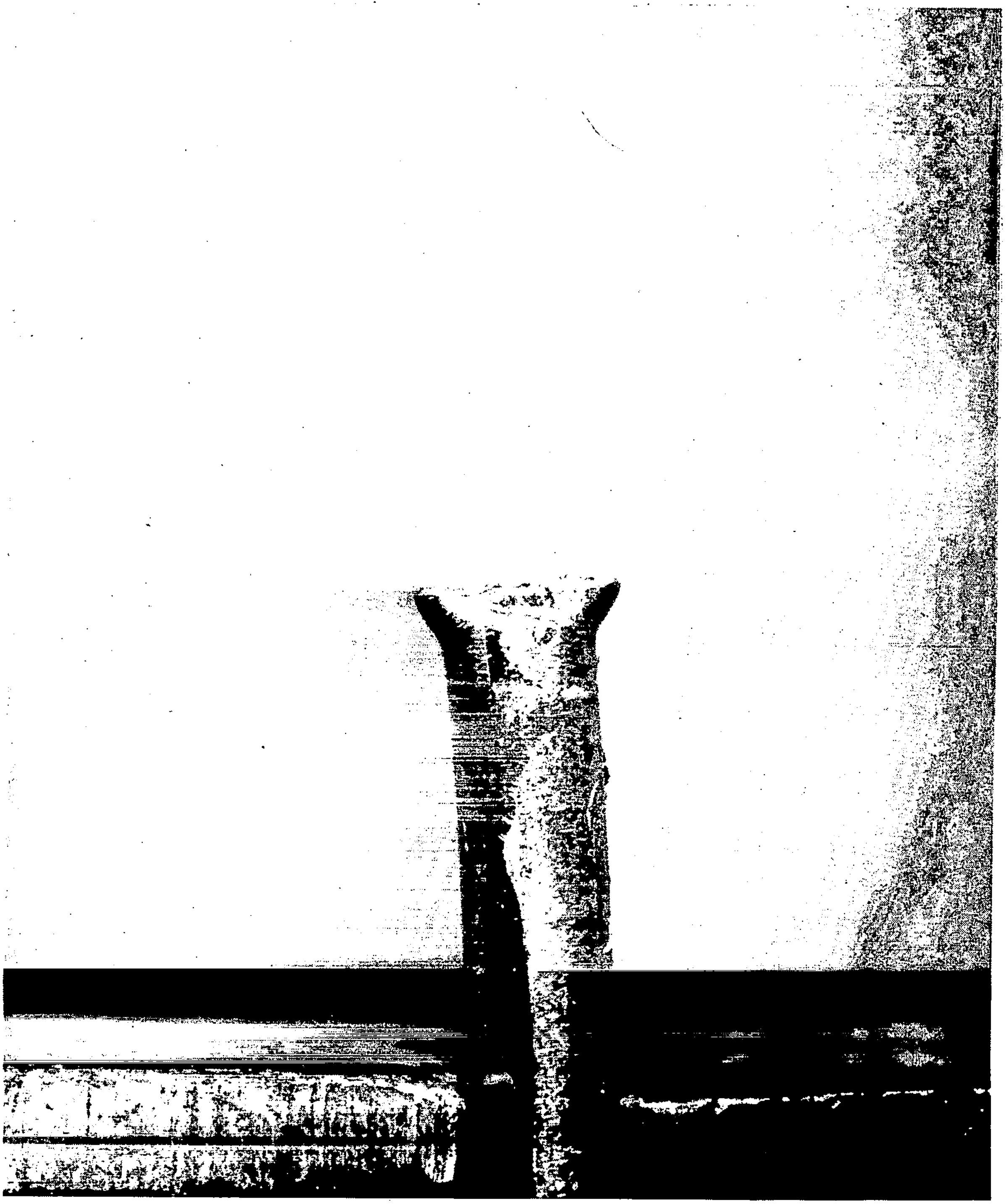

Figure 82 Drilled Copper Blade Locking Pin Showing Upset Deformation after 125-Pound Load

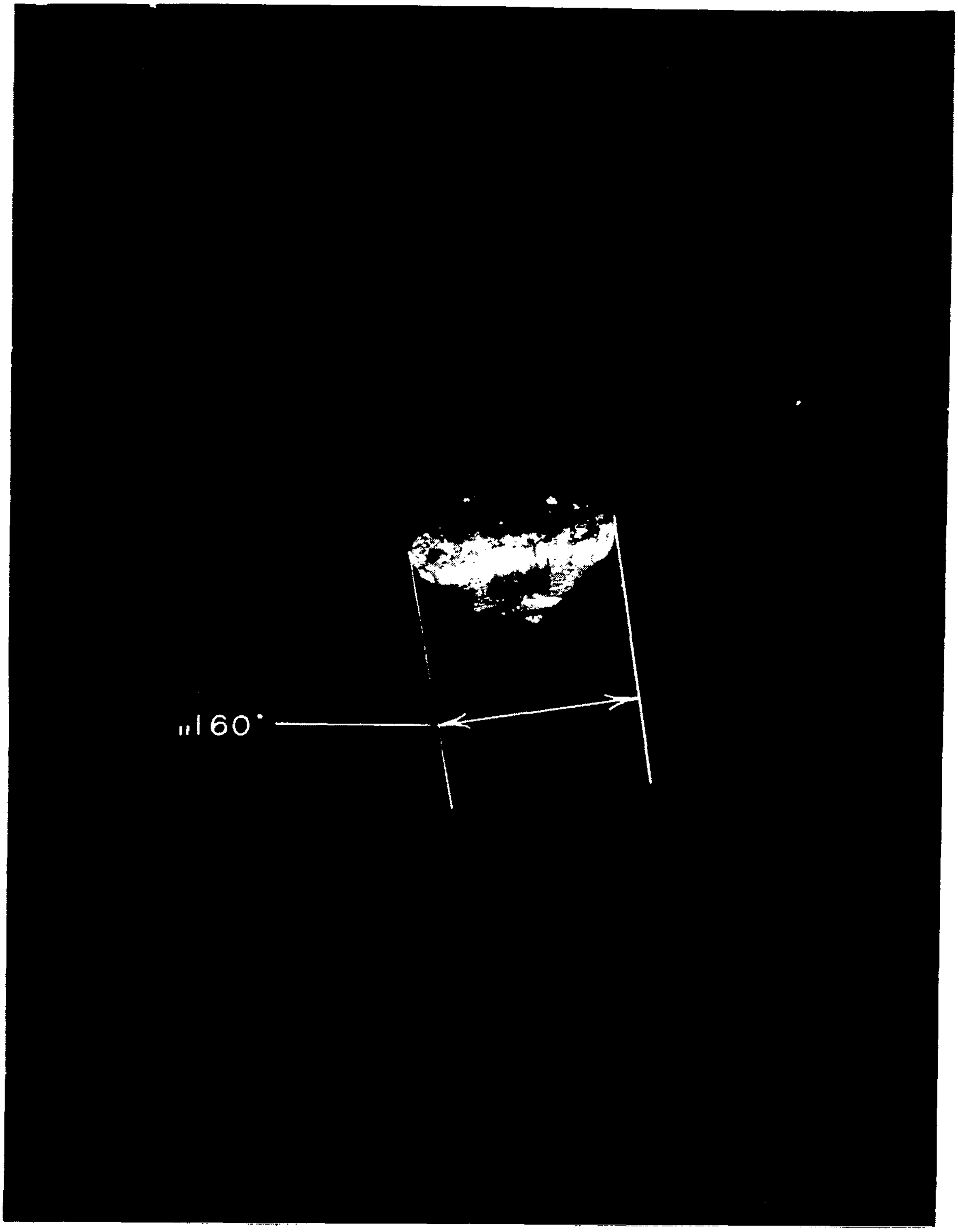

Figure 83 Deformed Rivet Head of Drilled Copper Blade Locking Pin after 125-Pound Load

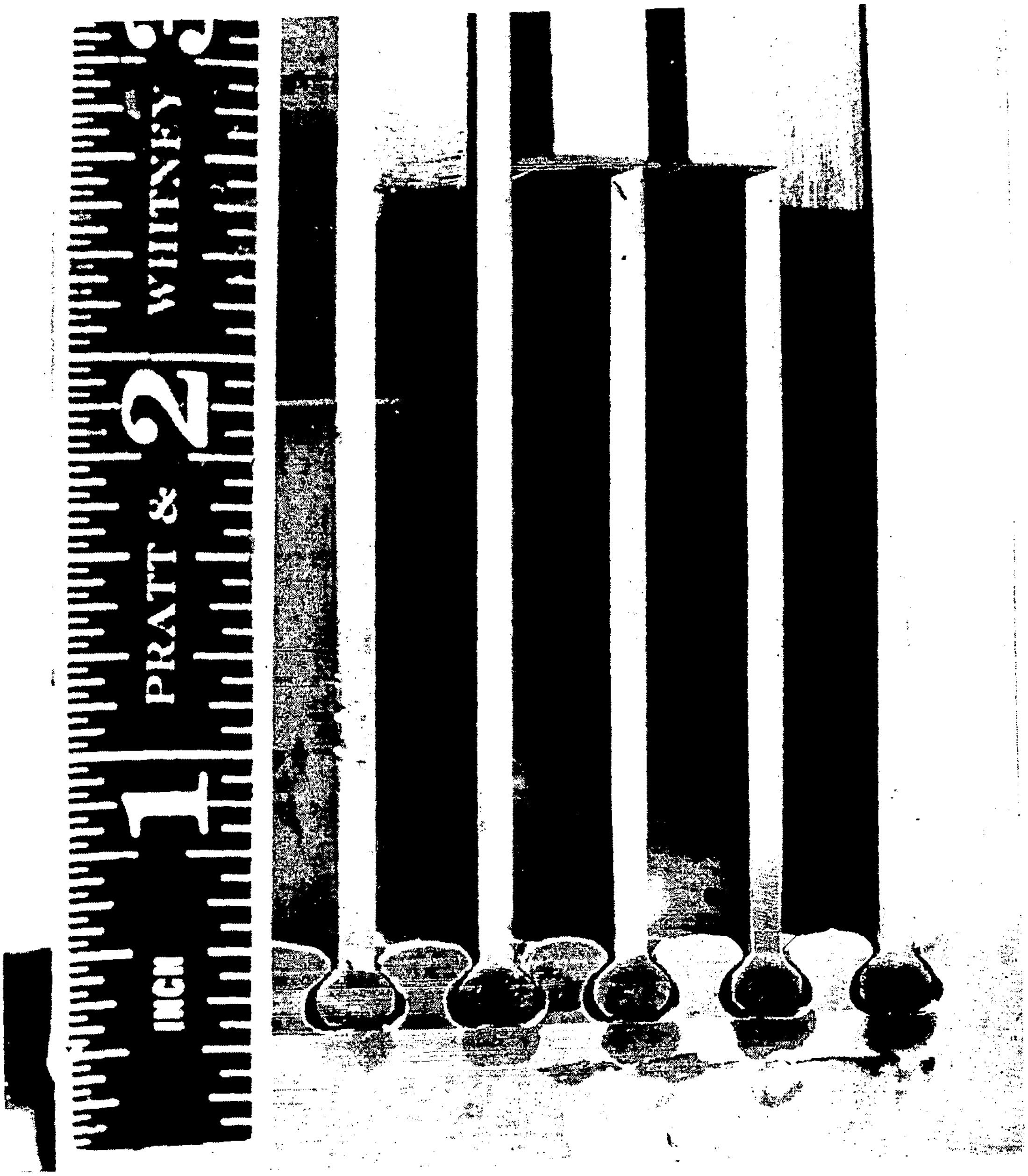
INCH
1
PRATT &
2
WHITNEY
3

Figure 84 Simulated Compressor Blade Root Test Parts

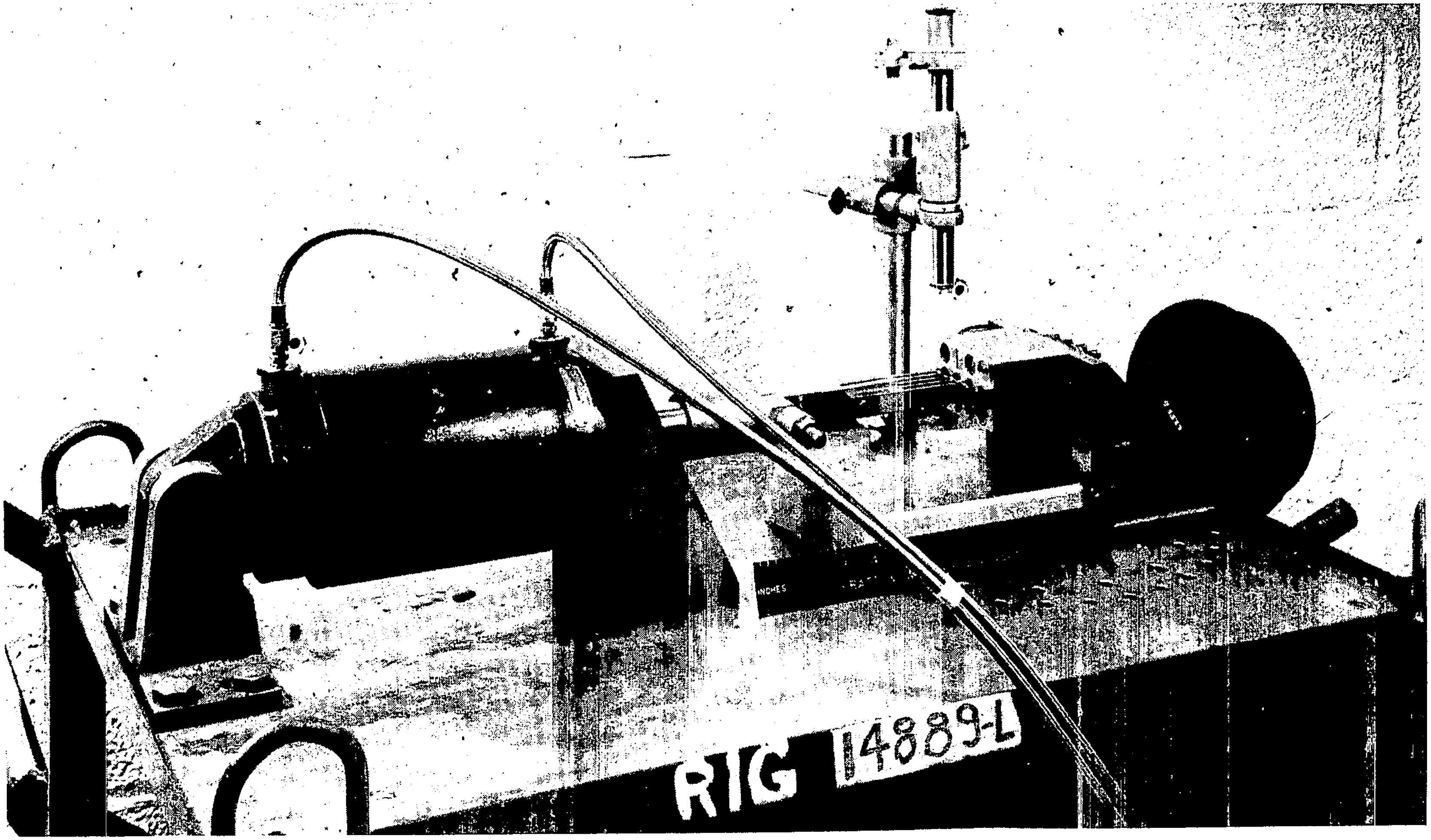
INCHES
RIG 14889-L

Figure 85 Test Setup for Applying Simulated Centrifugal Load to Compressor Blade Root Test Pieces

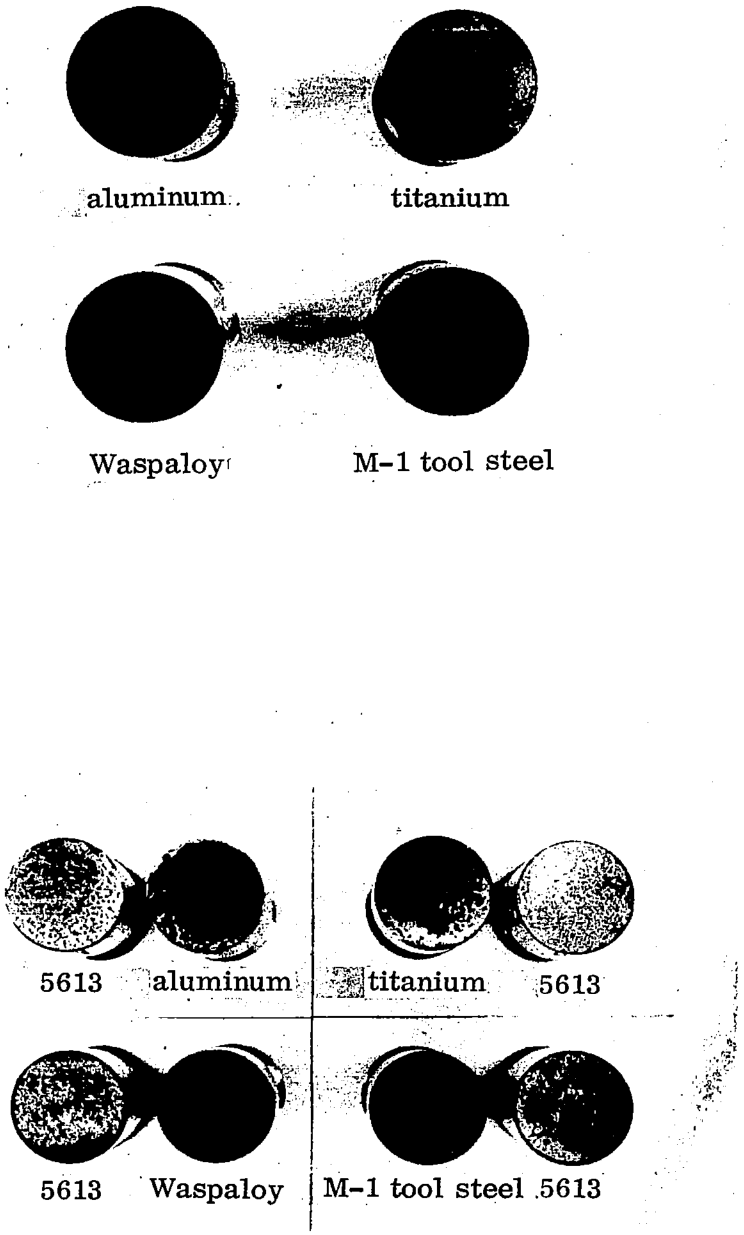
aluminum
titanium
Waspaloy
M-1 tool steel
5613
aluminum
titanium
5613
5613
Waspaloy
M-1 tool steel
5613

Figure 86 Linde LC-4 Process Bond Strength Specimens before and after Test

Mag: 500X

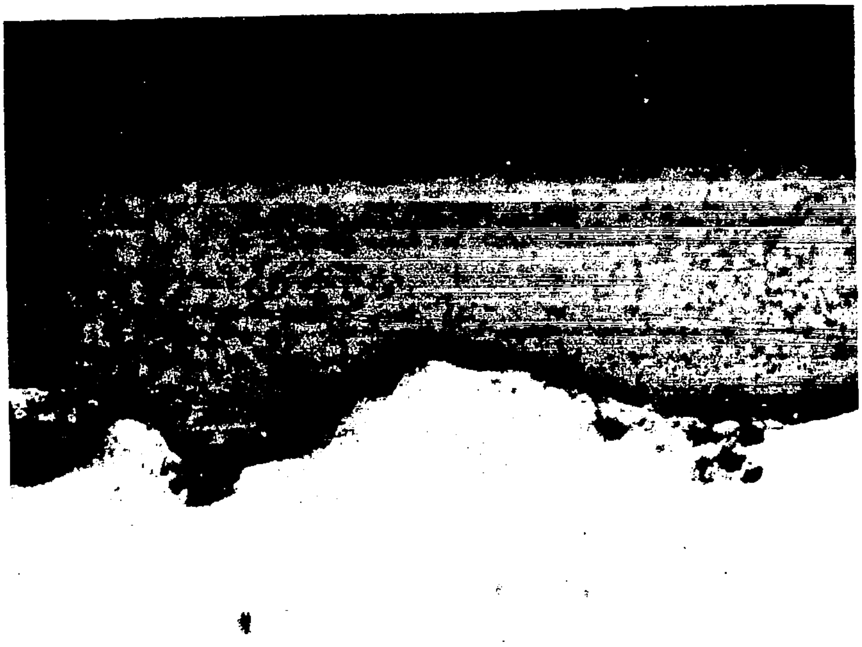
Mag: 500X

Figure 87 Waspaloy and Aluminum with Chrome Oxide Coating Applied by Linde LC-4 Process

Mag: 500X

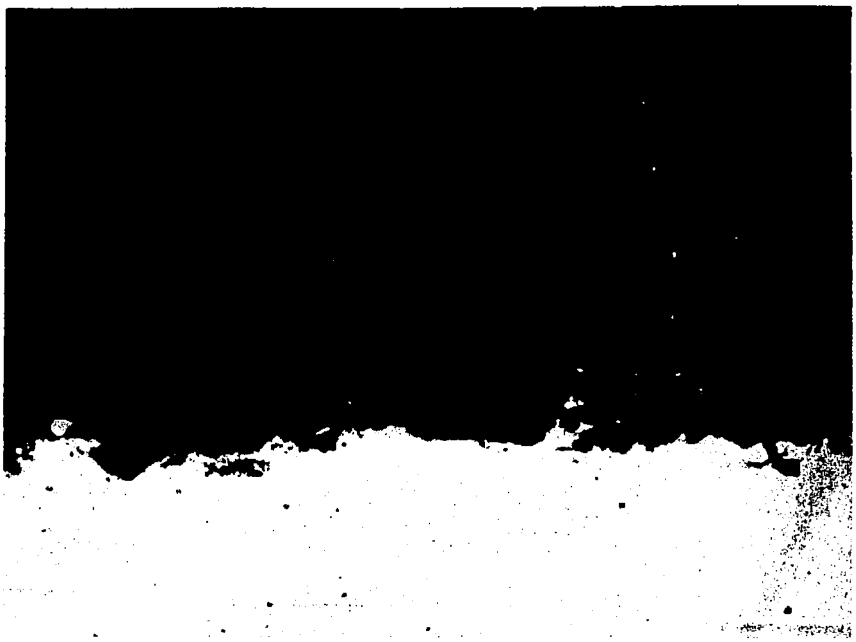

Mag: 500X

Figure 88 M-1 Tool Steel and Titanium with Chrome Oxide Coating Applied by Linde LC-4 Process

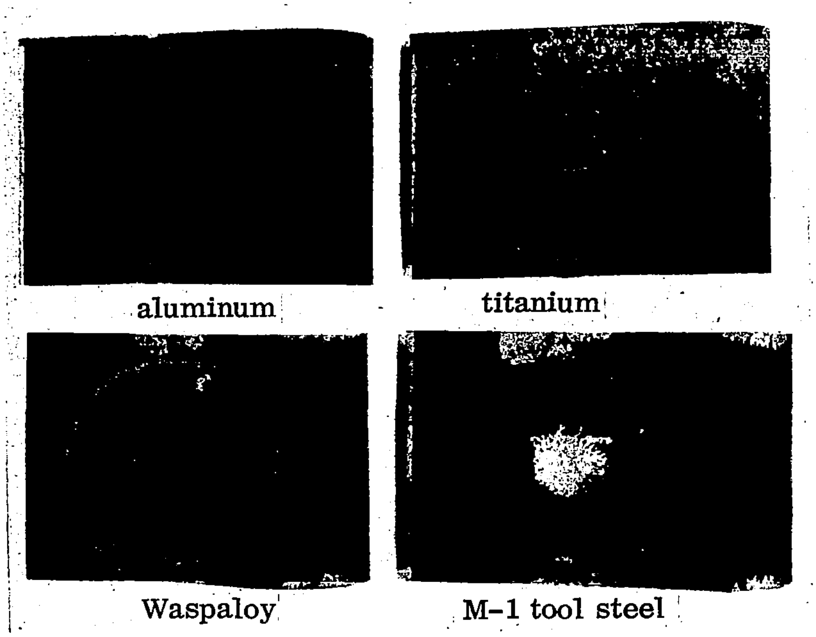

aluminum titanium

Waspaloy M-1 tool steel

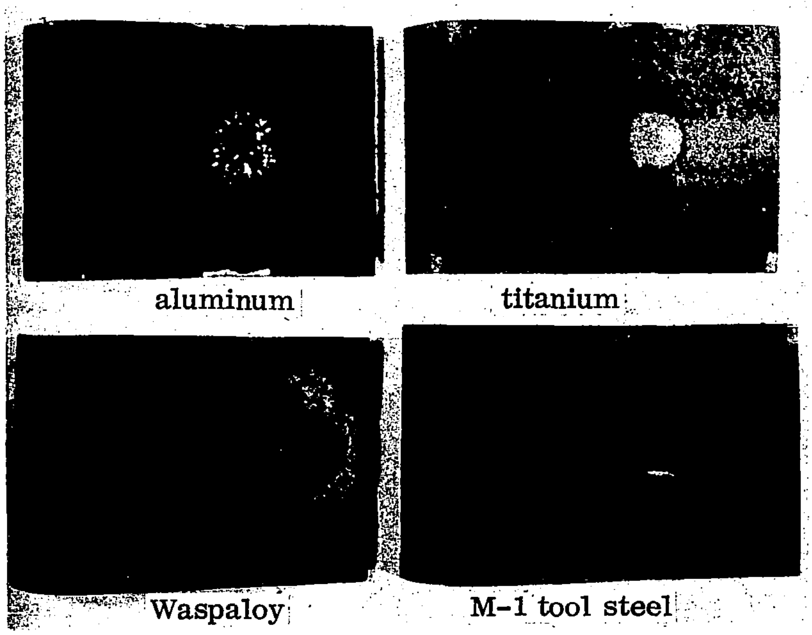

aluminum titanium

Waspaloy M-1 tool steel

Figure 89 Cup/Bend Specimens Coated by Linde LC-4 Process and Plasma-Spray Process after Test

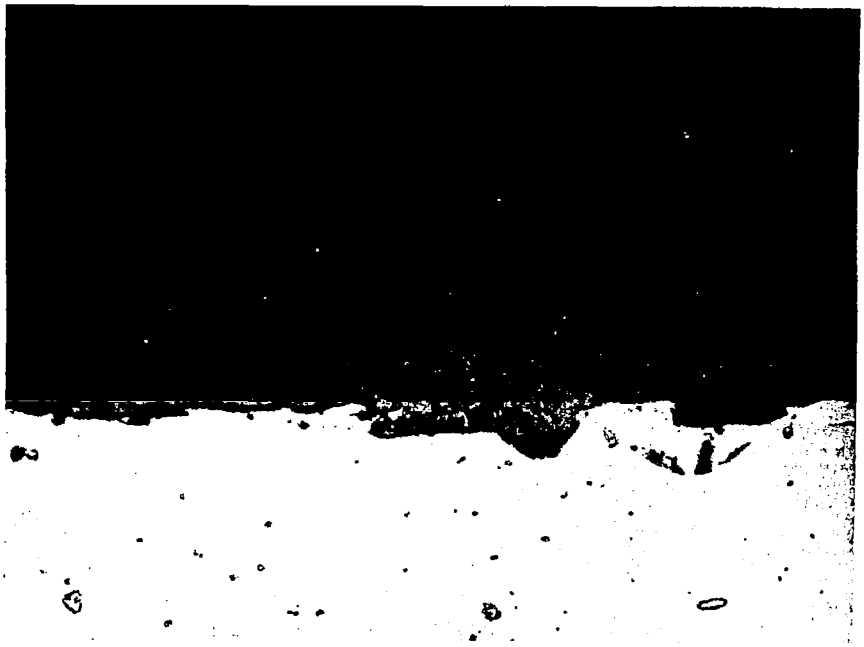

Mag: 500X

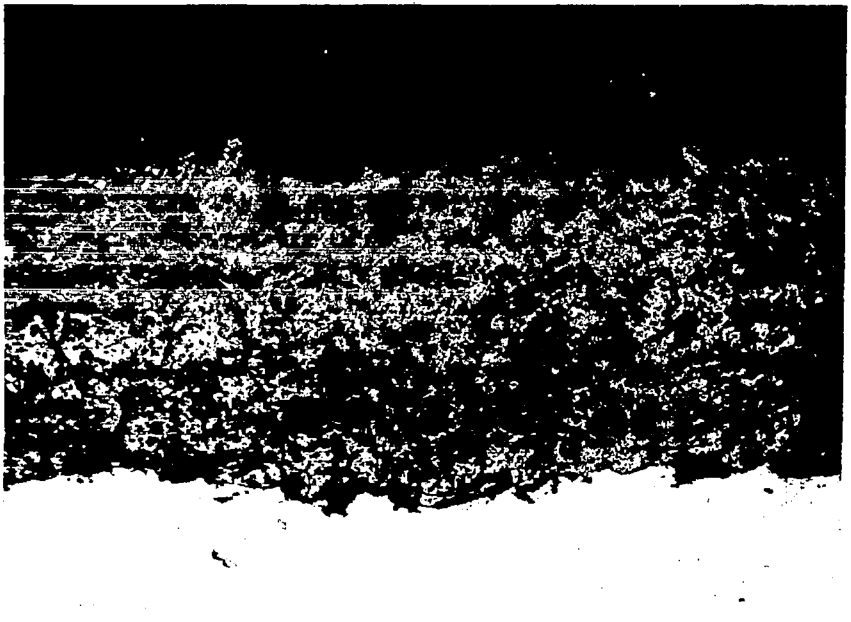

Mag: 325X

Figure 90 Thermally-Cycled Specimens of Linde LC-4 Coating and Plasma-Spray Coating on Waspaloy

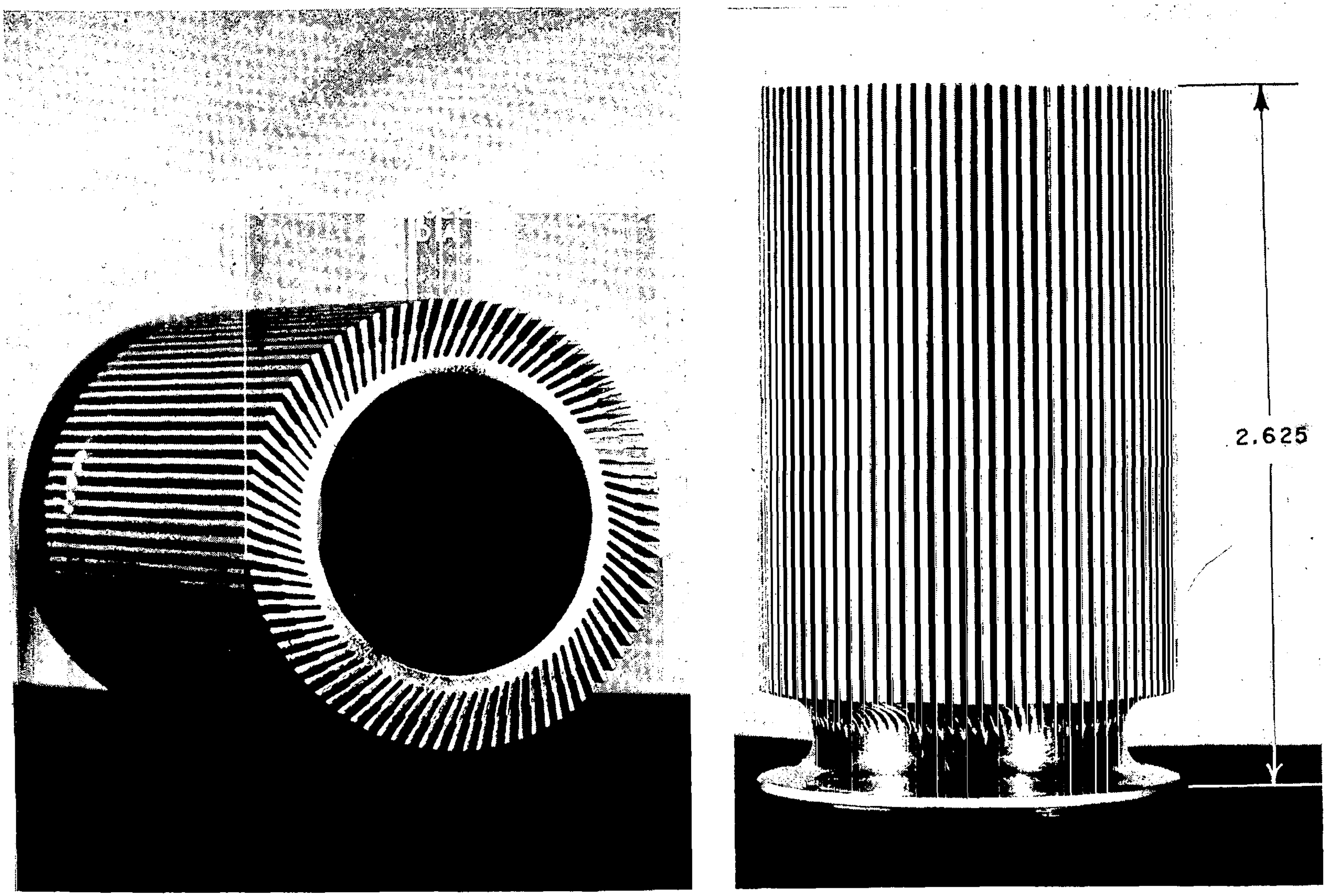

Figure 91 Two Views of Finned Element of Heat Exchanger for Number 2 Bearing

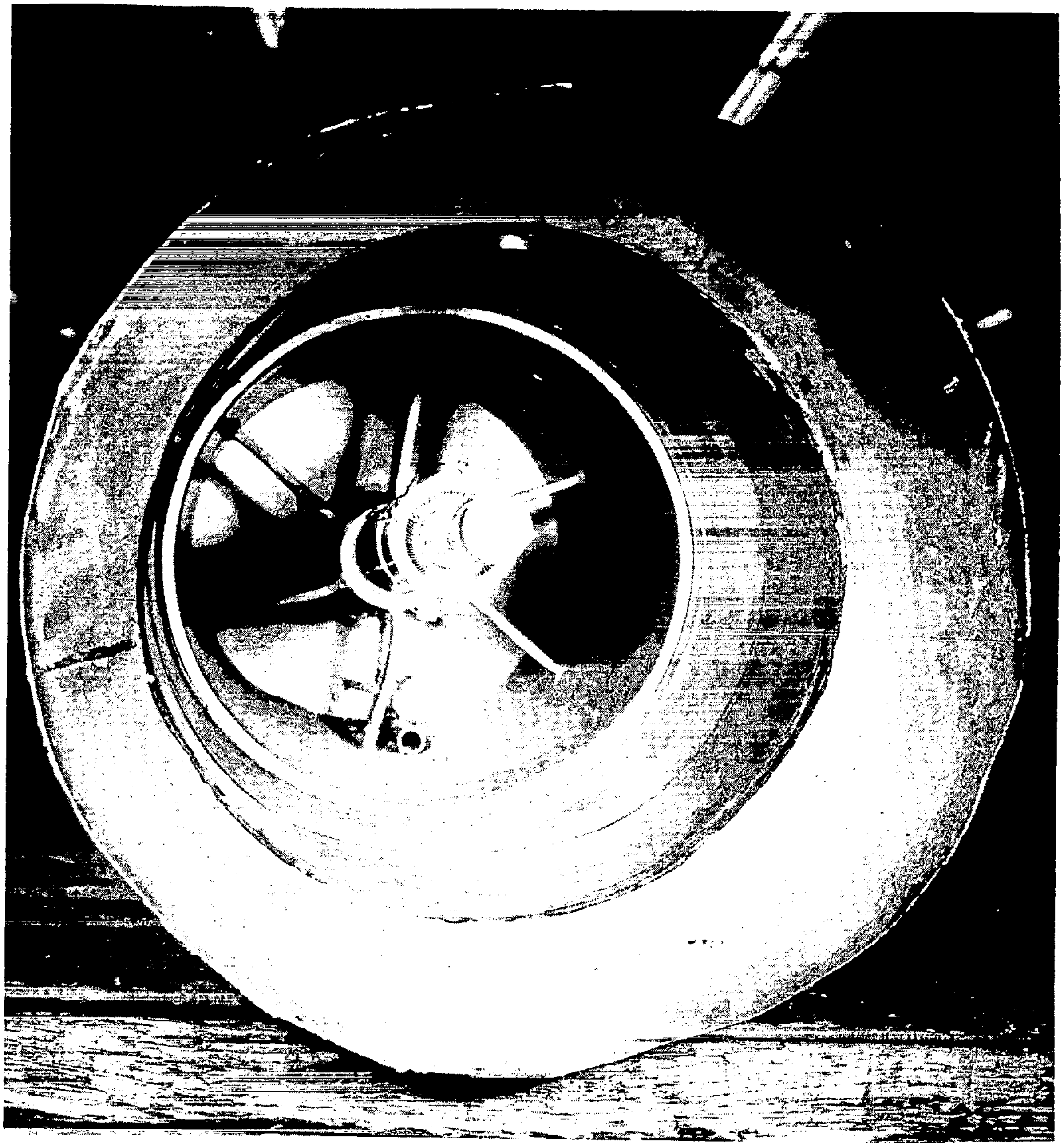

Figure 92 Simulated Shaft Assembly Mounted in Braze Retort

NASA-Langley, 1968 —— 3